REPUBLIQUE DU CAMEROUN
Paix-Travail-Patrie

UNIVERSITE DE YAOUNDE I

CENTRE DE RECHERCHE ET DE FORMATION DOCTORALE EN SCIENCES, TECHNOLOGIES ET GEOSCIENCES

UNITE DE RECHERCHE ET DE FORMATION DOCTORALE EN PHYSIQUES ET APPLICATIONS

B.P 812 Yaoundé
Email: crfd_stg@uy1.uninet.cm

REPUBLIC OF CAMEROON
Peace-Work-Fatherland

THE UNIVERSITY OF YAOUNDE I

POSTGRADUATE SCHOOL OF SCIENCES, TECHNOLOGY AND GEOSCIENCES

RESEARCH AND POSTGRADUATE TRAINING UNIT FOR PHYSICS AND APPLICATIONS

P.O. Box 812 Yaoundé
Email: crfd_stg@uy1.uninet.cm

Laboratoire de Mécanique, Matériaux et Structures

Laboratory of Mechanics, Materials and Structures

GENERATION OF SOLITONS IN NONLOCAL MEDIA

Thesis submitted in partial fulfillment of the requirements for the award of The degree of Doctor of Philosophy (Ph.D.) in Physics,

Specialty: **Fundamental Mechanics and Complex Systems**

By

ZANGA Dieudonné

Registration Number: **09W0851**

Master of Science in Physics

Under the Supervision of

FEWO Serge Ibraïd

Associate Professor

University of Yaounde I

KOFANÉ Timoléon Crépin

Professor

University of Yaoundé I

2021

UNIVERSITÉ DE YAOUNDÉ
THE UNIVERSITY OF YAOUNDE I

FACULTÉ DES SCIENCES
FACULTY OF SCIENCES

DÉPARTEMENT DE PHYSIQUE
DEPARTMENT OF PHYSICS

ATTESTATION DE CORRECTION DE LA THÈSE DE DOCTORAT/Ph.D

Nous, Professeur **TCHAWOUA CLEMENT** et Professeur **WOAFO PAUL**, respectivement Examinateur et Président du jury de la Thèse de Doctorat/PhD de Monsieur **ZANGA DIEUDONNE**, Matricule **09W0951**, préparée sous la direction des Professeurs **KOFANE TIMOLEON CREPIN ET FEWO SERGE IBRAID** (Université de Yaoundé I), intitulée : « **GENERATION OF SOLITONS IN NONLOCAL MEDIA** », soutenue le Vendredi, **28 Juillet 2022**, en vue de l'obtention du grade de Docteur/PhD en Physique, Spécialité **Mécanique, Matériaux et Structures,** option **Mécanique Fondamentale et Systèmes Complexes** attestons que toutes les corrections demandées par le jury de soutenance ont été effectuées.

En foi de quoi, la présente attestation lui est délivrée pour servir et valoir ce que de droit.

Fait à Yaoundé, le 20 FEV 2023

Examinateur	Le Président du jury	Le Chef de Département de Physique
Pr TCHAWOUA CLEMENT	Pr WOAFO PAUL	Pr NDJAKA JEAN-MARIE

UNIVERSITE DE YAOUNDE I * FACULTE DES SCIENCES * Le Chef de Département * DEPARTEMENT DE PHYSIQUE *

GENERATION OF SOLITONS IN NONLOCAL MEDIA

Thesis

Submitted in fulfillment of the requirements for the degree
of **Doctor of Philosophy** in Physics

Speciality: **Mechanics, Materials and Structures**

Option: **Fundamental Mechanics and Complex Systems**

By

ZANGA Dieudonné

Registration Number: 09W0851
Master in Physics, Option Mechanics and Materials

Under the Co-supervision of

KOFANÉ Timoleon Crépin

Professor, University of Yaounde I

FEWO Serge Ibraïd

Associate Professor, University of Yaounde I

September 17, 2022

Declaration

I declare that this work "**Generation of soliton in nonlocal media** " is my original work and that all the sources I have used or cited have been indicated and acknowledged by means of complete references, and that this document has not been submitted for degree purposes at any other academic institutions.

Dieudonné Zanga
Student Number: 09W0851(UY1)

Signed: ZD

Date: September 2021

Dedication

This work is dedicated to:

- My grand father and grand mother **Mr ZANGA DIEUDONNE AND NGO MAPOUTH SIPORA**.
- My mother **NGO BAMALE SERAPHINE**.
- AND ALL MENBERS OF FAMILY **ZANGA**.

Acknowledgements

The accomplishment of this thesis would not be possible without the assistance and the help of numerous individuals and institutions.

★ First of all, I would like to express my deepest thankfulness to my supervisor, Professor **KOFANE Timoleon Crepin**, for giving me the opportunity to complete successfully this thesis. His expertise, his vast knowledge in both nonequilibrium physics and coherent structures and his unique scientific feeling considerably shaped my current interest and experience in theoretical physics.

★ A very special acknowledgment goes out to my director, Professor **FEWO Serge**, for his guidance and help during the entire course of this work. His tremendous physical insight and unreserved willingness to share his understanding of physics with others have made this project very enjoyable and instructive. I owe her a debt of gratitude and respect.

★ I acknowledge in advance the scientists for accepting to examine this thesis, the President of Jury Professor WOAFO Paul and others members of jury: Professor TCHAWOUA Clement, Professor NANA NBENJO Blaise Roméo, and Professor DJUIDJE KENMOE Germaine at the University of Yaoundé I, and Professor MOHAMADOU Alidou at the University of Maroua.

★ I gratefully thank to Professor **TABI Bertrand Conrad** for his help during the preparation of different papers of this thesis.

★ I would like to acknowledge Professor **Jean-Marie Bienvenu NDJAKA**, the head of Department of Physics at the Faculty of Science at the University of Yaoundé I, for receiving me in his Department.

★ I am grateful to Professor **WOAFO Paul**, Chairman of the Cameroon Physical Society for his teaching specially in numerical methods.

★ It would be very pleasing to recognize trade and constructive discussions combined

with great moments of sharing with all the teachers of the Department of Physics in general and of the laboratory of Mechanics, Materials and Structures in particular. I have named Professor **TCHAWOUA Clement**, Professor **DJUIDJE Germaine**, Professor **NANA NBENDJO Blaise Roméo**, Professor **VONDOU Derbetini**.

★ I am grateful to Professor **ANNIE WAKATA BEYA**, Higher Teacher Training College Yaoundé, University of Yaoundé I Cameroon.

★ Special thanks to **Dr:DJOMO MBONG Thierry Landry Michel**,**Dr:TEMGOUA DJOUATSA Diane Estelle**,**Dr:BITANG AZIEM DANIEL CASSIDY**,**Dr:MADENG LUCIEN GNINZANLONG Carlos**, for the multitude exchanges and helps.

★ Special thanks to **NAHA NZOUPE FERNAND** for the multitude exchanges and helps.

★ I would like to acknowledge the World Bank through the "CETIC" project, which gave me the opportunity to perform a part of this thesis at the University of Yaounde I.

★ I am feelingly grateful to members of my familly, for the crucial role they have played

★ I acknowledge in advance the scientists who will accept to examine this thesis.

Contents

List of Figures

List of Abbreviations

AA: **A**ttractive-**A**ttractive
AR: **A**ttractive-**R**epulsive
AB: **A**khmediev-**B**reathers
BECs: **B**ose-**E**instein **C**ondensates
CQSCGLE: **C**ubic-**Q**uintic-**S**eptic **C**omplex **G**inzburg **E**quation
CSHE: **C**omplex **S**wift-**H**ohemberg **E**quation
CW: **C**ontinous **W**ave
FOD: **F**ourth-**O**rder **D**ispersion
FFOD: **F**ifth-**O**rder **D**ispersion
FPU: **F**ermi-**P**asta-**U**lam
mCSHE: **m**odified **c**omplex **S**wift-**H**ohemberg-**e**quation
MI: **M**odulational **I**nstability
NLSE: **N**onlinear **S**chrödinger **E**quation
RA: **R**epulsive-**A**ttractive
RE: **R**are **E**arth
RW: **R**ogue **W**ave
SPM: **S**elf-**P**hase **M**odulation
SOD: **S**ixth-**O**rder **D**ispersion

SSFM: **S**plit-**S**tep **F**ourier **M**ethod
TOD: **T**hird-**O**rder **D**ispersion

Résumé

Dans cette thèse, nous présentons une étude systématique, á la fois analytique et numérique, de la formation et la propagation de trains de solitons par instabilité modulationnelle dans des milieux nonlocaux et dopés. D'entrée de jeux, nous étudions, l'instabilité modulationnelle des ondes planes continues dans des milieux non linéaires faiblement nonlocaux de cubiques-quintique. Théoriquement, la transformation de Lenz et l'analyse de stabilité linéaire sont utilisées pour étudier l'impact des non-localités cubiques et quintiques sur l'instabilité modulationnelle à travers le diagramme de stabilité dans différents modes de non-linéarité. De plus, le critère dépendant du temps prédisant l'existence de l'instabilité modulationnelle, pour toute valeur du nombre d'onde, est établi. Dans la partie numérique, l'intégration directe de l'équation non linéaire de Schrödinger nonlinéaire, par la méthode d'intégration de Fourier à pas divisés, montre la dynamique de désintégration d'une onde plane dans des milieux a non-localité faiblement quintiques. Les prédictions théoriques sont en bon accord avec les résultats numériques. L'impact des non-localités cubiques et quintiques sur l'instabilité modulationnelle est tel que des valeurs plus élevées de la non-localité quintique contribuent à réduire l'instabilité modulationnelle dans le système. De plus, l'interaction à trois corps dans le modèle donne naissance à des ondes solitaires (Breather) d'Akhmediev, qui sont des manifestations nonlinéaires de l'instabilité modulationnelle.

Deuxièmement, nous présentons une génération de soliton optique dissipatif par instabilité de modulationnelle dans une fibre optique dopée avec des effets de correction. L'équation de Ginzburg-Landau complexe cubique-quintique-septique avec dispersion d'ordre supérieure et termes non linéaires de gradient, qui décrit bien la dynamique des impulsions ultracourtes dans la fibre optique dopée, est utilisée. L'analyse de stabilité linéaire nous permet d'obtenir le critère de Lange-Newell pour MI des ondes de Stocke, domaine des limites de MI et gain intégré de MI, pour le modèle considéré. Nous appliquons ensuite une méthode statistique pour observer l'influence de certains effets physiques sur le désaccord de fréquence critique simultanément. En régime normal, la forme pyramidale du gain maximum est obtenue pour les valeurs variables des coefficients de dispersion impairs. Pour l'équation du modèle complet, le nombre de régions d'instabilité varie de manière incohérente pour les coefficients de dispersion pairs, mais reste constant pour les coefficients de dispersion impairs dans le même régime de dispersion. Avec la méthode pseudo-spectrale, on observe la génération de train d'impulsions et on retrouve la

carte soliton induite par MI en fonction de certains effets physiques, à partir du diagramme de bifurcation. En l'absence des termes de gradient, les coefficients de dispersion même complexes augmentent le MI, et avec la présence d'un coefficient de dispersion impair, MI diminue.

Mots clés: Soliton; Instabilité modulationnelle ; Nonlocalité; Nonlinéarité; Soliton dissipatif; Transformée de Lenz; Analyse de la Stabilité linéaire; Méthode d'intégration de Fourier à pas divisés, Méthode statistique.

Abstract

In this thesis, we present a systematic study, both analytically and numerically, of the formation and propagation of soliton trains by modulational instability in nonlocal as well as doped media.

Firstly, we investigate, the modulational instability of continuous plane waves in weakly cubic-quintic nonlocal nonlinear media. Theoretically, the Lenz transformation and the linear stability analysis are used to study the impact of cubic and quintic nonlocalities on modualtional instability through the stability diagram in different modes of nonlinearity. Moreover, the time-dependent criterion predicting the existence of the modulational instability for any value of the wave number is expressed. In the numerical part, the direct integration of the nonlinear Schrödinger equation, with the split-step method, shows the disintegration dynamics of plane wave in weakly quintic media. Theoretical predictions are in good agreement with numerical results. Particularly, the impact of the cubic and quintic nonlocalities on modulational instability is such that higher values of the quintic nonlocality contribute to reduce the modulational instability in the system. Moreover, the three-body interaction in the model gives rise to Akhmediev breathers, which are the nonlinear manifestation of modulational instability.

Secondly, we present a generation of dissipative optical soliton through modulation instability (MI), in doped fiber with correction effects. The cubic-quintic-septic complex Ginzburg-Landau equation with higher-order dispersion and gradient nonlinear terms which governs the propagation of dispersive pulses in doped optical fiber is used. The linear stability analysis leads to the Lange-Newell's criterion for MI of Stokes waves, boundaries domain of MI and integrated gain of MI, for the model of under consideration. We apply a statistical method to observe the influence of any physical effect on the critical frequency detuning. In the normal regime, the pyramidal form of the maximum gain is obtained when varying the values of odd dispersion coefficients. For the full model equation, the number of instability regions varies incoherently for the even dispersion coefficients, but remains constant for the odd dispersion coefficients in the same dispersion regime. Using the pseudo-spectral method, we observe the generation of train of pulses and found the soliton map induced by MI as a function of some physical effects, through the bifurcation diagram. In the absence of the gradient terms, the even complex dispersion coefficients increase the MI, and with the presence of odd dispersion coefficient, MI decreases.

Keywords: Soliton; Modulational instabilty; Nonlocality; Nonlinearity; Dissipative soliton; Lenz transformation; linear stability analysis; Split-step Fourier method; Statistical method.

General Introduction

We introduce this thesis with the famous citation "knowledge is power". This sentence is short and simple, but very powerful. In the sense that knowledge is a set of information in one domain of life, information is the essence of life. It intervenes in several aspects of life such as biology, economics, religion, politic, education, sociology, history, and science. Despite its indispensability, information presents a great advantage for the ones who possess and manipulate it. That is why we have great structures that are based on the game of the manipulation of information, namely Central Intelligence Agency, Komitet GossoudarstvennoÃ¯ Bezopasnosti, INTERPOL just to cite a few. We note that, in this thesis we are not interest in the political and military implication in the manipulation of information. We will only focus our attention on the transport of this information. This latter transport has undergone great mutations through different centuries. For example, its nature changed from the use of musical instruments such as trump and tom-tom in ancient eras to the use of fire in the strategies adopted by Chinese and North people. Also, we have the transport by motion, exhibited by the animals such as eagles, pigeons, dogs...etc. Later in the recent centuries, we experienced transport of information by letters through the post office. These means of conveyance presented several disadvantages in mater of confidentiality, discretion, and speed of transport. The great question has been to find how to optimize and secure the transmission of information. Inspired by string toys, which functioning consists of the sound of the voice propagating through a string from one terminal to another, scientists and engineers elaborated several theories and technologies for the transport of sound over long distances. We can mention, as example, the telegraph and the Fax. Where the problem of confidentiality, loss of data and speed of transport are still (a major problem) persisting.

With the progress of science, the question of interaction between the propagating light and matter lead to elegant theories and the birth of new technologies such as crystallography, telecommunication [1]. These technologies shortcut distance and make life easy in the context of communication. One of the technologies that became famous is the physical substrate known as optical fiber. It is an optical material with a mode of a glass material such as silica, and can exhibit linear and nonlinear effects. An optical fiber consists of a central glass core surrounded by a cladding layer whose refractive index n_c is slightly lower than the core index n_1. This physical material has been subjected to evolution during the last century, especially due to

the manufacturing of uncladded glass fibers in the 1920s [2, 3, 4], and the production in the 1950s of the cladding layer that led to considerable improvement in the fiber characteristic [5, 6, 7, 8]. In the three next decades, the optical fiber was considerably optimized in the sense of manufacturing and information transmission speed. Then, several investigations of new phenomena in optical fiber have been done. We can cite the loss and high dispersion of linear effects, the stimulated Raman-and Brillouin scattering processes [9, 10, 11], the optically induced birefringence, the parametric four-wave mixing, and the self-phase modulation [12, 13, 14, 15, 16]. Another important feature which support optical fibers is nonlocality. It translates the dependence of the nonlinear intensity of waves at one point with respect to neighboring points [17]. It is a nonlinear phenomenon caused by molecular reorientation, a long-range drift the thermal nonlinearity [17, 18]. This property has a great consequence on telecommunication and is due to the presence of an optical field in optical fiber, and also the doped nature of the material components. The latter components can possess properties such as competing cubic Kerr nonlinearities and quintic non-Kerr nonlinearities.

Several types of materials are required for the fabrication of optical fiber, such as pure silica synthetic glass S_iO_2, dopants such as G_eO_2 and P_2O_5, which increase the refractive index of the pure silica and are suitable for the core, while materials such as boron and fluorine are used for the cladding since they can decrease the refractive index of silica [1]. With this architecture, optical fibers preserve a high percentage of the properties of the light that traverses them.

During the light propagation, there are contributions of dispersion/diffraction, loss, gain local, nonlocal and high- order nonlinearities. These contributions on the motion of light yield interesting phenomena. The more attractive of this phenomena is the generation and propagation the solitary waves, particularly solitons. Solitons occur from a balance between linear and nonlinear effects, and their robustness upon collision with obstacle is one of its particular proprieties [19]. In telecommunication, solitons are perfect candidates for the transport of information at a far distance. Because of its robustness, it has capacity to contain, conserve and transport data, and them prove their importance and necessity for the development of communication technologies. However, another phenomenon arising from nonlinearity in optical fibers is modulational instability (MI). Based on investigations of the dynamic of a perturbed plane wave in the scope of MI, it was found to be the justification for the existence of physical configurations that facilitate the propagation of solitons, and also impose propagation conditions such as Lange-Newell criteria.

In this thesis, we investigate the process of generation of soliton in an optical fiber that has intrinsic proprieties (spatial and temporal) being added to other extrinsic proprieties such as dopant. Firstly we will consider a synthesized material that exhibits competing nonlocal nonlinearities. With the aims to generate optical solitons for the treatment of information by light beams useful for the good transmission and conservative data. Secondly, we will generate optical soliton in dissipative media. We will recall the temporal nature of the nonlocality and

add dopants to create a dissipative character for the optical fiber. The dissipation will then be materialized by the gain and loss caused by the dopant. The reason of this being is to amplify the signal and increases its speed [1]. This work found its application in telecommunication, conservation of database, military application, cryptography. For the well understanding of the process of generation of solitons in nonlocal media, we design our thesis with respect to the following plan. In chapter one, we present the review of literature on solitons, mechanism of nonlinearity, and nonlocal materials. We also briefly explain the concept of modulational instability. Chapter two presents the different derivative models for the conservative system and dissipative system. Necessary analytical treatments such as the lens transformation and linear stability are explained in detail. In addition, for the numerical treatment, we describe methods such as the step by step method and the pseudo-spectral method (split-step- Fourier). The discussion and results of modulation instability for our model are expressed in Chapter three. A first, we illustrate the results coming from the model governed by the nonlinear Schrödinger equation with competing cubic Kerr and quintic Kerr nonlinearities. Next, we present the different results from the nonlinear dissipative model. This thesis ends with a conclusion and a presentation of some perspectives of our study .

Chapter 1

Literature review

1.1 Introduction

In modern physics, two complex processes have changed the view of scientists is the world, and also the daily life of human beings. One of these processes is the propagation of light that initiated the theory of relativity, and the other is about the thermodynamics of the quantum mechanics. The collision of light with obstacles during its propagation results in several phenomena. This greatly incited the physicists interest to the question of the interaction between light and matter. Subsequent to this interest was the rise of several disciplines in physics and engineering, such as geometric optics, crystallography, coherent optics, photonics, telecommunication, and nonlinear optics. To explain and extend different phenomena occurring from the interactions inside light propagating media, and also the behavior of light beams, we present in this chapter the different concepts that were taken as basis to develop our thesis. In section II, we present the concept of solitons and relate them to the faculty of acquiring the light of the beam during its propagation. Section III presents the different outcome behaviors of light during its propagation in a medium. The generation of trains of solitons, acting as a bridge between the notion of soliton and the propagation of light in a medium is presented in section IV. A brief conclusion ends the chapter.

1.2 Solitons

We can never stop the light from the sun. This sentence summarizes the brief journey of the concept of the solitary wave in the scientific world. Solitary waves have a complex story. At first, they have been observed in ancient times under the name "tsunami", then, said to have been discovered by Scottish. They have also been discovered in laboratories by Faraday[20], and obtained as results from numerous numerical investigations. Their story is the origin of a great debate that opposes mathematicians and physicists. Mathematicians present it as the solution of nonlinear equations, but physicists present it as the solution of the nonlinear equation which

preserves its physical properties such as the momentum, during their propagation. Specific type of solitary waves are solitons, which have the particularity to conserve their integrity upon collision with their kind. For more details, the word soliton is composed of radical "solit" coming from solitary waves and the suffix "on" giving a connotation of a particle in physics such as electron, proton, neutron, etc. Despite those different few divergences, scientists retained the tale of engineer John Scott Russell on meeting with solitons. History was nice, but the world attends to the birth of a new physical entity which will develop the part of nonlinear science with elegant theories and interesting applications in a several branches of science such as chemistry, biology, economics, engineering, and physics. In some branches of physics, the concept of soliton clears up several phenomena such as the beat of a heart pulse, the behavior of muscle, the transport of impulse nervous in biophysics. At the same time, this concept is also developed in the transport of current in transmission lines, and the conception of electrical networks. Indeed, solitons critically boost telecommunication as they allow the transport of Gigabits of information propagating down the optical fiber. As the concept of soliton is developed in a large number of fields of physics, in this thesis our work will be focused particularly in the context of nonlinear optics.

1.2.1 Optical solitons

Optical solitons result from the balance between dispersion and nonlinearity in conservative systems, with an additional balance between the loss and gain for the case of nonconservative systems (as illustrated in figure 1)[21, 22]. In addition, the nature of the nonlinearity and the dispersion specify the type of soliton we can have. Also when the linear effect is the dispersion and when the nonlinearity is caused by self-modulation phase (SPM) induced by Kerr nonlinearity, particle-wave results to this competing phenomena which is called the temporal soliton.

Its existence in optical fiber, and its use for optical communication was suggested in 1973 by Hasegawa and Tappert [23], and in 1980 these solitons had been observed experimentally by Mollenauer et al. [24]. Since then, the rapid progress in the studies has appointed the temporal soliton to be a practical candidate for designing modern light wave systems. In optical fiber, temporal solitons were presented in two forms: bright solitons in the case of anomalous dispersion, and dark or gray solitons in the case of normal dispersion [25]. In addition to these two types of solitons, the optical fiber can exhibit other phenomenon and the presence of other quantities, such as the loss managed and dispersion-managed soliton, the effect of amplifier noise, and the higher-order dispersive and nonlinear effects on temporal soliton. In doped fiber, the temporal soliton has several forms such as pulsating soliton, creeping soliton, exploding soliton, peak soliton. These different forms of dissipative soliton are illustrated in figure 2 [26, 27, 28, 29, 30, 31, 32].

Figure 1: Balance between linear effect and nonlinear effect [22].

Conversely to temporal solitons, spatial solitons result from the balance between the diffraction and self- focalization induced by Kerr nonlinearity. When the transverse coordinates form a couple (x, y), a vortex is obtained. In this coordinate framework, the stability of vortex solitons is preserved during their propagation. The framework also yields solitons such azimutons, vortex solitons, and cluster solitons [33, 34]. Now, the mixing of dispersion and diffraction occurs independently of the nature of nonlinearities in the medium. This can allow the creation of spatial-temporal solitons or optical bullets. Some soliton configurations are illustrated in figure 3. Figure 4 presents another type of solitons well-known as rogue waves (RW). Optical RW was initially investigated in nonlinear optics by Solli et al. [35] in 2007, and later on in a photonic crystal fiber by Buccolino et al [36]. The works were the pioneering studies in the field of optical RW. RWs can also be found in the output of laser radiation [37, 38, 39, 40, 41], and in some types of optical cavities [42, 43, 44, 45]. They can be influenced by Brillouin scattering [46] or by the Raman effect [47] . Indeed, there is a multiplicity of RW forms [48, 49, 50, 51, 52], and this can make them difficult to be classified.

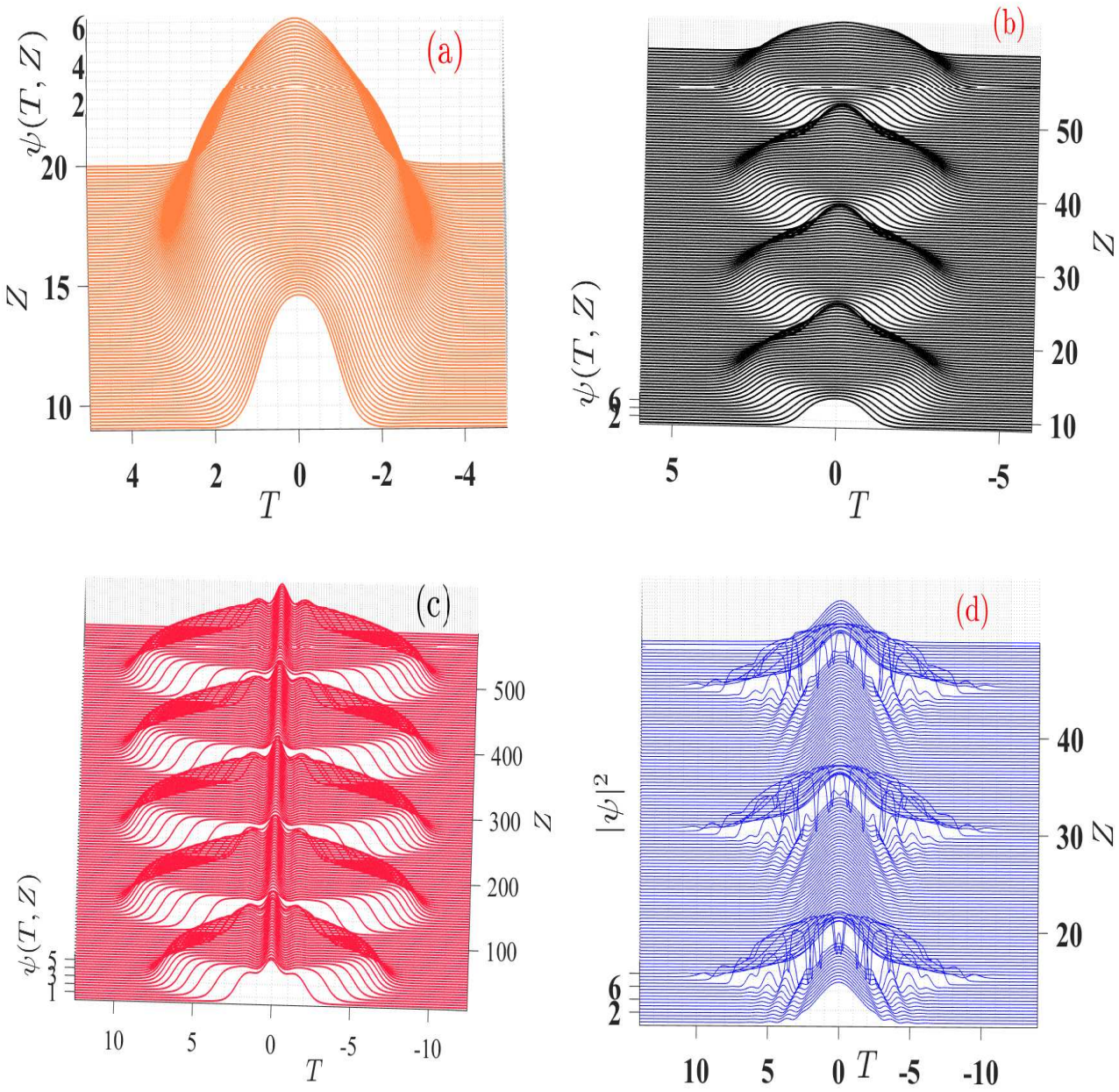

Figure 2: Dissipative solitons: (a) pain soliton, (b) pullsating soliton, (c) creeping soliton, (d) Volcanic soliton [29, 30]

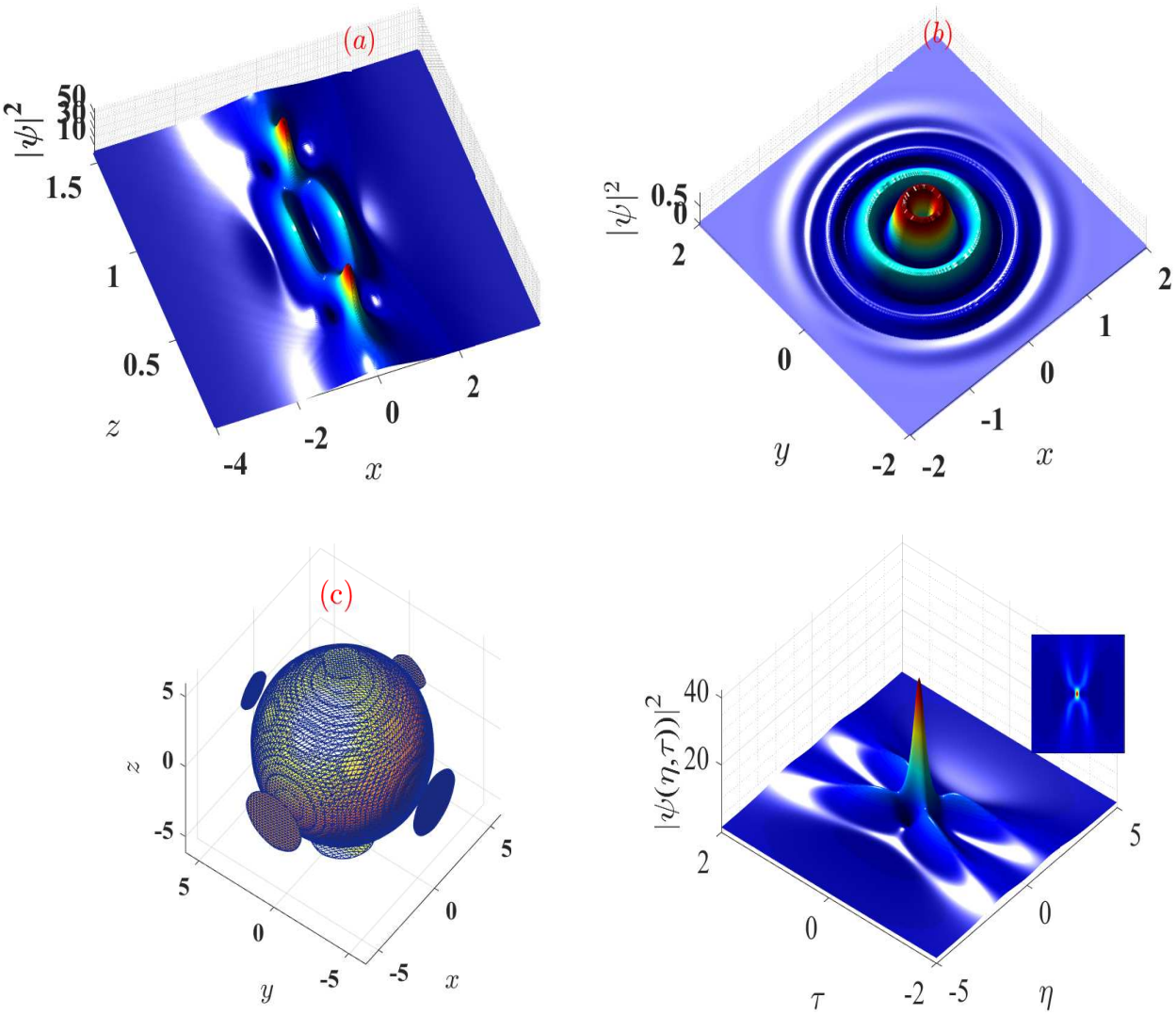

Figure 3: Spatial solitons: (a)(1+1)D soliton, (b) (2+1)D soliton (vortex soliton), (c) (3+1)D soliton (spatio-temporal soliton or light bullet), (d) rogue wave.

1.3 Nonlinearities and Materials

Nonlinear optics is the study of phenomena that occur due to the modification of the material properties in the presence of light of high intensity. The nonlinearity is associated with the fact that the material response varies in a nonlinear manner with the applied optical field. To study this effect, we consider the dependence of the dipole moment per unit volume or polarization $\tilde{P}(t)$ on the applied optical field strength $\tilde{E}(t)$. During the application of the optical field, there is the displacement of both electrons and the nuclei concerning the center of mass of the molecule. Considering the dipole approximation, an electric dipole is formed due to charge separation between the negatively charged electron cloud and the positively charged nucleus. At optical frequencies, due to much larger mass, the oscillations in the nucleus are much weaker than the electronic oscillations. Hence, the nuclear contributions are far weaker than the electronic contributions, at least for linear polarizability. The nonlinear susceptibility on the other hand (described in terms of Raman scattering), might be comparable or even larger depending on whether we are on or off-resonance [1]. But, for all practical purposes, we neglect the nuclear contributions for simplicity in our presentation. The bulk polarization of the entire material is thus a vector sum of the dipole moments of all the molecules [53, 54]. In a linear regime, the induced dipole also oscillates with the same frequency as the driving field and each molecule of the material can be viewed as a harmonic oscillator.

1.3.1 Nonlocality

Generally, the response of any physical system to an external field or force is nonlocal. This means that the applied force on one object of the system (or point of the media), spreads its influence to the other objects (points) too. Nonlocality is a consequence of the variety of forces and fields by which the particles or objects composing a physical system are interacting among themselves. In nonlinear optics nonlocality means that the refractive index in a particular point depends on the light intensity in certain neighborhood of this point. This nonlocality results from heat transport, reorientation of molecules [55, 56] and long-range interactions. Literature distinguishes four classes of nonlocal nonlinearities, and their can be described as the local nonlinearity, general nonlocal nonlinearity, strong nonlocality and weak nonlocality. Figure 4 illustrates these different situations [18].

The traditional wave motion in nonlinear optics is given by nonlinear Schrödinger equation.

$$i\partial_z\psi + \frac{1}{2}\partial_x^2\psi + \Delta n\left(I\right)\psi = 0. \tag{1.1}$$

When the nonlinear optical response of the medium is nonlocal, the refractive index change $\Delta n\left(I\right)$, induced by a beam with intensity

$$I\left(x,z\right) = \left|\psi\left(x,z\right)\right|^2, \tag{1.2}$$

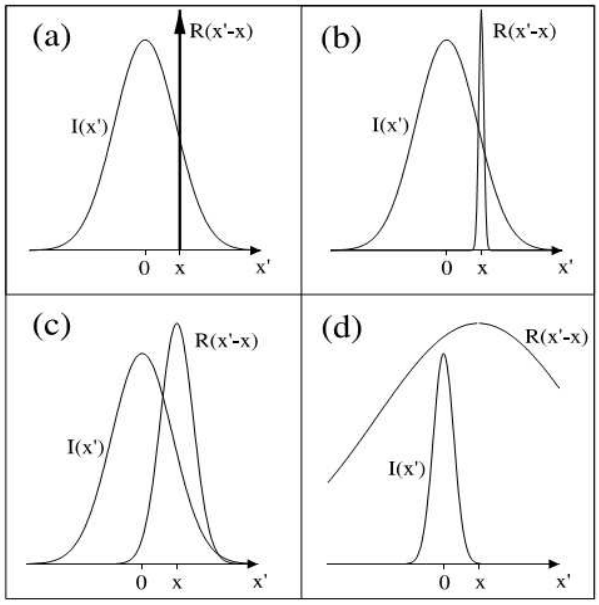

Figure 4: Different degrees of nonlocality, as given by the width of the response function R(x) and the intensity profile I(x).(a) is the local, (b) the weakly nonlocal, (c) a general nonlocal and (d) a strongly nonlocal response [18].

can be described by the following phenomenological nonlocal model:

$$\Delta n\left(I\right)=\Delta n\left(x,z\right)=\alpha\int R\left(x^{'}-x\right)I\left(x^{,},z\right)dx^{,}, \tag{1.3}$$

where the integral $\int dx$ is over all transverse dimensions and $\alpha=\pm1$, corresponds to a focusing or de-focusing medium, respectively. The real, localized, and symmetric function $R(x)$ is the response function of the nonlocal medium, that is normalized as follows: $\int Rdr=1$. As generally in the spatial NLSE, transient effects are neglected, the nonlocality is also assumed to be stationary. Further, the shape and the width of the response function are assumed to be the same along the propagation direction. Usually the degree of nonlocality is de

ned as the ratio between the beam width and the width of the nonlocal response function. In this sense, the phenomenological nonlocal nonlinearity model Eq (1.1) is more general and can be used to describe the local nonlinear and the highly nonlocal nonlinear case that corresponds to a linear waveguide problem [57]. This is evident, by simply considering the extreme limits of the width of the response function $R(r)$ relatively to the beam width. An illustration of the different degrees of nonlocalities is given in Fig.4. The local nonlinear case is accessible by letting the width of the normalized function $R\left(x\right)$ approaching zero, which transforms it to a delta response function $R\left(x\right)=\delta\left(x\right)$. In this case, the refractive index change becomes a local function of the light intensity,

$$\Delta n\left(I\right)=\alpha I\left(x,z\right), \tag{1.4}$$

i.e., the refractive index change at a given point is solely determined by the light intensity at that very point, and Eq.(1.1) simplifies to the ordinary NLSE. The case of a local nonlinearity has been the subject of many investigations and analytical treatment was shown to be possible [58, 59]. Thus, the properties of the ordinary NSE will not be considered here. There are two other important physical situations when the convolution term in equation Eq.(1.1) can be represented in a simplified form allowing for an extensive analytical treatment of the resulting equation. These are the weak nonlocality limit and the strong nonlocality limit. When the width of the response function is much less than the spatial extent of the beam, $I(x)$ can be formally expanded in a Taylor series and only the first significant terms be retained. This gives the nonlinearity in the following form:

$$\Delta n = \alpha \left(I + \gamma \partial_x^2 I \right), \gamma = \frac{1}{2} \int_{-\infty}^{\infty} x^2 R(x)\, dx, \tag{1.5}$$

where the positive definite γ is a measure of the strength of the nonlocality. Here the nonlocal contribution to the Kerr-type local nonlinearity is reflected by the presence of the Laplacian of the wave intensity in one dimension. It turns out that the nonlinearity in this particular form appears naturally in the theory of nonlinear effects in plasma [60]. It has been shown recently that Eq.(1.1) with nonlinearity Eq.(1.4) supports propagation of stable bright and dark solitons [61]. Another limiting case, the so-called highly nonlocal limit, refers to the situation when the nonlocal response function is much wider than the beam itself. It can be shown that in this limit the nonlinear term may be approximated by

$$\Delta n = \alpha R(x) P, \tag{1.6}$$

where $P = \int_{-\infty}^{\infty} I\left(x'\right) dx'$ is the total power of the beam, that is a conserved quantity. Interestingly enough, in this case, the propagation equation becomes linear. It describes the evolution of an optical beam trapped in an effective wave guide structure with the profile represented by the nonlocal response function. This highly nonlocal limit has been first explored by Snyder and Mitchell in the context of the so-called "accessible solitons" [57]. The same authors also illustrated the influence of nonlocality on the dynamics of beams for the special logarithmic nonlinearity, which allows exact analytical treatment [62]. Generaly in nonlinear optic we have three types of nonlocal responses function the smooth response despite in fig.5(a), peak response function in fig.5(b), and rectangular response. Even though it is quite apparent in some physical situations that the nonlinear response in general is nonlocal (as in the case of thermal lensing), the nonlocal contribution to the refractive index change was often neglected [63, 64]. This is justifed if the spatial scale of the beam is large compared to the characteristic response length of the medium (given by the width of the response function). However, for very narrow beams or beams with fine spatial features (such as dark solitons) the nonlocality can be of crucial importance. Intuitively, the basic properties of the nonlocal nonlinear medium will be

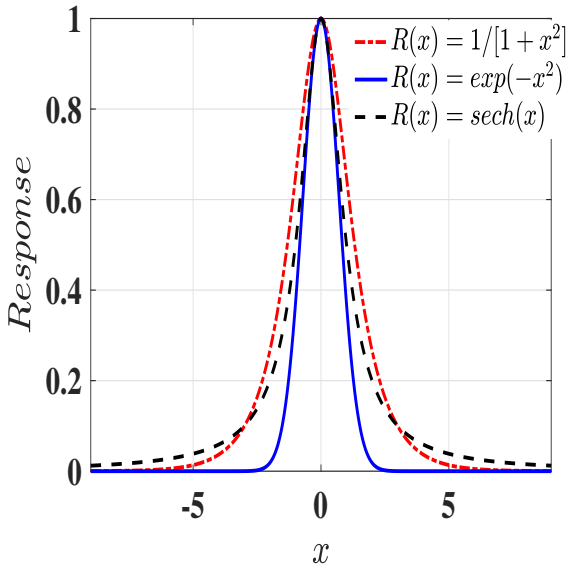

(a)

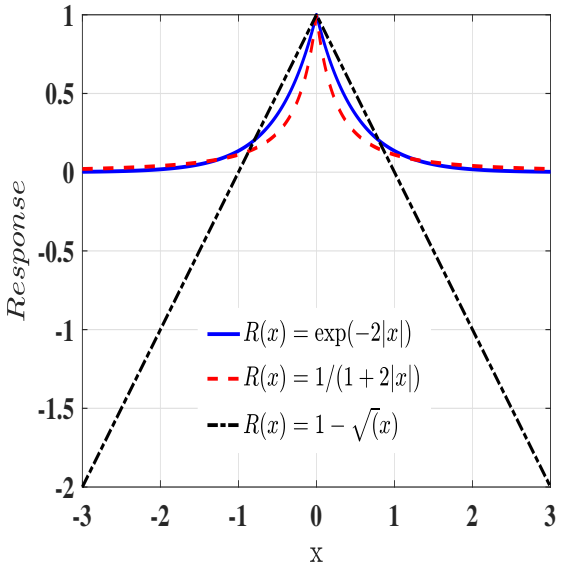

(b)

Figure 5: Spatial response functions: (a) Smooth response, (b) Peak response function

strongly dependent not only on the width of the response function, but also on the shape. The important case of exponential nonlocality will be thoroughly discussed later in the context of possibility to form bound statets of dark solitons in nonlocal media with cubic nonlinearity.

1.3.1.1 Bose-Einstein Condensate (BEC)

BECs inherently have a spatially nonlocal nonlinear response due to the finite range of the inter-particle interaction potential. The model describing the nonlinear interaction of ultra cold atoms in BEC is the Gross-Pitaevskii equation [65] :

$$i\hbar\frac{\partial\psi}{\partial t} = -\frac{\hbar^2}{2m}\frac{1}{2}\nabla^2\psi + V\left(r\right)\psi + \psi\int K\left(r-r'\right)\left|\psi\left(r'\right)\right|^2 dr. \tag{1.7}$$

This is exactly the nonlocal NLSE, but with the additional term for the external potential $V(r)$ [65]. Here, ψ is the wave function of N particles. Though the physics of the processes in BEC is different than the nonlocal nonlinearity in nonlinear optics and plasma physics, the same model used for their description, results in the same conclusions, i.e., collapse arrest [66], and soliton stabilization [67] in the presence of nonlocality. Naturally, any process in material or system caused by an external force or field needs a transition time to be developed. The delay of the response of the physical media can be considered as an analogue to the nonlocal distribution of the external induced changes of the materials properties. This means that the concept of nonlocal nonlinearity can be expanded to the time domain, i.e., into a noninstantaneous or delayed nonlinear response. Figure. 6 illustrates the Bose-Einstien condensate.

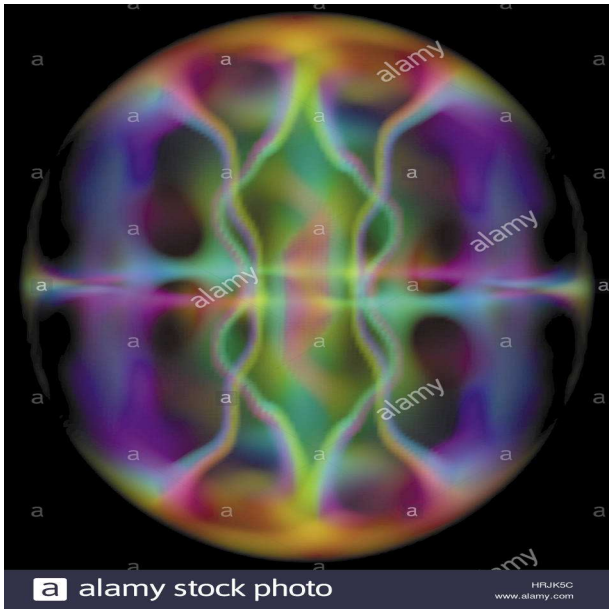

Figure 6: Bose-Einstein condensate [68]

1.3.1.2 Plasma

In nonlinear optics, a nonlocal distribution of the intensity induced refractive index is caused by additional physical mechanisms such as transport processes or inter-particle interaction. Transport processes can be either heat conduction [69] or diffusion of charges in photo-refractive materials [70, 71] or atoms in vapours [72]. The nonlocal response of an external field can be due to a variety of physical mechanisms. Here, only third-order intensity dependent nonlinear nonlocal effects are considered. Linear nonlocal effects as nonlocal dispersion [**?**, 73] and others are out the scope of this thesis. The propagation of light waves in a medium with a nonuniform distribution of the refractive index change is governed by the wave equation:

$$i\left[\frac{\partial}{\partial t}+V_g\frac{\partial}{\partial z}\right]\psi+\frac{\partial^2\psi}{\partial t^2}+\nabla_\perp^2\psi+\frac{2k^2}{n_0}\Delta n\left(x,y,z,t\right)\psi=-ik\alpha\psi. \tag{1.8}$$

Here, ψ is the envelope of the light wave, k the wave number, z the propagation coordinate, n_0 is the linear refractive index, Δn the change in the refractive index, and v_g is the group velocity. When considering the propagation of continuous-wave light beams, the second-order time derivative describing the dispersion is omitted. In a reference frame moving with the group velocity, Eq.(1.8) transforms to the general beam-propagation equation [74, 75]. When the change of the refractive index Δn is proportional to the light intensity $|\psi|^2$, Eq.(1.8) becomes the NLSE. There are many physical systems in which the induced refractive index change is nonlinear. Here, some examples of nonlinear systems in which the nonlocality of the nonlinear refractive index can not be neglected are given. These are the heat conduction and diffusion in absorptive liquids, ponderomotive force in plasmas, reorientation of molecules in liquid crystals, diffusion of electrons in photorefractive crystals, and inter-particle interaction in BECs. While propagating through an absorptive liquid media, a laser beam induces temperature and density gradients that change the refractive index profile. In this case, heat conduction and diffusion are the major processes that lead to the nonlocality of the light-induced refractive index. The refractive index change is, in general, a function of temperature and density changes inside the material [74].

$$\Delta n\left(x,y,z,t\right)=\left(\frac{\partial n}{\partial\rho}\right)_T\Delta\rho\left(x,y,z,t\right)+\left(\frac{\partial n}{\partial T}\right)_\rho\Delta T\left(x,y,z,t\right). \tag{1.9}$$

For times much longer than the acoustic transit time, the change of the density $\Delta\rho$ becomes directly proportional to the change of the temperature, $\Delta\rho=\frac{\partial\rho}{\partial T}$, where $\frac{\partial\rho}{\partial T}$ is a constant. For a laser heat source in liquids, the electrostriction can be neglected, and the temperature change $\Delta T=T-T_0$ is determined by:

$$c_p\rho\left(\frac{\partial T\left(x,y,z;t\right)}{\partial t}\right)-k\nabla^2T\left(x,y,z;t\right)=\alpha I(x,y,z;t). \tag{1.10}$$

In this way, the refractive index depends on the intensity of the light beam, thus the process is nonlinear. The nonlocality of the nonlinearity arises from the thermal diffusion, described by

the spatial derivatives in Eq.(1.10). The ponderomotive force in plasma illustrated in Fig(9),

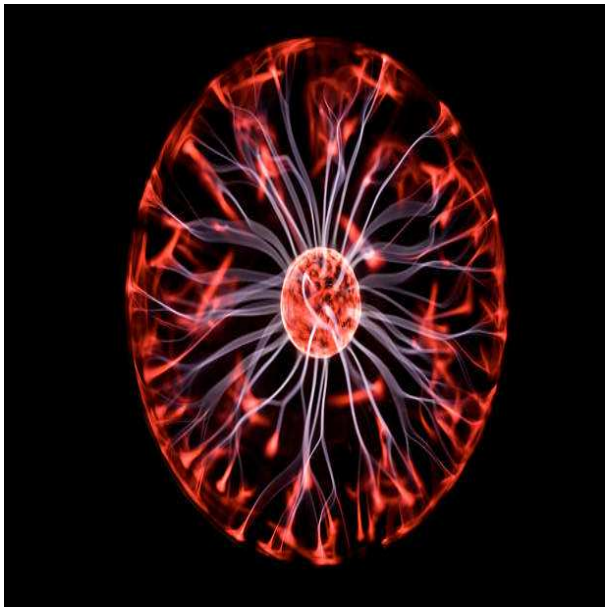

Figure 7: Plasma [68]

causes the drift of electrons and ions from regions with higher intensity to regions with lower intensity of the propagating electromagnetic wave. Thus, the induced spatial distribution of the plasma density leads to nonlinear response to the optical wave. Additional processes, such as heating or diffusion, lead to a nonlocal nonlinearity as well. For the case of nonlinear Landau damping in unmagnetized as well as magnetized plasmas[76, 77], the form of the nonlocal term is quite different, but still preserving the main features of the nonlocal nonlinearity.

1.3.1.3 Nematic crystal

The physical mechanism leading to nonlinear nonlocal response in liquid crystals is reorientation of molecules [78, 79]. Figure(8) shows example of nematicon. As the angle of rotation of the nematic molecules is finite, the nonlinearity is saturable. Due to the mutual molecular interaction, the induced nonlinear refractive index by the optical field is nonlocal. In this case the nonlocality of the nonlinear refractive index can not be expressed simply as a convolution integral of the optical intensity and the distributed response function. The model for the nonlocal nonlinearity in liquid crystals includes an additional differential equation for the molecular angle of rotation according to the constant external electric field. Thus, by the use of the variational approach and the slowly varying envelope approximation, the propagation of the optical beam in liquid crystals is described by a Schrödinger-type non linear equation Eq.(1.11), and the nonlocal nonlinearity is described by a separate differential equation describing the nonuniform director distribution as given in Eq.(1.12) [80]:

$$2ik\frac{\partial\psi}{\partial z} + \nabla_{\perp}^{2} + \frac{\omega_{e_a}^{2}}{C^{2}}\left[\sin^{2}\theta - \sin^{2}\theta_{0}\right]\psi = 0, \tag{1.11}$$

$$4k\nabla_{\perp}^{2} + e_a sin\left(2\theta\right)\left|\psi\right|^{2} = 0. \tag{1.12}$$

Here, ψ is the slowly varying envelope of the propagation beam, θ_0 is the initial tilt of the molecules, $e_a = n_{||}^2 - n_{\perp}^2$ is the optical anisotropy, and K elastic constant. As reported in Ref. [79], it is mainly the spatial nonlocality that contributes to the observation of stable spatial solitons in liquid crystals.

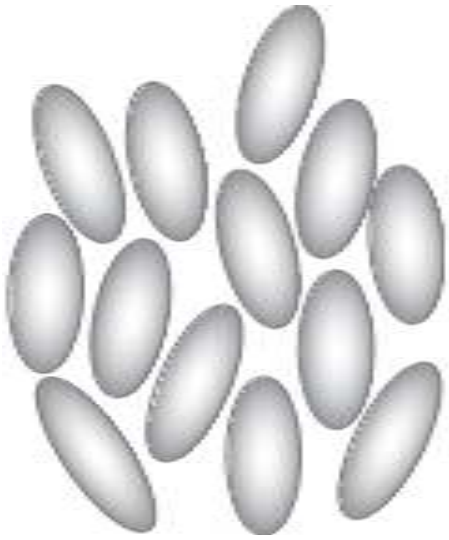

Figure 8: Nematicon [81]

1.3.1.4 Optical fiber

In nonlinear optics, the Raman effect is a noninstantaneous nonlinear response. The time delayed and the spatial nonlocal nonlinear effects are similar in the sense that they are modelled by similar equations. For example, if the orthogonal component of the Raman response is neglected, the equation describing the delayed nonlinear Raman response is non-instantaneous or "nonlocal in time":

$$\frac{\partial \psi}{\partial t} = -\mu\psi - \frac{i}{2}\frac{\beta_2}{2}\frac{\partial^2 \psi}{\partial \tau^2} + i\gamma\psi\left[(1-f_R)\left|\psi\right|^2 + f_R\int h_R\left(\tau - s\right)\left|\psi\left(s\right)\right|^2 ds\right]. \tag{1.13}$$

Here, ψ is the envelope of the complex linearly polarized optical field. The time $\tau = t - z/v_g$ is in a reference frame moving with the average group velocity, z is the propagation coordinate, μ is the loss, γ is the effective nonlinearity , and f_R is the fractional contribution of the Raman effect. To preserve the causality in time, the response function representing the delayed nonlinearity is $h_R = 0$ for $t = (-\infty, 0)$. Also, it should be noted that the Ramam response function h_R is not sign definite. Thus, the physical processes observed due to Raman delayed nonlinearity and the symmetric spatial nonlocal response are different.

Another example of delayed or non-instantaneous nonlinear optical response is the plasma formation by intense ultra-short light pulses in gases [82, 83]. This phenomenon occurs due to the self-focusing of intense light pulses in gases, which allows the beam intensity to be increased enough to generate plasma. The regions where plasma is generated have lower refractive index. Thus, further increase of the optical amplitude is prevented due to defocussing. The process of beam contraction and expansion that may repeat many times during pulse propagation in air is called "dynamic spatial replenishment in air" [84]. This process allows, self-guiding of short high-power light pulses in air. The next figure illustrates the example of optical fiber

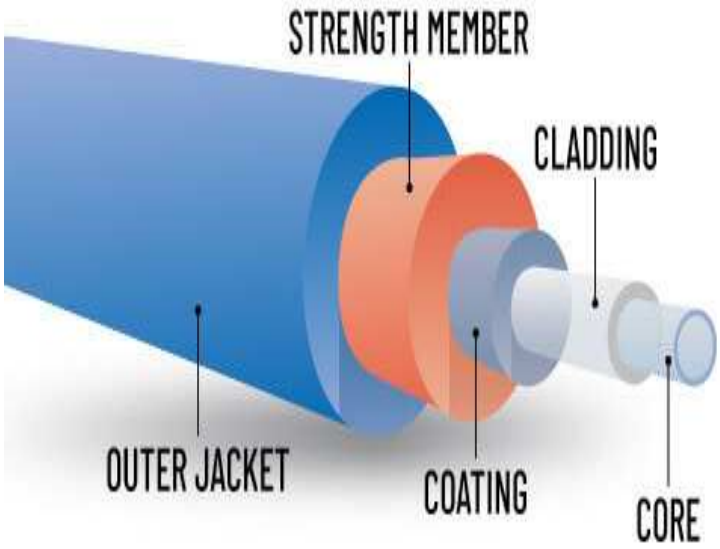

Figure 9: Optical fiber[68]

1.3.2 Rare Earth doped fibers

Rare Earth (RE) doped glass has been investigated and used as a laser media for more than four decades. Since the eighties, RE doped fibers have been available and fiber lasers and amplifiers have been an active field of research ever since. When RE elements are dissolved in a glass host, they become triply ionized by removal of the two outer 6s electrons and an inner 4f electrons [22]. The optical properties of the dopants are then determined by the partially filled 4f orbital and since the outer $5p$ and $5s$ electrons effectively shield the 4f electrons from the field of the host material, the laser characteristics such as wavelength and gain bandwidth are almost independent of the host. Today, optical fibers can be doped with a variety of REs with Erbium, Ytterbium (Yb), Neodynium and Thulium being the most used. The optical transitions in Yb take place between the $F_{5/2}$ and the $F_{7/2}$ levels. The field of the silica host causes Stark splitting as illustrated in figure 10 (left), and homogeneous broadening turns the discrete levels into energy bands [22]. It is noteworthy that these two bands are energetically isolated, so out-of-band transitions (excited state absorption) are not possible. The energy gap between the two "ground states" of the bands correspond to a wavelength of 976 nm. The system can therefore be pumped with commercially available telecommunication pump diodes. The most probable behavior for an electron excited to the ground state of $F_{5/2}$, is to return to the first Stark level of the lower band. This transition releases a photon with an energy corresponding to $\lambda = 1030nm$. In the same manner, excited atoms can relax into higher Stark levels in $F_{7/2}$ and wavelengths from 976 nm to almost 1200 nm can be realized. The transitions have different probabilities, as illustrated in figure 10 (right) which shows the cross-section of emission and

absorption as a function of wavelength. The upper state life time is approximately 900 μ_s, so spontaneous emission takes place on this time scale. Because of the tight confinement of light in optical fibers, the spontaneously emitted photons have a high probability to excite a guided mode and can therefore be amplified along the fiber. Amplified spontaneous emission (ASE) is a main limitation of the extractable energy from standard single mode Yb-doped fiber lasers.

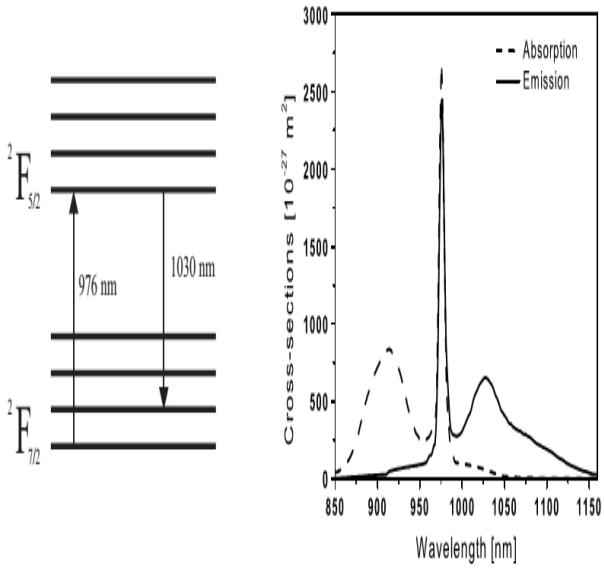

Figure 10: Transition phase of dopant [22]

1.4 Modulational instability of continuous waves

Modulational instability is referred to phenomenon when the continuous wave was disturbed initially and tends to brake itself spontaneously in soliton train waves, when propagating in nonlinear and dispersive media such as optical fiber [85, 86, 87]. Like solitons, MI arises in the presence of linear and nonlinear effects. Naturally, we distinguish temporal MI and spatial MI (self-filamentation) [88]. Temporal MI find its application directly in optical fiber and gives quite important results. Benjamin and Feir were the first to investigate the temporal process of MI in 1967[85]. They have demonstrated both theoretically and experimentally that uniform continuous wave trains can be unstable to the disturbance which modulating envelop [85]. Two years before Benjamin and Feir discovery, spatial case of MI was observed in nonlinear optic experiments by Pilipkiskie and Rustanov [89]. The next year in 1966, Bespalav and Talonov investigates the theoretical propagation of beams of continuous-wave in nonlinear focusing liquid, modeled by NLSE, and gave different characteristics of self- filamentation thanks to a perturbative approach [90, 91]. It has been found that a slight modulation comes to uniformly disturb the initial beam in focusing nonlinear media which then behaves like a convergent lens since the local refractive index grows up. Consequently, under certain conditions, the beams would tend to concentrate periodically in each one of the few regions and finally decompose in filaments as illustrated in Figure 10.

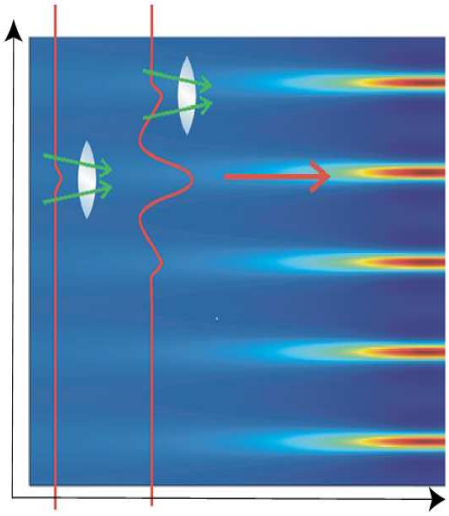

Figure 11: Transformation of beam wave in several peaks by modulation instability [81].

The spectral-domain interpretation of MI is very attractive as it presents the behavior characterizing the recurrence of Fermi-Pasta-Ulam (FPU). There, MI appears as a consequence of the nonlinear interaction of four mixing waves, when two photons (pumps) at the carrier frequency ω_0 interact with nonlinear Kerr medium, for will be converted to another two photons different

frequencies, first the stoke wave $(\omega_0 - \Omega)$ and another one $(\omega_0 + \Omega)$ the anti-stokes. Immediately, we note that the process respects the conservation of energy. We can also verify that it must have the conservation of momentum. For the waves, this conservation implies the realization of certain conditions of phase accord. It is fundamental for the investigation of MI because it gives unexpected conditions of instability and gain of unstable modulation. The stokes bands and anti-Stokes grow together to the detriment of the pump which is progressively depleting. This change of energy corresponds (temporally or spatially) to the growth of the modulation of the envelope of the wave to the training pulse. In the following, the transfer to those spectral band reaches the maximum, the energy flows in those band and their harmonics progressively to flow back to pump. So, that the continuous wave is completely reconstituted. Initially, this evolution of MI characterizes the recurrence of FPU. In nonlinear optics, MI was presented, spontaneously caused by noise. At the same time, theoretical investigation of MI in nonlinear optic was done by two different approaches. The perturbative approach that we describe in detail in the chapter of this manuscript and four mixing wave approaches. This MI phenomenon appears in diverse areas of physics such as fluid dynamics [92, 93], plasmas [94], discrete systems such as transmission lines [95], DNA chain [96, 97, 98], in neural networks[99, 100, 101, 102] and plasma systems [103, 104, 105], just to cite a few. It can also be observed in Bose- Einstein condensates (BECs) and vapor atomic in which it is responsible for the creation of bright solitons [106, 107, 108, 109, 110] and self-organization [111, 112], respectively. Recently, it has been proved that MI is the precursor of new structures, such as rogue waves in optical fibers, the generation of supercontinuum [113, 114, 115, 116]. In addition, appart from MI,a broad class of analytical solution of the 1D NLSE referred to as solitons on finite background or breathers have been identified. Among those are the Akhmediev breather (AB, periodic in time, localised in space) the Kuznetsov-Ma soliton (KM, localised in time, periodic in space) and the Peregrine soliton (PS, localised both in time and space). Many works on MI have been done using the local nonlinearities. In nonlinear optics it was found in meta materials [117], nonlocal systems [18, 118, 119], fiber Bragg gratings [120, 121, 122, 123], twin-core fiber [124], asymmetry dual-core fiber [125], micro-cavities [126], doped resonant fiber [127]. Agrawal studied the modulational instability in doped optical fiber with rare-earth[128].

1.5 Conclusion

The aims of this chapter were to present the different concepts that we will use in this thesis. Following a brief introduction, in Section II, we have presented the concept of solitons and the different cases of it appearance in the nonlinear optics. In section III, we have presented the nonlinearities and materials that will be accounted for in this thesis. The modulation instability was presented in section IV. In the next chapter, we will derive some nonlinear propagation wave equations and present different techniques for the investigation of MI.

Chapter 2

Methodology: Models and Numerical Methods

2.1 Introduction

Solitary waves arise in many physical substrates, such as water in fluid mechanics, condensate matter, DNA, atmosphere, plasma, electric transmission lines, and optical fiber, just to cite a few [19]. History teaches us that the first observation of solitary waves occurred in nature, and since then, several experimental attempts were done to reconstitute the phenomena. Although some laboratory investigations in different branches of physics tended to meet the latter goal, the high cost and time required for these investigations led scientists to aim for simple and easily manipulated models that could be helpful for qualitative investigations on the theory of soliton. The models presented in literature allowed the observation of rich behaviors. This subsequently yielded in the past two centuries to the definition and modification of propagation models, together with the surveys on the corresponding analytical methods helping for a throughout treatment. For example, we distinguish methods such as the inverse scattering method [129, 130], the bilinear Hirota method [131, 132] F-expansion method [133, 134], Jacobian-elliptic function method [135, 136]. These methods are mostly found to be based on exact or approximated analytical approaches. Moreover, some semi-analytical methods are also present in literature, the latter methods generally reduce the problem to a problem of solving a set of ordinary differential equations. To cite some of such methods, we have the moment method, the collective coordinates method, and the variational approach [137] . It is important to note that propagation models are not all analytically solvable, it is sometimes necessary to address the issue with numerical approaches. Indeed, numerical methods have played a crucial role in the development of the theory of soliton. Methods such as the finite difference methods, the pseudo-spectral method, and the Cranck-Nickolson method are some of the numerical methods frequently employed in this theory. All the above-cited methods have been of great contribution to explain the generation and the propagation of solitons in physical systems.

Theoretically, the study of the generation of solitons needs a strong mathematical asset. Linear stability has been proven to be a good approach, as it provides a framework to investigate the modulation instability process of the generated waves to obtain not only their stability conditions, but also the dispersion relation governing the dynamics of the system. Pursuing the treatment then enables the observation of the birth of train waves, the formation of plane waves with localized energy landscapes, and several other numerical characteristics.

In this chapter, we present the different steps for the derivation of a nonlocal Schrödinger equation modeling conservative systems, specifically weakly nonlocal nonlinear systems displaying competing Kerr and non-Kerr nonlinearities. For dissipative systems, we first derive the model with in dopant described by the complex Ginzburg-Landau equation with higher-order dispersion, high order nonlinearities, higher-order self-stepping, self-shifting effects. Next, we explain how a nonlinear nonlocal Schrödinger equation can be transformed into a management nonlinear nonlocal Schrödinger equation via the Lenz transformation [138]. Later on, we apply a linear stability analysis to obtain the stability conditions and the dispersion relation from the new management nonlocal Schrödinger equation. Then, we expose in detailed the pseudo-spectral method, also known as the split-step Fourier method and statiscal method sensitivity analysis. A concise conclusion finally ends the chapter.

2.2 Derivation of the Models

2.2.1 Nonlocal Model

2.2.1.1 Temporal nonlocality

The mathematical description of the dynamics of electromagnetic fields in optical fibers (medium without free charges and non-magnetic properties) can be done using the classical NLSE:

$$i\psi_z + \frac{\beta}{2}\psi_{xx} + \alpha\left|\psi\right|^2\psi = 0, \tag{2.1}$$

where β and α are the dispersion and nonlinear coefficients, respectively. In order to understand why the nonlocality is introduced in the dynamics of the electromagnetic field, we first need to present the different steps of the derivation. Consequently, we begin with the Maxwell equations proper to the optical fiber. These equations are defined as :

$$\overrightarrow{rot}\left(\overrightarrow{E}\right) = -\frac{\partial\overrightarrow{B}}{\partial t}; \tag{2.2}$$

$$\overrightarrow{rot}\left(\overrightarrow{H}\right) = \frac{\partial\overrightarrow{D}}{\partial t}; \tag{2.3}$$

$$div\left(\overrightarrow{D}\right) = 0; \tag{2.4}$$

$$div\left(\overrightarrow{B}\right)=0. \tag{2.5}$$

The relations between the field vectors $\overrightarrow{D}$, $\overrightarrow{E}$, $\overrightarrow{B}$ and $\overrightarrow{H}$ are given as : $\overrightarrow{D}=\varepsilon\overrightarrow{E}+\overrightarrow{P}$, $\overrightarrow{B}=\mu\overrightarrow{H}$, where ε is the dielectric permittivity, μ the magnetic permeability of the medium, and $\overrightarrow{P}$ the induced electric polarization. Applying the rotational operator on both sides of equation (2.2), and accounting for the relation between the field vector in the other Maxwell equations yields to the wave equation :

$$\Delta\overrightarrow{E}-\frac{1}{c^2}\frac{\partial^2\overrightarrow{E}}{\partial t^2}-\frac{\partial^2\overrightarrow{P}}{\partial t^2}=0. \tag{2.6}$$

The induced polarization consists of two parts such that:

$$\overrightarrow{P}\left(\overrightarrow{r},t\right)=\overrightarrow{P}_L\left(\overrightarrow{r},t\right)+\overrightarrow{P}_{NL}\left(\overrightarrow{r},t\right), \tag{2.7}$$

where $\overrightarrow{P}_L$ is the linear part, and $\overrightarrow{P}_{NL}=\overrightarrow{P}_{NL}^{(3)}+\overrightarrow{P}_{NL}^{(5)}+\overrightarrow{P}_{NL}^{(7)}$..... the nonlinear part. These two components are related to the electric field by the general relation [139]

$$\overrightarrow{P}_L\left(\overrightarrow{r},t\right)=\varepsilon_0\int_{-\infty}^{t}\chi^{(1)}\left(t-t^{'}\right)\overrightarrow{E}\left(\overrightarrow{r},t^{'}\right)dt^{'}, \tag{2.8}$$

for the third order of nonlinear polarization,

$$\overrightarrow{P}_{NL}\left(\overrightarrow{r},t\right)=\varepsilon_0\iiint_{-\infty}^{t}\chi^{(3)}\left(\delta t_1,\delta t_2,\delta t_3\right)\overrightarrow{E}.\left(\overrightarrow{r},t_1\right)\overrightarrow{E}.\left(\overrightarrow{r},t_2\right).\overrightarrow{E}\left(\overrightarrow{r},t_3\right)dt_1.dt_2.dt_3, \tag{2.9}$$

where $\delta t_1=t-t_1$, $\delta t_2=t-t_2$ and $\delta t_3=t-t_3$. Here, we consider the approximation of slowly varying envelope with the aim to separate the rapidly varying part of the electric field writing as :

$$\overrightarrow{E}\left(\overrightarrow{r},t\right)=\frac{1}{2}\left[E\left(\overrightarrow{r},t\right)*\exp(-i.\omega_0 t)+C.C.\right]\overrightarrow{a}, \tag{2.10}$$

where $\overrightarrow{E}\left(\overrightarrow{r},t\right)$ is function that slowly varies with time, compared with the optical period $\overrightarrow{a}$ and the polarization direction and C. C. denotes the complex conjugate. One obtains the same type of expressions for $\overrightarrow{P}_L\left(\overrightarrow{r},t\right)$ and $\overrightarrow{P}_{NL}\left(\overrightarrow{r},t\right)$

$$\overrightarrow{P}_L\left(\overrightarrow{r},t\right)=\frac{1}{2}\left[P_L\left(\overrightarrow{r},t\right)*\exp(-i.\omega_0 t)+C.C.\right]\overrightarrow{a}, \tag{2.11}$$

$$\overrightarrow{P}_{NL}\left(\overrightarrow{r},t\right)=\frac{1}{2}\left[P_{NL}\left(\overrightarrow{r},t\right)*\exp(-i.\omega_0 t)+C.C.\right]\overrightarrow{a}. \tag{2.12}$$

In the nonlocal case, the nonlinear response is non instantaneous, the time-dependence of the third-order susceptibility is given by [1, 25]

$$\chi^{(3)}\left(t-t_1,t-t_2,t-t_3\right)=\chi^{(3)}R\left(t-t_1\right)\delta\left(t-t_2\right)\delta\left(t-t_3\right), \tag{2.13}$$

where $R(t)$ is the normalized nonlocal nonlinear response function. By inserting (2.13) into (2.9), the nonlocal nonlinear polarization is written as

$$\overrightarrow{P}_{NL}\left(\overrightarrow{r},t\right)=\varepsilon_0\chi^{(3)}\overrightarrow{E}\left(\overrightarrow{r},t\right)\int_{-\infty}^{t}R\left(t-t_1\right)\left|\overrightarrow{E}\left(\overrightarrow{r},t\right)\right|^2dt_1. \tag{2.14}$$

Substituting (2.13) into (2.14), the nonlinear part of the polarization is reduced to:

$$P_{NL}\left(\overrightarrow{r},t\right)=\varepsilon_0\varepsilon_{NL}E\left(\overrightarrow{r},t\right), \tag{2.15}$$

where the nonlinear contribution to the dielectric constant is defined by

$$\varepsilon_{NL}=\frac{3}{4}\chi^{(3)}\int_{-\infty}^{t}R\left(t-t_1\right)\left|\overrightarrow{E}\left(\overrightarrow{r},t_1\right)\right|^2dt_1. \tag{2.16}$$

At this step, the derivation of the equation governing the spectral (Fourier) domain of the electric field $\overrightarrow{E}$ becomes more approachable.
The Fourier transform of the slowly varying amplitude $\overrightarrow{E}\left(\overrightarrow{r},t\right)$ and the response function $R\left(t\right)$ are given by:

$$\tilde{E}\left(\overrightarrow{r},\omega-\omega_0\right)=\int_{-\infty}^{\infty}\overrightarrow{E}\left(\overrightarrow{r},t\right)\exp(i\left(\omega-\omega_0\right)t)dt, \tag{2.17}$$

where ω_0 is initial frequency, and

$$\tilde{R}\left(\omega-\omega_1\right)=\int_{-\infty}^{\infty}R\left(t-t_1\right)\exp(i\left(\omega-\omega_1\right)t_1)dt_1. \tag{2.18}$$

Substituting (2.10) and (2.12) into (2.6) leads to:

$$\Delta\tilde{E}+n^2\left(\omega\right)k_0^2\tilde{E}=\frac{\chi^3\omega^2}{c}\iint_{-\infty}^{\infty}\tilde{R}\left(\Omega_1\right)\tilde{E}\left(\omega_1,\tau\right)\tilde{E}\left(\omega_2,\tau\right)\tilde{E}\left(\Omega_2\right)d\omega_1d\omega_2, \tag{2.19}$$

where $\Omega_1=\omega-\omega_1$ and $\Omega_2=\omega_1+\omega_2-\omega$. It is well known that, the nonlinear part of the induced polarization is treated as a small perturbation of the linear part. Therefore, the term in the right hand side of (2.19) can be neglected. By using a method of separation of variables, we assume a solution of the form

$$\tilde{E}\left(\overrightarrow{r},\omega-\omega_0\right)=F\left(x,y\right)\tilde{A}\left(z,\omega-\omega_0\right)exp\left(i\beta_0z\right), \tag{2.20}$$

where $F\left(x,y\right)$ and $\tilde{A}\left(z,\omega-\omega_0\right)$ denote respectively a slowly varying function of z, and the mode distribution function in the plane $(x;y)$. The substitution of (2.20) into (2.19) yields

$$\frac{\partial^2F}{\partial x^2}+\frac{\partial^2F}{\partial y^2}+\left[\varepsilon\left(\omega\right)k_0^2-\tilde{\beta}^2\right]F=0, \tag{2.21}$$

and

$$2i\beta_0\frac{\partial\tilde{A}}{\partial z}+\left(\tilde{\beta}^2-\beta_0^2\right)\tilde{A}=0. \tag{2.22}$$

The dielectric constant $\varepsilon\left(\omega\right)$ in (2.21) can be approximated by

$$\varepsilon\left(\omega\right)=\left(n+\Delta n\right)^2\approx n^2+2n\Delta n \tag{2.23}$$

with

$$\Delta n=\int_{-\infty}^{t}R\left(t-t^{'}\right)\left|\overrightarrow{E}\left(\overrightarrow{r},t^{'}\right)\right|^2dt^{'}.$$

Taking into consideration the effect of Δn in (2.23), the eigenvalue $\tilde{\beta}$ becomes

$$\tilde{\beta}(\omega) = \beta(\omega) + \Delta\beta(\omega), \tag{2.24}$$

with

$$\Delta\beta(\omega) = \frac{\omega^2 n(\omega) \iint_{-\infty}^{\infty} \Delta n(\omega) |F(x,y)|^2 dxdy}{c^2 \beta(\omega) \iint_{-\infty}^{\infty} |F(x,y)|^2 dxdy}. \tag{2.25}$$

The Fourier transform $\tilde{A}(\tau, \omega - \omega_0)$ of $A(z,t)$ satisfying (2.21) can then be written as

$$\frac{\partial \tilde{A}}{\partial z} = [\beta(\omega) + \Delta\beta(\omega) - \beta_0]\tilde{A}. \tag{2.26}$$

The propagation equation for $A(z,t)$ can now be obtained by taking the inverse Fourier transform of (2.26). However, it is useful to expand $\beta(\omega)$ in a Taylor series around the carrier frequency ω_0 i.e.,

$$\beta(\omega) = \Delta\beta_0 + (\omega - \omega_0)\Delta\beta_1 + \frac{(\omega-\omega_0)^2}{2}\Delta\beta_2 + \frac{(\omega-\omega_0)^3}{6}\Delta\beta_3 + \frac{(\omega-\omega_0)^4}{24}\Delta\beta_4..... \tag{2.27}$$

where

$$\Delta\beta_m = \left(\frac{d^m\beta}{d\omega^m}\right)_{\omega=\omega_0}.$$

. In most cases of practical interest, it is sufficient to retain only the first two terms in this expansion. By substituting (2.25) and (2.27) into (2.26), and applying the inverse Fourier transform, we obtain

$$A(z,t) = \frac{1}{2\pi}\int_{-\infty}^{\infty} \tilde{A}(z, \omega - \omega_0) exp(-i(\omega - \omega_0)t) d\omega, \tag{2.28}$$

and the resulting equation for $A(z,t)$ yields

$$\frac{\partial A}{\partial z} + \sum_{n=1} \beta_n \frac{i^{n-1}}{n!}\frac{\partial^n \psi}{\partial t^n} = i\Delta\beta A. \tag{2.29}$$

When applying the Fourier-transform, $\omega - \omega_0$ is replaced by the differential operator $i\frac{\partial}{\partial t}$. The term with $\Delta\beta$ includes the effect of the nonlinearity of the fiber. By using (2.26) and (2.29), we then obtain, after some cumbersome algebra, the equation for pulse evolution inside a single-mode fiber:

$$\frac{\partial A}{\partial z} + \beta_1\frac{\partial A}{\partial t} - i\frac{\beta_2}{2}\frac{\partial^2 A}{\partial t^2} = i\gamma(\omega_0)\left(A(z,t)\int_{-\infty}^{t} R\left(t - t'\right)\left|A\left(z,t'\right)\right|^2 dt'\right). \tag{2.30}$$

Here, the nonlinear parameter is expressed as: $\gamma(\omega_0) = \frac{n_2(\omega_0)\omega_0}{cA_{eff}}$, and the nonlinear response function $R(t)$ should include both the electronic and nuclear contributions. Assuming that the electronic contribution is nearly instantaneous, the functional form of $R(t)$ can be written as:

$$R(t) = (1 - f_R)\delta(t - t_e) + f_R h_R(t), \tag{2.31}$$

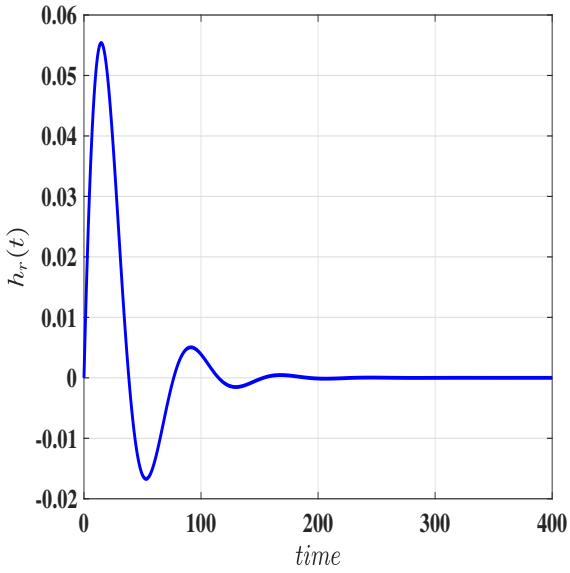

Figure 12: Time response function $t_1 = 12.2fs$, $t_2 = 30fs$,

where t_e account for a negligibly short delay in electron response ($t_e < 1fs$), and f_R represents the fractional contribution of the delayed Raman response to nonlinear polarization P_{NL} [140]. Attempts have been made to determine an approximate analytic form of the Raman response function. A useful form has been written as [141]:

$$h_R(t) = \frac{t_1^2 + t_2^2}{t_1 t_2^2} \exp\left(-\frac{t}{t_2}\right) \sin\left(\frac{t}{t_2}\right) \tag{2.32}$$

Applying the change of variables, $T = t - \beta_1 z$ in (2.30), it takes a new form given by:

$$i\frac{\partial A}{\partial z} + \frac{\beta_2}{2}\frac{\partial^2 A}{\partial T^2} + \gamma\left(A(z,T)\int_0^\infty R\left(T - T'\right)\left|A\left(z,T'\right)\right|^2 dT'\right) = 0 \tag{2.33}$$

2.2.1.2 Spatial nonlocality model

Here, we consider a phenomenological model, in which the nonlocal nonlinearity, induced by a wave e.g., an optical beam with the intensity I in nonlinear optic appears naturally as a result of many-body interaction processes in the description of Bose-Einstein condensates [18, 142]. It can be represented in a general form given by the Gross-Pitaevskii Equation (GPE)

$$i\hbar\frac{\partial\psi}{\partial t} = -\frac{\hbar^2\nabla^2\psi}{2m} + V(r)\psi + \psi\left(\int_{-\infty}^{\infty} R(r - r')\left|\psi(r')\right|^2 dr'\right). \tag{2.34}$$

Here $\psi(r,t)$ is the wave function of N particles, and $V(r)$ is the external potential. The one dimensional form of (2.34) is given by

$$i\frac{\partial\psi}{\partial t} + \frac{\partial^2\psi}{\partial x^2} + V(r)\psi + \alpha\psi\left(\int_{-\infty}^{\infty} R\left(x - x'\right)\left|\psi\left(x'\right)\right|^2 dx'\right) = 0. \tag{2.35}$$

Physically, we consider the situation where the response functions are narrow compared to the intensity of beam light (the weakly nonlocal case). We make Taylor series expansion of two components of nonlinearity [18]. This is such as:

$$I(\xi) \approx |\psi(\xi,z)|^2 + \frac{1}{2!}(\xi - x)^2 \frac{\partial^2 |\psi(\xi,z)|^2}{\partial x^2} + \frac{1}{4!}(\xi - x)^4 \frac{\partial^4 |\psi(\xi,z)|^2}{\partial x^4} ..... \tag{2.36}$$

$$\int_{-\infty}^{+\infty} R_1(x-\xi) I(\xi) d\xi \approx |\psi(\xi,z)|^2 + \frac{\gamma_1}{2!}\frac{\partial^2 |\psi(\xi,z)|^2}{\partial x^2} + \frac{\mu_1}{4!}\frac{\partial^4 |\psi(\xi,z)|^2}{\partial x^4}, \tag{2.37}$$

where

$$\gamma = \frac{1}{2!}\int_{-\infty}^{+\infty} R(x) x^2 dx,$$

and

$$\mu = \frac{1}{4!}\int_{-\infty}^{+\infty} R(x) x^4 dx.$$

2.2.1.3 Weak nonlocal nonlinear media with competing Kerr and non-Kerr nonlinearities

In this context, the study of the dynamics of the normalized wave function $\psi(x,z)$ is done, in the presence of a harmonic potential. This wave function can represent the macroscopic in BEC [106, 107, 108, 109, 110], or the paraxial wave in nonlinear optics [1, 143]. Where z and x are longitudinal and transverse coordinates, respectively. The nonlinear dynamics of this wave function is governed by the NLSE:

$$i\frac{\partial \psi}{\partial z} = -\psi_{xx} + V(x)\psi + \Delta n(I)\psi. \tag{2.38}$$

In the right-hand side of (2.38), the first term is the diffraction of optical beam. The second term materializes the external effect describes by the harmonic potential $V(x)$, and the last term includes the effect of the nonlinear refractive index $\Delta n(I)$.
Here we consider the harmonic potential as $V(x) = \mu x^2$, with μ being a positive number. The synthetic medium which exhibits the competing nonlocal nonlinearities is expressed as

$$\Delta n(I) = \Delta n_1(I,x) + \Delta n_2(I,x), \tag{2.39}$$

$$\Delta n(x,z) = S_1 \int_{-\infty}^{+\infty} R_1(x-\xi) |\psi(\xi,z)|^2 d\xi + S_2 \int_{-\infty}^{+\infty} R_2(x-\xi) |\psi(\xi,z)|^4 d\xi. \tag{2.40}$$

Here, S_1 and S_2 represent respectively, the strength of nonlocal Kerr and nonlocal non-Kerr nonlinearity contribution. The nonlocal character is due to the presence of the response functions R_1 and R_2. We turn our attention to the competing case ($S_1 S_2 < 0$), and higher-order

contribution case ($S_1 S_2 > 0$). Applying Taylor series expansion, i.e.,

$$\int_{-\infty}^{+\infty} R_2(x-\xi) I^2(\xi) d\xi \approx |\psi(x,z)|^4 + \frac{\gamma_2}{2!}\frac{\partial^2 |\psi(x,z)|^4}{\partial x^2} + \frac{\mu_2}{4!}\frac{\partial^4 |\psi(x,z)|^4}{\partial x^4}, \tag{2.41}$$

we restrict ourselves, without loss of generalities, to the fourth order term of the Series. Inserting (2.37) and (2.41) into (2.39), we obtain the nonlinear refractive index

$$\Delta n(x,z) = S_1\left(|\psi(x,z)|^2 + \gamma_1\frac{\partial^2 |\psi(x,z)|^2}{\partial x^2}\right) + S_2\left(|\psi(x,z)|^4 + \gamma_2\frac{\partial^2 |\psi(x,z)|^4}{\partial x^2}\right). \tag{2.42}$$

With the help of (2.42), we finally get the governing propagation equation as

$$\begin{aligned} i\frac{\partial\psi}{\partial z} =& -\psi_{xx} + V(x)\psi + S_1\left(|\psi(x,z)|^2 + \gamma_1\frac{\partial^2 |\psi(x,z)|^2}{\partial x^2}\right)\psi \\ &+ S_2\left(|\psi(x,z)|^4 + \gamma_2\frac{\partial^2 |\psi(x,z)|^4}{\partial x^2}\right)\psi \end{aligned} \tag{2.43}$$

The last two terms of (2.43) account for the contribution of competing nonlocalities. At a first sight, these terms are of the same nature as the higher-order perturbation terms introduced in the model considered by Wamba et al. in BEC [109]. Neglecting the effect of the harmonic potential and taking $S_2 = 0$, the equation is reduced to the model treated by Krolikowski et al. [18] for nonlocal media. A similar model has also been investigated in the context of BEC by Xiui et al. [110].

2.2.1.4 Cubic-quintic-septic complex Ginzburg-Landau equation with higher-order dispersion and correction terms

It is necessary to note that in the dopant, the population inversion is produced only in the electrons of the atoms. This phenomenon is essential for stimulated emission of photons in the operation of all lasers or amplifiers. The atomic response which can be included through the susceptibility of two level system is given by :

$$\chi_a = \frac{g_p\left((\omega-\omega_a)T_2 - i\right)}{\left(1+(\omega-\omega_a)^2 {T_2}^2\right)k_0}, \tag{2.44}$$

where g_p is the peak gain, [144, 145], ω_a is the atomic resonance frequency and ω is optical frequency. The susceptibility of two level system is of great importance in solving problems of pulse propagation in doped fibers. The complex dielectric constant is defined as

$$\varepsilon(\omega) = n_f^2 + 2in_f(c/\omega)\alpha + \chi_a(\omega), \tag{2.45}$$

where α account for the fiber loss, and n_f is the refractive index of the fiber. Considering the refractive index in the strong focusing case, this refractive index is expressed by

$$n_f = n(\omega) + n_2 I + n_4 I^2 + n_6 I^3. \tag{2.46}$$

The last term of (2.46) arises from seventh-order of susceptibility χ_e^7 [144], and was shown to be determinant in the investigating optical Bullets [34, 146, 147, 148]. This term can be defined as the second order correction of the Kerr nonlinearity. To derive the Maxwell equation [25], the following process must be followed : At first, the Taylor expression of the susceptibility up to sixth order is performed, and we obtain :

$$\begin{aligned}
\chi_a = & -\frac{g_p\,(-\delta+i)}{(1+\delta^2)\,k_0} \\
& + \frac{g_p\,(1-\delta^2+2\,i\delta)\,(\omega-\omega_0)\,T_2}{(1+\delta^2)^2\,k_0} \\
& - \frac{g_p\,(3\,\delta-\delta^3-i+3\,i\delta^2)\,(\omega-\omega_0)^2\,{T_2}^2}{(1+\delta^2)^3\,k_0} \\
& - \frac{g_p\,(1+\delta^4-6\,\delta^2)\,(\omega-\omega_0)^3\,{T_2}^3}{(1+\delta^2)^4\,k_0} \\
& + \frac{g_p i\,(-4\,\delta+4\,\delta^3)\,(\omega-\omega_0)^3\,{T_2}^3}{(1+\delta^2)^4\,k_0} \\
& - \frac{g_p\,(-5\,\delta+10\,\delta^3-\delta^5)\,(\omega-\omega_0)^4\,{T_2}^4}{(1+\delta^2)^5\,k_0} \\
& - i\frac{g_p\,(1-10\,\delta^2+5\,\delta^4)\,(\omega-\omega_0)^4\,{T_2}^4}{(1+\delta^2)^5\,k_0} \\
& + \frac{g_p\,(1-15\,\delta^2+15\,\delta^4-\delta^6)\,(\omega-\omega_0)^5\,{T_2}^5}{(1+\delta^2)^6\,k_0} \\
& + i\frac{g_p\,(6\,\delta+6\,\delta^5-20\,\delta^3)\,(\omega-\omega_0)^5\,{T_2}^5}{(1+\delta^2)^6\,k_0} \\
& - \frac{g_p\,(7\,\delta-35\,\delta^3+21\,\delta^5-\delta^7)\,(\omega-\omega_0)^6\,{T_2}^6}{(1+\delta^2)^7\,k_0} \\
& - i\frac{g_p\,(-1+21\,\delta^2-35\,\delta^4+7\,i\delta^6)\,(\omega-\omega_0)^6\,{T_2}^6}{(1+\delta^2)^7\,k_0},
\end{aligned} \tag{2.47}$$

where $\delta = (\omega_0 - \omega_a)\,T_2$ is the difference between the vibration frequency of the electric field ω_0, and the vibration frequency of atoms of dopant ω_a. In parallel, β is also expanded up to the sixth order, yielding :

$$
\begin{aligned}
\beta =& \beta_0 + (\omega-\omega_0)\partial_\omega\beta \\
&+ \frac{1}{2}(\omega-\omega_0)^2\partial_\omega^2\beta + \frac{1}{6}(\omega-\omega_0)^3\partial_\omega^3\beta \\
&+ \frac{1}{24}(\omega-\omega_0)^4\partial_\omega^4\beta + \frac{1}{120}(\omega-\omega_0)^5\partial_\omega^5\beta \\
&+ \frac{1}{720}(\omega-\omega_0)^6\partial_\omega^6\beta + |\psi|^2\frac{\partial\beta}{\partial|\psi|^2} \\
&+ \frac{1}{2}|\psi|^4\frac{\partial\beta}{\partial|\psi|^4} + \frac{1}{6}|\psi|^6\frac{\partial\beta}{\partial|\psi|^6} \\
&+ (\omega-\omega_0)|\psi|^2\partial_\omega\left(\frac{\partial\beta}{\partial|\psi|^2}\right) \\
&+ \frac{1}{2}(\omega-\omega_0)|\psi|^4\partial_\omega\left(\frac{\partial\beta}{\partial|\psi|^4}\right) \\
&+ \frac{1}{6}(\omega-\omega_0)|\psi|^6\partial_\omega\left(\frac{\partial\beta}{\partial|\psi|^6}\right) \\
&+ \left(\frac{\partial\beta}{\partial|\psi|_t^2}\right)|\psi|_t^2 + \\
&\frac{1}{2}\left(\frac{\partial\beta}{\partial|\psi|_t^4}\right)|\psi|_t^4 + \frac{1}{6}\left(\frac{\partial\beta}{\partial|\psi|_t^6}\right)|\psi|_t^6.
\end{aligned}
\tag{2.48}
$$

Eq.(2.48) can be reduced as follows :

$$
\begin{aligned}
-i\frac{\partial\psi}{\partial z} = & \left(\frac{g_p\delta}{2n\left(1+\delta^2\right)}\right)\psi - i\left(-\alpha+\frac{g_p}{2n\left(1+\delta^2\right)}\right)\psi \\
& + \left(-\frac{2g_p\delta T_2}{2n(1+\delta^2)^2}\right)\frac{\partial\psi}{\partial t} + i\left(\beta_1+\frac{g_p\left(1-\delta^2\right)T_2}{2n\left(1+\delta^2\right)^2}\right)\frac{\partial\psi}{\partial t} \\
& + \left(-\frac{\beta_2}{2}+\frac{g_p\left(3\delta-\delta^3\right)T_2^2}{2n\left(1+\delta^2\right)^3}\right)\frac{\partial^2\psi}{\partial t^2} + i\left(\frac{g_p\left(-1+3\delta^2\right)T_2^2}{2n\left(1+\delta^2\right)^3}\right)\frac{\partial^2\psi}{\partial t^2} \\
& + \left(\frac{g_p\left(-4\delta+4\delta^3\right)T_2^3}{2n\left(1+\delta^2\right)^4}\right)\frac{\partial^3\psi}{\partial t^3} - i\left(\frac{\beta_3}{6}+\frac{g_p\left(-1-\delta^4+6\delta^2\right)T_2^3}{2n\left(1+\delta^2\right)^4}\right)\frac{\partial^3\psi}{\partial t^3} \\
& + \left(\frac{\beta_4}{24}-\frac{g_p\left(-5\delta+10\delta^3-\delta^5\right)T_2^4}{2n\left(1+\delta^2\right)^5}\right)\frac{\partial^4\psi}{\partial t^4} - i\left(\frac{g_p\left(1-10\delta^2+5\delta^4\right)T_2^4}{2n\left(1+\delta^2\right)^5}\right)\frac{\partial^4\psi}{\partial t^4} \\
& + \left(-\frac{g_p\left(6\delta+6\delta^5-20\delta^3\right)T_2^5}{\left(1+\delta^2\right)^6}\right)\frac{\partial^5\psi}{\partial t^5} + i\left(\frac{\beta_5}{120}+\frac{g_p\left(1-15\delta^2+15\delta^4-\delta^6\right)T_2^5}{2n\left(1+\delta^2\right)^6}\right)\frac{\partial^5\psi}{\partial t^5} \\
& + i\frac{\partial}{\partial_\omega}\left(\frac{\partial\beta}{\partial|\psi|^2}\right)\left(|\psi|^2\psi\right)_t - \left(\frac{\beta_6}{720}+\frac{g_p\left(7\delta-35\delta^3+21\delta^5-\delta^7\right)T_2^6}{2n\left(1+\delta^2\right)^7}\right)\frac{\partial^6\psi}{\partial t^6} \\
& + \frac{i}{2}\left(\frac{\partial}{\partial_\omega}\left(\frac{\partial\beta}{\partial|\psi|^4}\right)\right)\left(|\psi|^4\psi\right)_t \\
& - i\left(\frac{g_p\left(-1+21\delta^2-35\delta^4+7\delta^6\right)}{2n\left(1+\delta^2\right)^7}\right)\frac{\partial^6\psi}{\partial t^6} + \frac{i}{6}\left(\frac{\partial}{\partial_\omega}\left(\frac{\partial\beta}{\partial|\psi|^6}\right)\right)\left(|\psi|^6\psi\right)_t \\
& + \left(\partial_{|\psi|^2}\left(\beta\right)+\frac{k_0A_{eff}^{-1}}{4}\left(n_2+i\frac{\alpha n_2}{nk_0}\right)\right)|\psi|^2\psi + \frac{1}{6}\left(\frac{\partial\beta}{\partial|\psi|_t^6}\right)|\psi|_t^6\psi \\
& + \left(\frac{1}{2}\frac{\partial\beta}{\partial|\psi|^4}+\frac{k_0A_{eff1}^{-1}}{4}\left(\frac{n_2^2}{2n}+n_4+i\frac{\alpha n_4}{nk_0}\right)\right)|\psi|^4\psi + \left(\frac{\partial\beta}{\partial|\psi|_t^2}\right)|\psi|_t^2\psi \\
& + \left(\frac{1}{6}\frac{\partial\beta}{\partial|\psi|^6}+\frac{k_0A_{eff2}^{-1}}{4}\left(n_6+\frac{n_2n_4}{n}+i\frac{\alpha n_6}{k_0n}\right)\right)|\psi|^6\psi + \frac{1}{2}\left(\frac{\partial\beta}{\partial|\psi|_t^4}\right)|\psi|_t^4\psi
\end{aligned}
\tag{2.49}
$$

which can be rewritten as

$$
\begin{aligned}
& i\frac{\partial\psi}{\partial z} + i\beta_1^{eff}\psi_t + \left(d_{2r}+id_{2s}\right)\psi_{2t} + \left(d_{3r}+id_{3s}\right)\psi_{3t} + \left(d_{4r}+id_{4s}\right)\psi_{4t} \\
& \quad + \left(d_{5r}+id_{5s}\right)\psi_{5t} + \left(d_{6r}+id_{6s}\right)\psi_{6t} + \left(\gamma_r+i\gamma_s\right)\psi \\
& \quad + \left(q_{1r}+iq_{1s}\right)|\psi|^2\psi + \left(q_{2r}+iq_{2s}\right)|\psi|^4\psi + \left(q_{3r}+iq_{3s}\right)|\psi|^6\psi \\
& \quad + m_{r1}|\psi|_t^2\psi + m_{r2}|\psi|_t^4\psi + m_{r3}|\psi|_t^6\psi \\
& \quad + in_{s1}\left(|\psi|^2\psi\right)_t + in_{s2}\left(|\psi|^4\psi\right)_t + in_{s3}\left(|\psi|^6\psi\right)_t = 0.
\end{aligned}
\tag{2.50}
$$

Assuming $\tau = t - \beta_1^{eff} z$ and $z = \xi$, we obtain the final form

$$i\psi_\xi + \sum_{j=2}^{6} d_{jrs}\psi_{j\tau} + \sum_{k=1}^{3}\left[\left(q_{krs}|\psi|^{2k} + m_{kr}|\psi|_\tau^{2k}\right)\psi + in_{ks}\left(|\psi|^{2k}\psi\right)_\tau\right] + \gamma_{ri}\psi = 0, \tag{2.51}$$

where, d_{jrs} are the complex dispersion coefficients, which can be defined by $d_{jrs} = d_{jr} + id_{js}$, with d_{jr} and d_{js} the real and the imaginary part, respectively. The different coefficients of Eq.(51) are expressed in the following:

$d_{2r} = -\left(\frac{\beta_2}{2} + \frac{g_p\left(-3\delta+\delta^3\right)T_2^2}{2n\left(1+\delta^2\right)^3}\right)$,

$d_{2s} = -\frac{g_p\left(1-3\delta^2\right)T_2^2}{2n\left(1+\delta^2\right)^3}$.

$d_{3r} = -4\delta\frac{g_p\left(1-\delta^2\right)T_2^3}{2n\left(1+\delta^2\right)^4}$,

$d_{3s} = -\left(\frac{\beta_3}{6} + \frac{g_p\left(-1-\delta^4+6\delta^2\right)T_2^3}{2n\left(1+\delta^2\right)^4}\right)$.

$d_{4r} = \frac{\beta_4}{24} - \frac{g_p\left(-5\delta+10\delta^3-\delta^5\right)T_2^4}{2n\left(1+\delta^2\right)^5}$,

$d_{4s} = -\left(\frac{g_p\left(1-10\delta^2+5\delta^4\right)T_2^4}{2n\left(1+\delta^2\right)^5}\right)$.

$d_{5r} = -\frac{2g_p\delta\left(3+3\delta^4-10\delta^2\right)T_2^4}{2n\left(1+\delta^2\right)^6}$,

$d_{5s} = \frac{\beta_5}{120} + \frac{g_p\left(1-15\delta^2+15\delta^4-\delta^6\right)T_2^5}{2n\left(1+\delta^2\right)^6}$.

$d_{6r} = -\frac{\beta_6}{720} - \frac{g_p\left(7\delta-35\delta^3+21\delta^5-\delta^7\right)T_2^6}{2n\left(1+\delta^2\right)^7}$,

$d_{6s} = -\frac{g_p\left(-1+21\delta^2-35\delta^4+7\delta^6\right)}{2n\left(1+\delta^2\right)^7}$.

The constants q_{krs} represent the complex coefficients of nonlinearity, the real part are nonlinear coefficient and imaginary are nonlinear gain/loss.

For *k=1*, q_{1r} is the nonlinear Kerr coefficient, q_{1s} the gain or loss term of nonlinearity, and k the order of correction, with

$q_{1r} = \frac{\partial\beta}{\partial|\psi|^2} + \left(\frac{n_2k_0}{4}\right)A_{eff}^{-1}$,

$q_{1s} = \left(\frac{\alpha n_2}{4n}\right)A_{eff}^{-1}$.

For *k=2*, we obtain the first correction of the Kerr effect, commonly known as quintic nonlinearity coefficients,

$q_{2r} = \frac{1}{2}\left(\frac{\partial\beta}{\partial|\psi|^4}\right) + \frac{k_0}{4}\left(\frac{n_2^2}{2n} + n_4\right)A_{eff1}^{-1}$,

$q_{2s} = \left(\frac{\alpha n_4}{4n}\right)A_{eff1}^{-1}$.

For *k=3*, we have second correction of Kerr effect. This is also known as septic nonlinearity coefficients, $q_{3r} = \frac{1}{6}\left(\frac{\partial\beta}{\partial|\psi|^6}\right) + k_0\left(n_6 + \frac{n_2n_4}{4n}\right)A_{eff2}^{-1}$,

$q_{3s} = \left(\frac{\alpha n_6}{4n}\right)A_{eff2}^{-1}$.

Here A_{eff}^{-1}, A_{eff1}^{-1}, A_{eff2}^{-1}, keep the same definition as in Ref [146]. The coefficients m_{kr} are the self steepening coefficients, m_{r2} and m_{r3} being, respectively, the first and second order correction terms of m_{1r}, with

$m_{r1} = \frac{\partial\beta}{\partial|\psi|_t^2}$,
$m_{r2} = \frac{1}{2}\frac{\partial\beta}{\partial|\psi|_t^4}$,
$m_{r3} = \frac{1}{6}\left(\frac{\partial\beta}{\partial|\psi|_t^6}\right)$.

The real parameters n_{ksi} denote the intra-pulse Raman scattering coefficient, with
$n_{1s} = \frac{\partial}{\partial_\omega}\left(\frac{\partial\beta}{\partial|\psi|^2}\right)$,
$n_{2s} = \frac{1}{2}\left(\frac{\partial}{\partial_\omega}\left(\frac{\partial\beta}{\partial|\psi|^4}\right)\right)$,
$n_{3s} = \frac{1}{6}\left(\frac{\partial}{\partial_\omega}\left(\frac{\partial\beta}{\partial|\psi|^6}\right)\right)$.

The complex coefficient of absorption γ_{rs} is defined as $\gamma_{rs} = \gamma_r + i\gamma_s$, with $\gamma_r = \frac{g_p\delta}{2n(1+\delta^2)}$, $\gamma_s = -\alpha + \frac{g_p}{2n(1+\delta^2)}$.

The different models that we have presented provide the possibility to study new properties of the dynamics of waves propagating in doped optical fiber and condense matter physics. This study can the be implemented with the use of some analytical and numerical tools.

2.3 Analytic and numerical methods

This section presents analytical and numerical methods that we have used in order to achieve the results presented in this thesis.

2.3.1 Analytic methods

2.3.1.1 Lens type transformation

Generally, excepts for the linear and nonlinear effects, the wave motion can be affected by other effects such as exterior effects (magnetic, optical, homogeneity), and management. Commonly expressed by an explicit function of the coordinates equation (transverse or longitudinal), it is usually not easy to treat the wave motion with those effects. To investigate efficiently without changing the dynamics of waves, It is necessary to do some transformations which lead to new equations with intrinsic exterior effects or management. We note that certain transformations lead to the discrete equation when the exterior effect is optical. It is for example the case of Time-building approximation[149, 150]. The other methods conserve the scale of dynamics such as similarity transformation, and Lens type transformations for exterior effects are magnetic effects [109]. The Lens transformation is the optical denotation of mathematical pseudo-conformal transformation. In nonlinear optics, this transformation is used to move the space dependence in the non-autonomous NLSE to obtain the standard NLS. In the condensed matter physics it is used to transform a space-time dependent Gross-Pitaevskii equation into a GP equation without explicit local dependence. We note that this transformation has a great variety of forms that depend on the nature of external potentials. Besides, this method gives the integrability condition of equations, and a smooth MI investigation.

2.3.1.2 Application of Lens type transformation to the nonlocal Schrödinger equation with quadratic potential

Let us consider the nonlocal Schrödinger given by (2.35), where $V(x)$ is the potential energy. Generally, the complex form of this potential is writing as

$$V(x) = \beta x^2 + \eta x + \varepsilon_r + i\varepsilon_i, \tag{2.52}$$

where the first term accounts for the magnetic field, the second term results from the influence of the laser or gravitational field, and the last term is a complex term which may account for an arbitrary nonlocal field or atomic exchange with the background. In our context, we restrict our study to the quadratic term of potential. The form of Lens-type transformation is

$$\psi(x,t) = \frac{\delta(X,T)}{\sqrt{l(t)}} \exp\left(if(t)\, x^2\right), \tag{2.53}$$

where $T(t)$ and $X(t)$ are the scale variables, and $f(t)$ and $l(t)$ are the real functions of time. The Lens transformation may have distinct forms, but the latter form is not considered at this stage yet. Introducing (2.53) into (2.35) and collect to the degree of$x$, we obtain the differential equations :

$$\frac{df}{dt} = -4f(t) - \beta, \tag{2.54}$$

$$\frac{dl}{dt} = 4f(t)\, l(t), \tag{2.55}$$

$$\frac{dT}{dt} = \frac{1}{l(t)^2}, \tag{2.56}$$

and

$$X = \frac{1}{l(t)}.$$

The solutions of these equations depend on the nature of the potential energy. In the case of a potential well ($\beta > 0$), the solutions of the equations are

$$f(t) = -\frac{\sqrt{\beta}}{2} \tan\left(2\sqrt{\beta}t\right), \tag{2.57}$$

$$l(t) = \left|\cos\left(2\sqrt{\beta}t\right)\right|, \tag{2.58}$$

$$T(t) = \frac{1}{2\sqrt{\beta}} \tan\left(2\sqrt{\beta}t\right). \tag{2.59}$$

Here, the frequency shift of the wave is periodic and induces the current. This induction is characterized by the periodic oscillation of $f(t)$ at the frequency $4\sqrt{\beta}$.
In the case of a barrier potential ($\beta < 0$), we have

$$f = \pm\frac{1}{2}\sqrt{-\beta}, \tag{2.60}$$

$$l(t) = \exp(2ft), \tag{2.61}$$

$$T(t) = \frac{1 - \exp(-8ft)}{8ft}. \tag{2.62}$$

We note that with a barrier potential, the frequency shift is constant. Consequently, no current is induced. Using the latter solutions with Lens function, one can obtain a new equation with intrinsic potential.

Here, we are interested in the case of the potential well, and a new form of the nonlocal Schrödinger equation is obtained as :

$$i\delta_T + \delta_{XX} + \alpha g(T)\delta \int_{-\infty}^{\infty} (R(X - X')|\delta(X')|^2)dX' = 0, \tag{2.63}$$

where $g(T) = 1 + 4\beta T^2$. When $\beta = 0$, (2.63) it equivalent to the nonlocal model equation used by Krolikowski [18].

2.3.1.4 Linear Stability

We present the linear stability analysis of the plane waves in the new nonlocal which derives from Lens transformation (2.63). We assume that the amplitude of the wave is time-independent during propagation in the system. This allow to consider the plane waves of the form :

$$\delta(X,T) = \delta_0 \exp\left[i\left(kx - \int_0^T \omega(s)\,ds\right)\right], \tag{2.64}$$

where δ_0, is a constant amplitude. Substituting this solution in NNSLE yields the associated nonlinear dispersion relation

$$\omega(t) = k^2 - \alpha\delta_0^2 g(T), \tag{2.65}$$

which is the same as for the standard local GP equation

$$i\delta_T + \delta_{XX} + \alpha g(T)|\delta|^2\delta = 0. \tag{2.66}$$

In the linear stability framework, the MI is examined using linearisation. Therefore we use the ansatz

$$\delta(X,T) = [\delta_0 + \phi(X,T)] \exp\left[i\left(kx - \int_0^T \omega(s)\,ds\right)\right], \tag{2.67}$$

In this ansatz, $\phi(X,T)$ is a small perturbation, say $|\phi| \ll \delta_0$, $kx - \int_0^T \omega(s)\,ds$ is the modulation phase in which k and ω are, respectively, the wave number and the frequency of the modulation. We substitute the perturbed plane wave (2.67) into (2.66), considering the above dispersion relation. Then, neglecting terms of order higher than zero (ϕ), we obtain the equation describing the dynamics of the perturbation $\phi(X,T)$ as

$$i\phi_T + \phi_{XX} + 2ik\phi_x + 2\alpha g(T)\delta_0^2 \int_{-\infty}^{\infty} (R(X - X')R_e(\phi))dX' = 0. \tag{2.68}$$

Using the Fourier transform inverse as well as the Fourier transform of this equation we obtain:

$$i\phi_T + \phi_{XX} + 2ik\phi_x + 2\alpha g\left(T\right)\delta_0^2 \tilde{R} R_e\left(\phi\right) = 0, \tag{2.69}$$

where $\tilde{R}$ is the Fourier transform of the response function R. We consider a perturbation of the form $\phi = U\left(X,T\right) + iV\left(X,T\right)$. Then, the real and imaginary parts of ϕ obey to the coupled set of equations:

$$\begin{cases} U_T + V_{XX} + 2kU_X = 0 \\ -V_T + U_{XX} - 2kV_X + 2\alpha g(T)\tilde{R}\delta_0^2 U = 0 \end{cases} \tag{2.70}$$

We suppose that the perturbations are plane wave solutions defined by to the following expressions:

$$\begin{aligned} U &= R_e\left\{U_0 \exp\left[KX - \int_0^T \Omega\left(s\right) ds\right]\right\}, \\ V &= R_e\left\{V_0 \exp\left[KX - \int_0^T \Omega\left(s\right) ds\right]\right\} \end{aligned} \tag{2.71}$$

Inserting (2.71) into (2.70), we obtain a system of first order equation in U_0, V_0

$$\begin{bmatrix} \Omega(t) - 2kK & -K^2 \\ 2\alpha g(T)\tilde{R}K^2\delta_0^2 & \Omega(t) - 2kK \end{bmatrix}$$

Such a system may have solution only of its determinant is zero. This correspond to the following explicitly time-dependent dispersion relation for the parameter of the perturbation

$$\left(\Omega\left(t\right) - 2kK\right)^2 - K^2\left(-K^2 + 2\alpha g\left(T\right)\tilde{R}K^2\delta_0^2\right) = 0. \tag{2.72}$$

From this relation, we can derive the condition of onset of the MI. In fact, the perturbation may undergo the exponential growth if the modulation frequency is a complex number with positive imaginary part. This condition should be realized when the discriminant of the above quadratic equation in Ω is negative, say

$$K^2 - 2g\left(T\right)\alpha\tilde{R}\delta_0^2 > 0. \tag{2.73}$$

This condition combines the perturbation wave number K to the amplitude δ_0 of initial plane wave and the strength of nonlocal cubic nonlinearity, the width of nonlocality and the parameter of the trapping potential. Then, the instability results from the interplay between dispersion and nonlinearity. The confinement of the condensate in a trap modifies the dispersion, so that the range of nonlinear phenomena may be correspondingly broader. Under the condition (2.73), the MI sets in within the system under study with a gain (or instability growth rate). The nonlocal-instability growth rate is given by:

$$G = K^2\sqrt{2g\left(T\right)\tilde{R}(K)\left(\frac{\delta_0}{K}\right)^2 - 1} \tag{2.74}$$

2.3.2 Numerical methods

In nonlinear optics, several methods are used to solve the NLSE. Analytical methods such as the inverse scattering method, Dressing Darboux method, and Bilinear Hirota method can give an exact solution for integrable equations. But obtaining exact analytical solutions for non-integrable equations can be either difficult or impossible. Nevertheless, non-integrable systems can show rich behaviors as far as the propagation of solitons is concerned. Thus, to address the issues of the treatment of non-integrable problems, numerical simulations are usually implemented. We recall that numerical simulations present the disadvantage of being time-consuming. So, we describe in this section a famous optical method that can solve the nonlinear propagation equation. Before describing the method, let us recall some of the useful transforms we encounter in optics.

This method relies on the steps that will be explained briefly. Mathematically, (2.35) can be expressed in the following form:

$$\frac{\partial A}{\partial z} = \left[\hat{L} + \hat{N}\right] A, \tag{2.75}$$

where $\hat{L}$ is linear differential operator that takes into account the dispersion and the absorption in the medium, and $\hat{N}$ is a nonlinear operator that accounts for the effect of fiber's nonlinearities in pulse propagation [1]. These operators are defined as:

$$\hat{L} = i\frac{\partial^2}{\partial x^2}, \tag{2.76}$$

and

$$\hat{N} = i\left(V(x) + \alpha\left(\int_{-\infty}^{\infty} R\left(x - x'\right)\left|\psi\left(x'\right)\right|^2 dx'\right)\right). \tag{2.77}$$

Both the linear and the nonlinear parts have analytical solutions.
Under the assumption of a small step h taken along z direction, two parts can be treated to act separately with only a small numerical error. One can therefore first take a small nonlinear step while $\hat{L} = 0$, and in the second step, dispersion acts alone, and $\hat{N} = 0$. Mathematically, for the standard SSFM, the solution of the differential equation at step $z = jh$ is given by:

$$A(x, z+h) = \Im^{-1}\left[\exp\left(h\hat{L}(i\omega)\right)\Im\left\{\exp\left(h\hat{N}\right)A(x,z)\right\}\right], \tag{2.78}$$

where j is an integer, $j = 1, 2, , N$, $N = L/h$ is the number of steps of length h, with L being the total fiber length. The operation on $\hat{L}$ is performed in the frequency domain. By taking the inverse Fourier transform, the pulse has thus been propagated in a small step h. Next, the procedure is repeated so that the pulse can be propagated over a total length of L. The Fourier transforms of this algorithm can be computed relatively fast using the fast Fourier transform (FFT).
The SSFM is accurate to first order in the step size h [1]. The algorithm of SSFM is given in next figure.

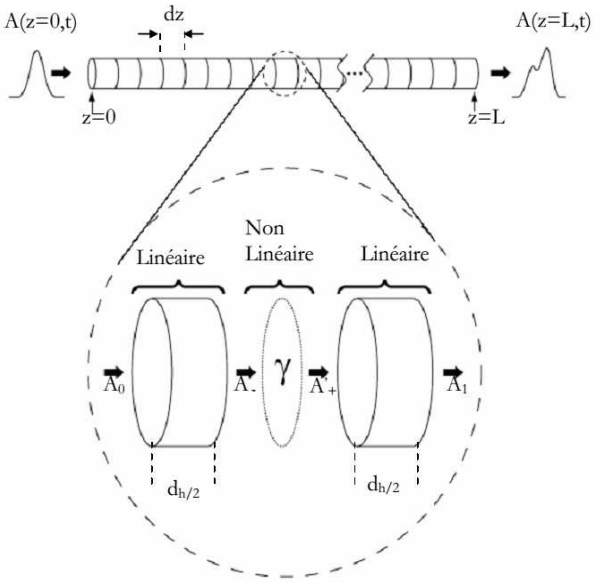

Figure 13: Split-step Fourier method algorithm

2.3.3 Sensitivity analysis

In this manuscrip we had used the analytical and numerical methods to investigated MI. In the order to observed simultonously different physical on MI, we use the statiscal method. This method has been applied in biology, in supra transmission phenomena [151, 152, 153, 154, 155]. It is first application of this method our knowlege. Sensitivity analysis (SA) is a method for quantifying uncertainty in any type of complex model. The objective of SA is to identify critical inputs (parameters and initial conditions) of a model and quantifying how input uncertainty impacts model outcome(s). When input factors such as parameters or initial conditions are known with little uncertainty, we can examine the partial derivative of the output function with respect to the input factors. This sensitivity measure can easily be computed numerically by performing multiple simulations varying input factors around a nominal value. This technique is called a local SA because it investigates the impact on model output, based on changes in factors only very close to the nominal values. In biology, input factors are often very uncertain and therefore local SA techniques are not appropriate for a quantitative analysis; instead global SA techniques are needed. These global techniques are usually implemented using Monte-Carlo(MC) simulations and are, therefore, called Sampling-based methods. In this study sensitivity analysis is performed with LHS and partial rank correlation coefficient (PRCC) methods, The LHS method assumes that the sampling is performed independently for each parameter, although a procedure to impose correlations on sampled values has also been developed [151]. The sampling is done by randomly selecting values from each pdf (Fig. 14(A)). Each interval for each parameter is sampled exactly once (without replacement), so that the

entire range for each parameter is explored (Fig. 14(A)). A matrix is generated (which we call the LHS matrix) that consists of N rows for the number of simulations(sample size) and of k columns corresponding to the number of varied parameters (Fig. 14 (B)). The LHSmatrix (X) is then built by assembling the samples from each pdf. Each row of the LHS matrix represents a unique combination of parameter values sampled without replacement. The hypothetical model (in our case a parameter) is then evaluated, the corresponding output generated and stored in the matrix (Y). Each matrix is then rank transformed (XR and YR). N model solutions are then simulated, using each combination of parameter values (each row of the LHS matrix, (Fig. 14(B))). The rank-transformed LHS matrix (X) and the output matrix (Y) are used to calculate the CC Pearson, Spearman or rank correlation coefficient (RCC) and the partial rank correlation coefficient (PRCC)(Fig.14(C)). Correlation provides a measure of the strength of a linear association between an input and an output. A CC between x_j and y is calculated as follows:

$$r_{x_j,y} = \frac{Cov\left(x_j, y\right)}{\sqrt{Var\left(x_j\right) Var\left(y\right)}} = \frac{\sum_{i=1}^{N}\left(x_{ij} - \bar{x}\right)\left(y_i - \bar{y}\right)}{\sqrt{\sum_{i=1}^{N}\left(x_{ij} - \bar{x}\right)^2 \sum_{i=1}^{N}\left(y_i - \bar{y}\right)^2}}, \tag{2.79}$$

with $j = 1, 2..., k$ and $r_{x_j,y}$ varies between -1 and 1, $Cov\left(x_j, y\right)$ represents the covariance between x_j and y while $Var(x_j)$ and $Var(y)$ are respectively the variance of x_j and y. If the data x_j and y have not been analyzed, then the coefficient r is called sample or Pearson CC (Fig.14 (C)). If the data are rank transformed, thus the result is a Spearman or rank correlation coefficient(also refers to Fig.14(C)). Partial correlation characterizes the linear relationship between input x_j and output y after the linear effects on y of the main inputs are discounted. note that, the PCC between x_j and y is the CC between the two residuals $(x_j - \hat{x_j})$ and $(y - \hat{y})$ where $\hat{x_j}$ and $\hat{y}$ are the following linear regression models:

$$\hat{x_j} = a_0 + \sum_{p=1}^{k} a_p x_p, \tag{2.80}$$

$$\hat{y} = b_0 + \sum_{p=1}^{k} b_p x_p, \tag{2.81}$$

with $p \neq j$. similarly to PCC, partial rank correlation (PRC) performs a partial correlation on rank-transformed data: x_j and y are first rank transformed, and then the linear regression models defined $\hat{x_j}$ and y are built. PRCC is a robust sensitivity measure for nonlinear but monotonic relationships between x_j and y, as long as little to no correlation exists between the inputs.

2.4 Conclusion

In this chapter, we presented different type of models that we have considered in this thesis. We explained the transformation of the governing equation from a non-management to a manage-

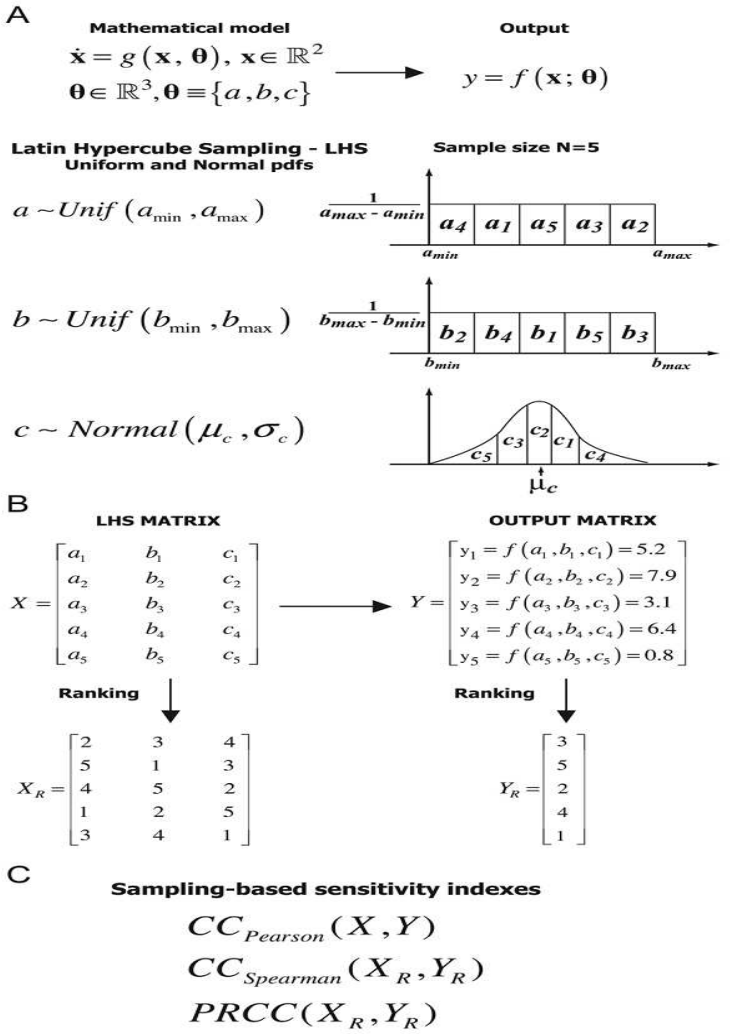

Figure 14: Scheme performed for sensitivity analysis with LHS and PRCC methods [151],(A) Mathematical model specification (dynamical system, parameters, output) and the corresponding LHS scheme. Probability density functions (pdfs) are assigned to the parameters of the model (e.g. a, b, c). We show an example with sample size N equal to 5. Each interval is divided into five equiprobable subintervals, and independent samples are drawn from each pdf (uniform and normal)The subscript represents the sampling sequence.

ment equation. We derive the stability condition of the resulting management equation as well as the growth rate. We explain step-by-step the numerical methods which we have employed in the thesis. In the next chapter, we will present and discuss the different results obtained from analytical and numerical treatments described in this chapter.

Chapter 3

Results and discussions

3.1 Introduction

In this chapter, we present and discuss some important results obtained from the investigations using both analytical and numerical methods as presented in chapter II. This chapter is organized as follows: In the second Section, we present modulational instability in nonlocal media in the presence of magnetic effect. In the third Section, Modulational instability in weak nonlocal nonlinear media with competing Kerr and non-Kerr nonlinearities is discussed in the presence of an external potential. In the fourth Section, we perform the process of generation of solitons in doped fiber with higher-order correction of cubic-quintic nonlinearities, accounting for dispersion and gradient nonlinear terms. The fifth section concludes this chapter.

3.2 Modulational instability in nonlocal nonlinear media

In this Section, we present results from different techniques we have presented in chapter II for nonlocal model. With the aim to highlight the impact of nonlocality on MI, Fig. 15 shows the impact of different response functions on the critical distance z_c. We observe the presence of many lobes around the zero values of the wave number for rectangular response, but none exist for the Gaussian response. For the Gaussian response, we note that z_c is not null at $k = 0$. This implies that MI exist for all wave numbers.

The above result can be confirmed in Fig. 16, where Fig. 16(a) presents many lobes of MI when increasing the width of nonlocality σ. Fig. 16(b) shows an asymmetry of lobes of the growth rate for an increase of the strength of nonlinearity coefficients. The rectangular response induces MI with defocusing nonlinearity. Fig. 16(c) and Fig. 16(d) represent MI taking the case of a Gaussian function. Here, we observe a decrease of the band width of gain with an increase of nonlocality.

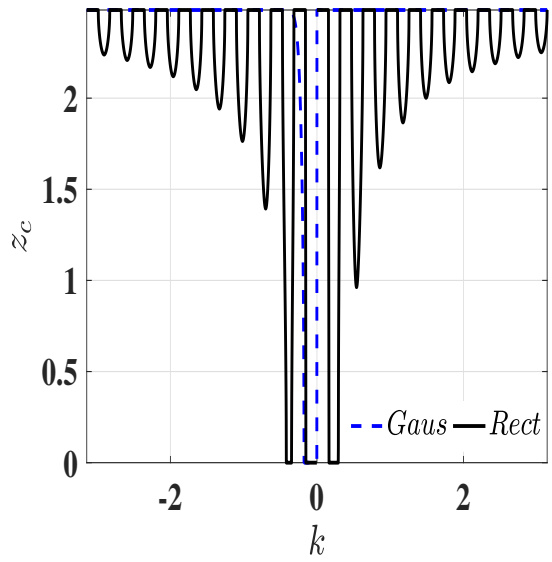

Figure 15: Critical distance z_c as a function of wave number k. Dash line represents the impact of Gaussian response function and the solid line is the impact of rectangular response function on critical distance. $\sigma = 1, \alpha = 1, \beta = 0.01, \delta_0 = 2$.

The same result is observed in Fig. 18 with the increase of the nonlinear coefficient α. The response exhibits MI with defocusing nonlinearity. Applying the split-steps Fourrier method described Sec. II.3.2, we a train of soliton has been generated for rectangular and Gaussian response function without an external trapping potential. A skecth of the wave train is done in Fig. 17.

3.3 Modulational instability in weak nonlocal nonlinear media with competing Kerr and non-Kerr nonlinearities

Investigations on interactions between optical light and matter, in nonlinear optics, resulted in several observations, which have led to considerable applications in telecommunications, and elegant theories in discrete and continuous systems [1, 156]. The propagation of optical beam is accompanied by two principal effects: linear effects, due to dispersion or/and diffraction, and nonlinear effects, due to phenomena such as self-phase modulation (SPM) and cross-phase modulation (XPM) [1, 156, 157]. The balance between these effects leads to localized structures and modulational instability (MI) [1, 25, 156], which is characterized by the exponential growth of the amplitude of a (quasi) monochromatic wave propagating in weakly nonlinear dispersion media [158]. In presence of competing cubic and quintic nonlinearities, discrete systems were found to support a great variety of stable solitons, including discrete breathers in the one-dimensional lattice models [159, 160].

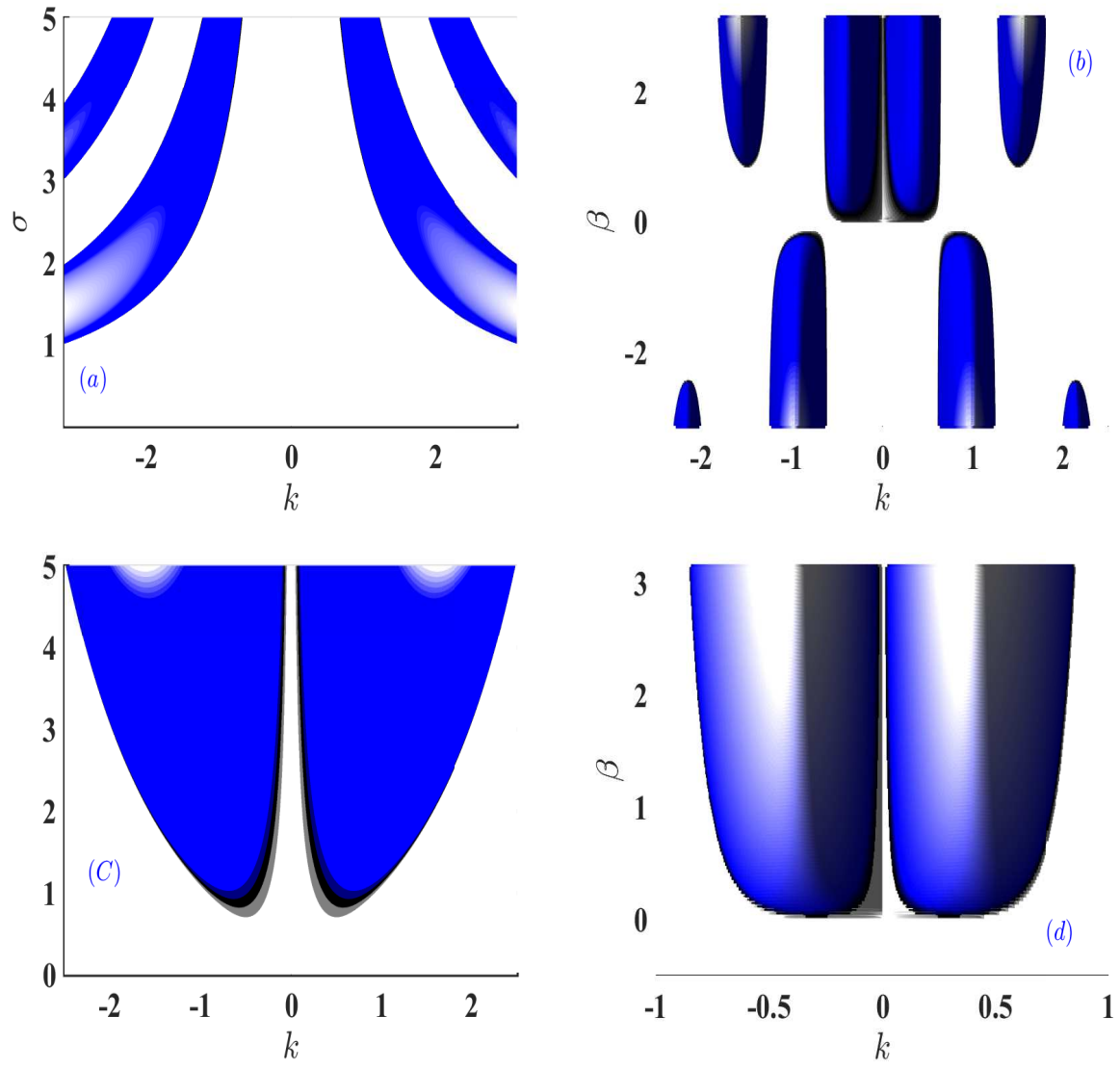

Figure 16: On the top 2D surface is a plot showing the gain, in the plane (k, σ) and (k, α) when the response function is rectangular. On the bottom, the response function is Gaussian. Physical parameters are :(a),(c) $\alpha = 1, \beta = 0.01, \delta_0 = 2$, (b) , (d) , $\sigma = 1$.

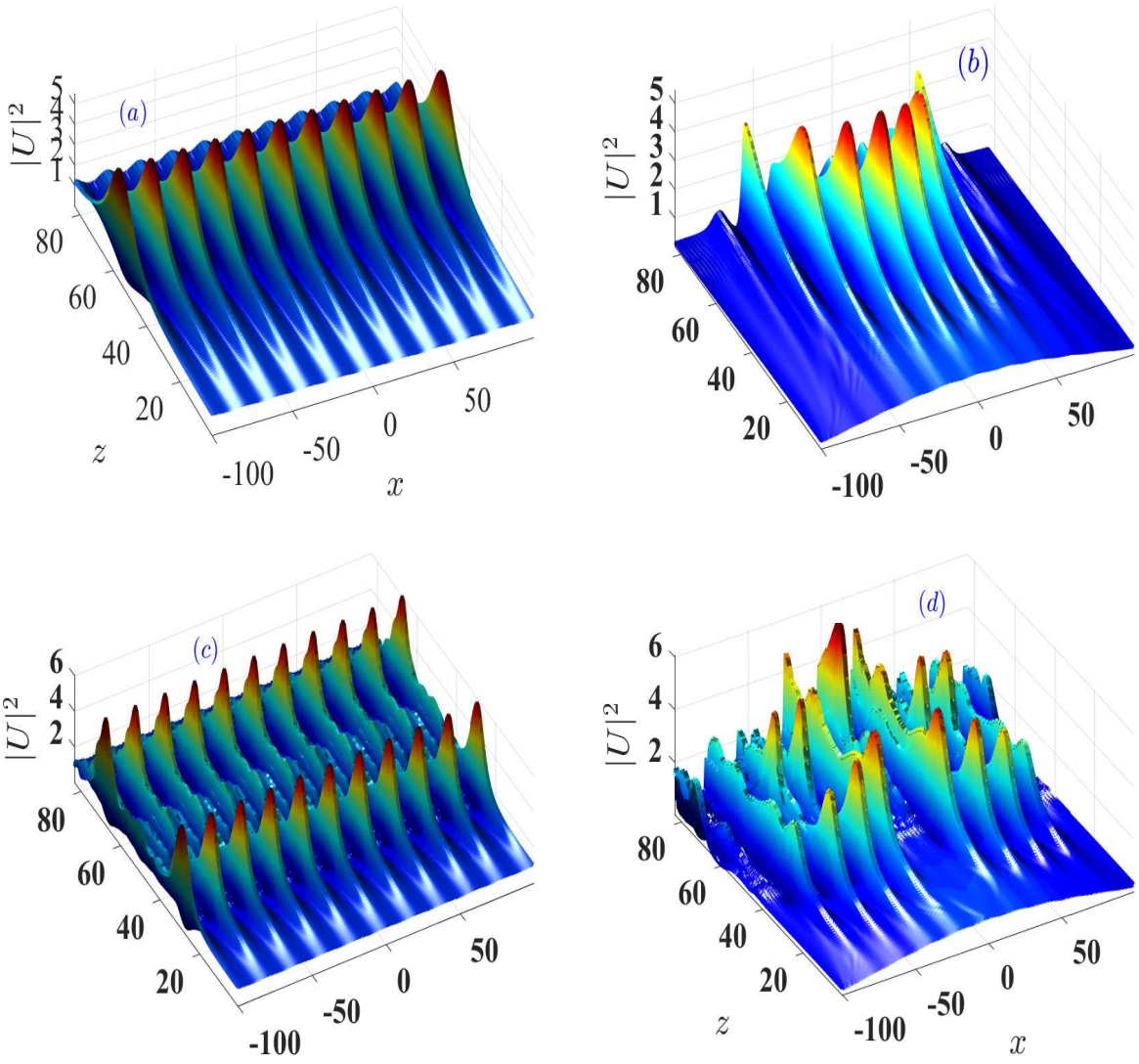

Figure 17: Generation of wave train: (a) rectangular response without potential.(b) Rectangular with potential.(c) Gaussian response without external potential.(d) Gaussian response with external potential. Physical parameters are $\sigma = 1, \alpha = 1, \beta = 0.01$.

Effects of nonlocality are possible in those media where nonlocality results from single process of nonlinearity. These fascinating patterns or phenomena occur when two or more competing nonlinearities contribute to the processing of nonlinearity. It is well known that exotic patterns or phenomena occur in media where two or more physical processes or effects participate in building the overall nonlinear response. This kind of media is the so-called synthetic media with competing nonlinearities, with practical examples being local and nonlocal (dipole-dipole) interactions in BECs [161, 162, 163], thermal and orientational nonlinearity response to the presence of a light beam in nematic liquid crystals [164]. When the order of nonlinearity is the same as the cubic focusing and cubic defocusing, the bright soliton is attractive or repulsive with Gaussian response function [165].

We investigate MI in a weakly regime of competing cubic and quintic nonlocalities in the presence of magnetic effect, with the aim of observing the impact of weakly Kerr and weakly non-Kerr effects on physical mechanisms of generation of optical pulse waves. The model and the results of analytical treatment based on the Lens-type transformation and linear stability analysis are presented below.

3.3.1 Model and mathematical background

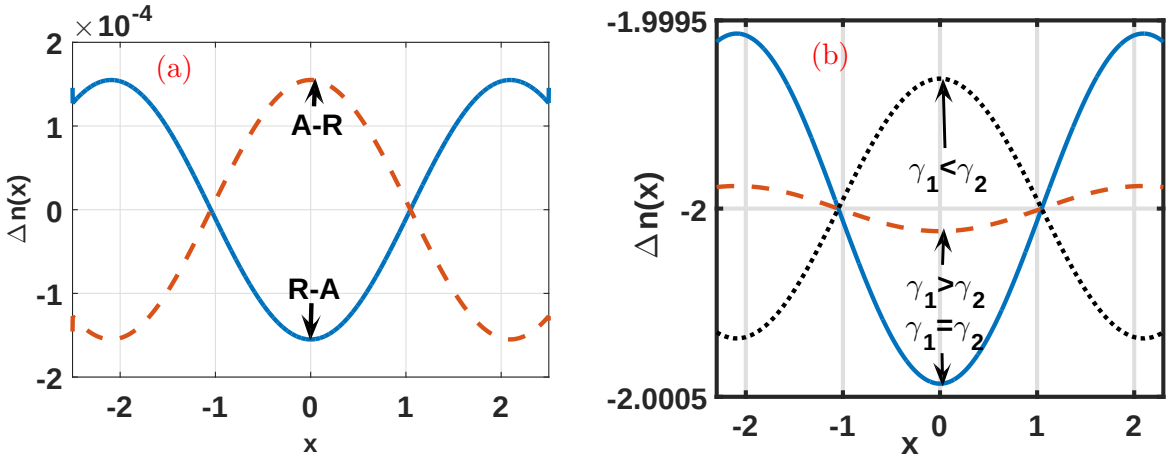

Figure 18: The panels show different profiles of the nonlinear refractive index: (a) the competing index, where the blue line shows the repulsive-attractive case, with $\gamma_1 = \gamma_2 = 0.1$. (b) The double attractive case with $\gamma_1 = \gamma_2 = 0.1$(solid blue line),$\gamma_1 > \gamma_2$ (dashed red line), and $\gamma_1 < \gamma_2$ (dotted black line). In (a) the first mode in blue line (repulsive (Kerr)-attractive (non-Kerr)) presents a maximum at the point $x = 0$. In (b) the refractive index change of the model assumes a comparison between the strength of the interaction effect in red line and the three-body interaction effect in black line.

We study the dynamics of the normalized wave function $\psi(x, z)$. in a nonlinear nonlocal medium with external effects characterized by a harmonic potential. $\psi(x, z)$ represents the macroscopic wave function in BECs [106, 107, 108, 109, 110], and it is a paraxial wave function in nonlinear optics [1, 143]. This exploration is done through the longitudinal coordinate z and transverse coordinate x, of the NLSE, which is phenomenologically given by

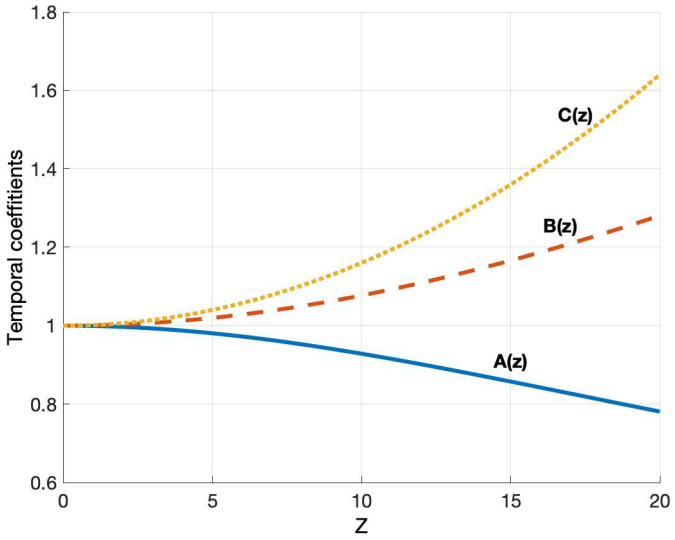

Figure 19: Variable coefficients versus the propagation distance, with the trapping parameter $\alpha = 0.0004$, where the two-body interaction is in solid blue line, two-body nonlocal interaction is in dashed red line and a the three-body nonlocal interaction is in yellow-dotted line.

$$i\frac{\partial\psi}{\partial z} = -\frac{\partial^2\psi}{\partial x^2} + V(x)\,\psi + \Delta n(I)\,\psi. \tag{3.1}$$

On the right-hand side of Eq. (3.1), the first term reflects the diffraction of the optical beam, the second term introduces the external effects described by the quadratic potential $V(x)$ and the last term captures the nonlinear refractive index change $\Delta n(I)$. Here, we take the potential in the form $V(x) = \nu x^2$, with $\nu > 0$, and a synthetic medium allowing the competing nonlocal nonlinearities or double nonlinearities. The nonlinearity is defined by [143]

$$\Delta n(x,z) = S_1 \int_{-\infty}^{+\infty} R_1(x-\xi)\,|\psi(\xi,z)|^2\,d\xi + S_2 \int_{-\infty}^{+\infty} R_2(x-\xi)\,|\psi(\xi,z)|^4\,d\xi, \tag{3.2}$$

which represents nonlocal two-body interaction with potential interaction R_1 and nonlocal three-body interaction with potential R_2, respectively. S_1 and S_2 are corresponding strengths of these two inter- atomic interactions. The first term of Eq. (3.2) represents the Kerr nonlocal nonlinearity recently used to observe different kinds of solitons [166, 167]. The second term represents the statured nonlocal nonlinearity, initially introduced by Mihalache et al. [143] to study the stability of even-parity solitons and their dipole mode counterparts. The sign of the product of S_1 and S_2 allows to distinguish the major cases of nonlinearities. For the first case $S_1S_2 > 0$ implies a double nonlinearity, where a single process contributes to obtain this nonlinearity. In our situation, we have nonlocal nonlinear saturation. The second case, $S_1S_2 < 0$,

responsible for competing nonlinearities, corresponds to two different processes contributing to the nonlinearity. In optics, these kinds of nonlocal nonlinearities have been used to investigate MI [168, 169] and the properties of dark solitons [170, 171]. We pay attention to the weak nonlocality by performing a Taylor expansion of $|\psi(\xi,z)|^2$ and $|\psi(\xi,z)|^4$ around $\xi = x$. This leads to the following expansion of the nonlinear interaction:

$$\Delta n(x,z) = S_1 |\psi(x,z)|^2 + S_2 |\psi(x,z)|^4 + S_1\gamma_1 |\psi(x,z)|^2_{xx} + S_2\gamma_2 |\psi(x,z)|^4_{xx}. \tag{3.3}$$

Obviously, Eq. (3.3) depends strongly on the sign of S_1, S_2 and the nonlocal parameters $\gamma_1 = \frac{1}{2}\int_{-\infty}^{+\infty} x^2 R_1(x)\,dx$ and $\gamma_2 = \frac{1}{2}\int_{-\infty}^{+\infty} x^2 R_2(x)\,dx$. Naturally, this dependence, which affects the shape of the nonlinear refractive index, helps to specifically address different regimes of nonlinearities and predict the kind of solitons that may exist in such media. Fig. 18 shows different profiles of the nonlinear refractive index versus the transverse coordinate taking, as test solution, the ansatz $\psi(x) = \rho_0[a_0 + \epsilon\cos(kx)]$ [18]. Inserting of Eq. (3.3) into Eq. (3.1) leads to

$$i\frac{\partial\psi}{\partial z} = -\frac{\partial^2\psi}{\partial x^2} + V(x)\psi + S_1|\psi|^2\psi + S_2|\psi|^4\psi + S_1\gamma_1\left(\frac{\partial^2|\psi|^2}{\partial x^2}\right)\psi + S_2\gamma_2\left(\frac{\partial^2|\psi|^4}{\partial x^2}\right)\psi, \tag{3.4}$$

which models the trapped BECs with two and three-body interactions with two additional terms. The nonlocal terms appear as the correction of the nonlinearities. The two and three-body interactions appear with their respective corrections. This equation is the starting point of our study which describes the dynamics of the wave function effects. The great advantage of weak nonlinearity is the possibility of analytical manipulation of Eq. (3.4) without the need of the response function as used by Wamba et *al.* [109] in a recent contribution. However, they discarded the nonlocal contribution combined to two-boody and three-body interactions, which was studied separately some years after [107, 108]. Ignoring external and non-Kerr effects reduces our model to the model of Krolikowski et *al.* [18] in nonlocal media, also used in BECs by Xiui et *al.* [110] in presence of magnetic effects. Recently, a generation of solitons in media with arbitrary degree of nonlocality has been reported [172].

3.3.2 Linear stability analysis

Due to the presence of trapping terms, the transformation of Eq. (3.4) is required to ensure analytical tractability and treatment of the linear stability analysis. For this purpose, we apply the Lens- type transformation [106, 107, 108, 109, 110], which is used by employing the optical beam represented by

$$\psi(x,z) = \frac{1}{\sqrt{l(z)}}\phi(X,Z)\,e^{i\chi(z)x^2}, \tag{3.5}$$

where $\chi(z)$ is a real function of z. We assume the change of variables as in [106, 107]. The NLS equation with nonlocal competing and management coefficients then becomes

$$i\phi_Z = -\phi_{XX} + \alpha_1 A(Z)|\phi|^2\phi + \alpha_2|\phi|^4\phi + \alpha_1\gamma_1 B(Z)\frac{\partial^2|\phi|^2}{\partial X^2}\phi + \alpha_2\gamma_2 C(Z)\frac{\partial^2|\phi|^4}{\partial X^2}\phi, \quad (3.6)$$

with $A(Z) = (1+4\alpha Z^2)^{\frac{-1}{2}}$, $B(Z) = (1+4\alpha Z^2)^{\frac{1}{2}}$, $C(Z) = (1+4\alpha Z^2)$. Fig. 19 represents the evolution of the variable coefficients versus the propagation distance Z. The cubic coefficient $A(Z)$ decreases with increasing the value of the propagating distance, while the cubic-nonlocal coefficient $B(Z)$ and the quintic-nonlocal coefficient $C(Z)$ increase with Z. We perform the linear stability analysis on Eq. (3.6) using the normalized function

$$\phi = (\eta_0 + \eta(X,Z))\exp\left[-i\int_0^Z \theta(v)dv\right], \quad (3.7)$$

where η_0 is a real constant, η is the amplitude of perturbation and $\theta(Z)$, a real function that defines the nonlinear frequency shift. Inserting Eq. (3.7) into Eq. (3.6) and preserving the low terms in η and its conjugate $\eta*$, the dynamics of the amplitude of perturbation is governed by the equation

$$i\eta_z = -\eta_{xx} + \Delta Q(\eta + \eta^*), \quad (3.8)$$

where

$$\Delta Q = \eta_0^2\left[\alpha_1 A(Z) + 2\alpha_2\eta_0^2 + \left(\alpha_1\gamma_1 B(Z) + 2\eta_0^2\alpha_2\gamma_2 C(Z)\right)\frac{\partial^2}{\partial X^2}\right]. \quad (3.9)$$

The frequency shiff is derived as

$$\theta(Z) = \eta_0^2\left[\alpha_1 A(Z) + \alpha_2\eta_0^2\right], \quad (3.10)$$

from which the nonlocality does not affect the nonlinear frequency shift. This agrees with the results in the case of the cubic-quintic nonlinearity. Substituting the relation $\eta = U + iV$ into Eq. (3.8) and separating the real form imaginary parts leads to the following equations

$$U_Z = -V_{XX} \quad (3.11)$$

$$U_{XX} - 2\Delta QU = V_Z. \quad (3.12)$$

The solutions of perturbations are defined as

$$U = u\cos\left[\left(KX - \int_0^Z \lambda(v)dv\right)\right], \quad (3.13)$$

and

$$V = v\sin\left[\left(KX - \int_0^Z \lambda(v)dv\right)\right]. \quad (3.14)$$

The arguments of Eq. (3.13) and Eq. (3.14) represent physically the modulation phase, where K denotes the wave number and λ is the frequency of the modulation phase. Introducing Eq. (3.13) and Eq. (3.14) into Eq. (3.11) and Eq. (3.12), we obtain the nonlinear dispersion relation

$$\lambda = K^2\sqrt{1+\frac{2\eta_0^2}{K^2}\left[\alpha_1 A(Z)+2\alpha_2\eta_0^2-K^2\left(\alpha_1\gamma_1 B(Z)+2\alpha_2\gamma_2 C(Z)\eta_0^2\right)\right]}. \tag{3.15}$$

This allows to study two cases, depending on the sign of the term under the square root. If λ is real, the perturbation evolves in the form of a traveling wave out of phase. In this situation, we have no gain and no loss. This leads the stable waves. In opposite, if λ is imaginary, there is an exponential amplification of the wave associated with the perturbation. This implies that the right-hand side of Eq. (3.15) must be negative. The latter situation applies only when the condition

$$1+\frac{2\eta_0^2}{K^2}\left[\alpha_1 A(Z)+2\alpha_2\eta_0^2-K^2\left(\alpha_1\gamma_1 B(Z)+2\alpha_2\gamma_2 C(Z)\eta_0^2\right)\right]<0 \tag{3.16}$$

is satisfied. We note that the sign between the local and the correction terms is negative, which leads to a decrease of MI without suppressing it completely by the correction terms. The subsequent growth rate is given by

$$\mathrm{Im}\left(\lambda\right)=K^2\sqrt{-\left\{1+\frac{2\eta_0^2}{K^2}\left[\alpha_1 A\left(Z\right)+2\alpha_2\eta_0^2-K^2\left(\alpha_1\gamma_1 B\left(Z\right)+2\alpha_2\gamma_2 C\left(Z\right)\eta_0^2\right)\right]\right\}}. \tag{3.17}$$

Considering the approximation $0<\left(1+4\alpha Z^2\right)^{-\frac{1}{2}}\leq 1$, the required condition for MI takes a simple form without variable coefficients, i.e.,

$$1+\frac{2\eta_0^2}{K^2}\left[\alpha_1+2\alpha_2\eta_0^2-K^2\left(\alpha_1\gamma_1+2\alpha_2\gamma_2\eta_0^2\right)\right]<0. \tag{3.18}$$

The critical wave number K_c, function of the nonlocality, is obtained as

$$K_c=\sqrt{\frac{2\left(\alpha_1+2\alpha_2\eta_0^2\right)\eta_0^2}{2\left(\alpha_1\gamma_1+2\alpha_2\eta_0^2\gamma_2\right)\eta_0^2-1}}, \tag{3.19}$$

so that $K<K_c$. This agrees with the result of [109], where the nonlocal effect is ignored. Moreover, we solve Eq. (3.16), in order to find the critical distance Z_c which depends strongly on nonlocality, i.e,

$$z_c=0.5\alpha^{-0.5}\arccos\left(T_{real}\right), \tag{3.20}$$

where

$$T_{real}=\frac{\left[A+\left(k^2+4\,{\eta_0}^4\alpha_2\right)\left(\frac{k^2+4\,{\eta_0}^4\alpha_2}{A}-1\right)\right]}{6{\eta_0}^2\alpha_1}, \tag{3.21}$$

with

$$
\begin{aligned}
A &= \sqrt[3]{B + 6\sqrt{6}k\sqrt{C}{\eta_0}^3\alpha_1},\\
B &= -k^6 - 12\,k^4{\eta_0}^4\alpha_2 + \left(108\,{\eta_0}^6{\alpha_1}^3\gamma_1 - 48\,{\eta_0}^8{\alpha_2}^2 + 216\,{\eta_0}^8{\alpha_1}^2\gamma_2\alpha_2\right)k^2 - 64\,{\eta_0}^{12}{\alpha_2}^3,\\
C &= C_0 + C_1k^2 + C_2k^4 + C_3k^6,\ \ C_0 = -64\,{\eta_0}^{12}\alpha_1\gamma_1{\alpha_2}^3 - 128\,{\eta_0}^{14}\gamma_2{\alpha_2}^4,\\
C_1 &= -48\,{\eta_0}^8\alpha_1\gamma_1{\alpha_2}^2 + 54\,{\eta_0}^6{\alpha_1}^4{\gamma_1}^2 - 96\,{\eta_0}^{10}\gamma_2{\alpha_2}^3 + 216\,{\eta_0}^{10}{\alpha_1}^2{\gamma_2}^2{\alpha_2}^2 + 216\,{\eta_0}^8{\alpha_1}^3\gamma_1\gamma_2\alpha_2,\\
C_2 &= -12\,{\eta_0}^4\alpha_1\gamma_2\alpha_2 - 24\,{\eta_0}^6\gamma_2{\alpha_2}^2,\ \ C_3 = -2\,{\eta_0}^2\gamma_2\alpha_2 - \alpha_1\gamma_1.
\end{aligned}
\tag{3.22}
$$

3.3.3 Numerical analysis

3.3.3.1 Attractive-Repulsive case (AR)

To start, we consider competing nonlinearities that include a cubic focusing and a quintic defocusing nonlinearities. These competing nonlinearities are used to find the fundamental solution for even and odd-parity solitons [143]. Then, for a weakly competing nonlocality, the growth rate of MI is illustrated in Fig. 20, where panel (a) shows stable and unstable areas of plane wave, with different contributions of nonlinearities. We choose the values of strength $S_1 = -1$ (*attractive*) and $S_2 = 1$ (*repulsive*) to plot the growth rate of Eq. (3.17). The stability/instability diagram of plane wave presents two areas as shown in Fig. 20(a). The red area indicates the unstable zone and the blue area corresponds to the stable zone of the plane wave. We note that in this mode of nonlinearity, MI arises for the parameter value ranges $\gamma_1 \in [0, 0.58]$ and $\gamma_2 \in [0.77, 1]$.

The middle panel presents the decreasing maximum value of the growth rate with increasing the value of the quintic parameter γ_2. One can notice that higher values of γ_2 contribute to reduce MI in the system. Fig. 20(c) shows the behaviors of the critical distance Z_c with increasing the value of the quintic parameter. This is in agreement with the growth rate evolution presented in Fig. 20(b), where there is a large delay of appearance of MI when γ_2 increases. It also comes out that the interplay between the nonlinearity parameters gives rise to MI for all the values of the wave number k associated with the plane wave. We now focus on the direct numerical integration of Eq. (3.4). Implementing the split-step Fourier method, we consider as initial condition

$$
\psi\left(x, z = 0\right) = \psi_{TF}\left[1 + \varepsilon\cos(kx)\right], \tag{3.23}
$$

where ψ_{TF} is the Thomas-Fermi function approximated as $\psi_{TF} \approx 1 - V\left(x\right)/2$ [109], and ε is a small perturbation. The values of the parameters are chosen to be $\varepsilon = 10^{-2}$, $k = 1$, $\gamma_1 = 0.2$, $\gamma_2 = 1$ and the results of the numerical integration are presented in Fig. 21. Fig. 21(a) depicts the development of MI in the system at position $z = 8$. The generation of several modulated waves with different magnitudes is observed at this position. We note that the magnitude of the pulse

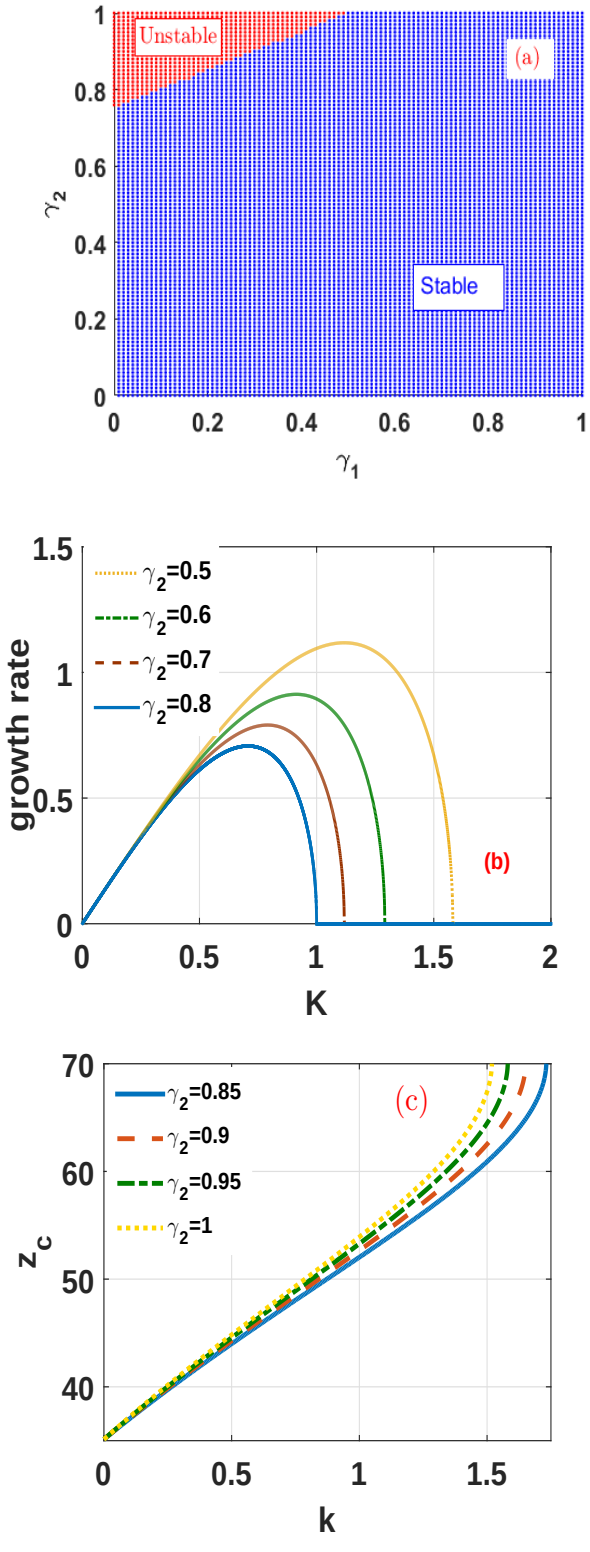

Figure 20: Analytical results on MI in the **AR** mode: (a) The stability diagram shows two areas. Regions of stability are in blue, while red regions are those for instability, with the parameters $S_1 = -1$, $S_2 = 1$, $\eta_0 = 1$, $k = 1$. (b) Profile growth rate of instability for different values of γ_2. (c) Critical distance scale $z_c(k)$ with increasing the values of three-body interaction. The physical parameters are: $\gamma_1 = 1$ and $\alpha = 0.0005$.

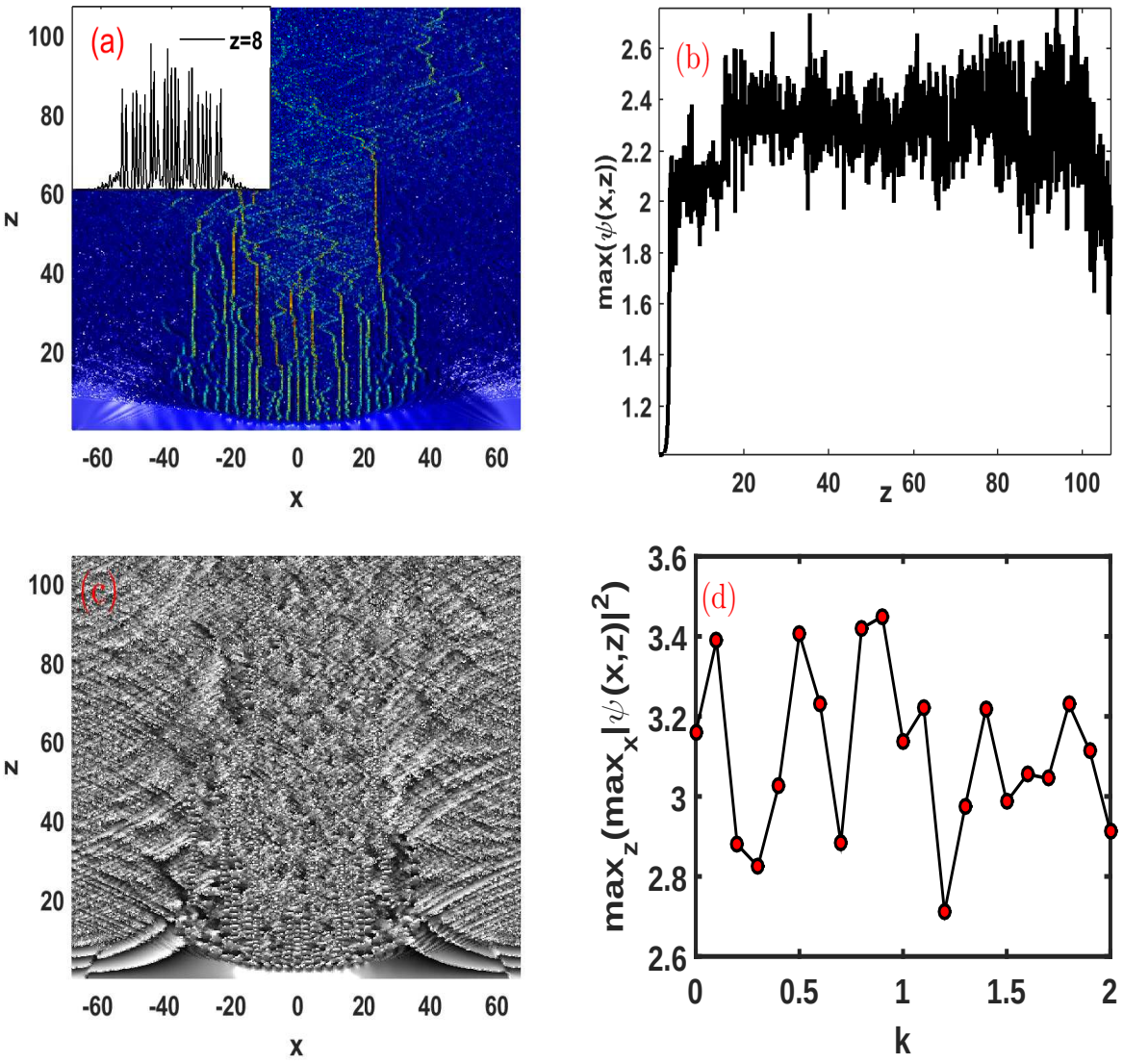

Figure 21: MI patterns in the **AR** mode: (a) Spatiotemporal evolution of the modulated plane wave. (b) Evolution of peak of intensity versus the propagation distance. (c) Dynamics of phase and maximal peak versus the wave number, with the characteristic parameters of the medium being: $S_1 = -1$, $S_2 = 1$, $\phi_0 = 1$, $k = 1$, $\gamma_1 = 1$, $\gamma_2 = 0.2$, $\alpha = 0.0005$, and $\varepsilon = 0.01$.

increases while the width decreases. The evolution of maximum intensity and phase of intensity are illustrated respectively in Fig. 21(b) and Fig. 21(c) and support the emergence of MI. We note that the plane wave does not return to its initial position, but increases continuously. In Fig. 21(d), we observe the impact of the wave number on MI as predicted by Eq.(3.43), where all real values of the wave number predict MI. We note that for $k = 0$, we get MI and it is accentuated around $k = 1.5$ and not far from $k = 1.8$, where the magnitude of MI gets lower. From analytical and numerical treatments, we can conclude that the system supports MI depending on the nonlocal contribution of the cubic and quintic parameters.

3.3.3.2 Repulsive-Attractive case (RA)

We are now interested in the case where the two-body nonlinearity is repulsive $(S_1 > 0)$, while the three-body nonlinearity is attractive $(S_2 < 0)$. The permutation of the sign of strength of nonlinearity is possible with double Feshbach resonance technique. Analytical plots are shown in Fig. 22, where the right panel illustrates the symmetry distribution of areas of stability, considering $S_1 = 1$ and $S_2 = -1$. Fig. 22(b) presents the reduction of the growth rate with increasing the value of the three-body nonlocality as a function of the wave number. Fig. 22(c) depicts the critical distance as a function of the wave number. For greater values, above the wave number $k = 0.5$, we observe that the critical distance decreases with increasing the value of the three-body nonlocality γ_2. This can be understood as a *reduction* of the MI process when the value of γ_2 increases. The numerical results of MI in repulsive-attractive mode are illustrated in Fig. 23. The direct numerical integration was done with $\gamma_1 = 1$ and $\gamma_2 = 0.4$. In the inset of Fig. 23(a), we have the transverse profile of intensity at position $z = 8$, where we observe the generation of nine sub-pulses. We note that the behaviors of magnitude and width of pulse are similar to the ones in the previous regime. The discrepancy between those regimes lies on the number of generated sub-pulses, which is smaller than in the AR mode. The intensity of modulated wave is maximal at $x = 0$. conversely to the case of RA, where it is minimal. In Fig. 23(b), we present the evolution of the maximum of intensity with respect to the propagation distance, and Fig. 23(d) shows the evolution of the maximum peak of the plane wave as a function of the wave number. Here, the maximum of MI occurs at $k = 2$ and the minimum intensity at $k = 1.2$. As a whole, it is obvious that the competing effects (AR and RA) lead to the generation of MI despite the observed discrepancies.

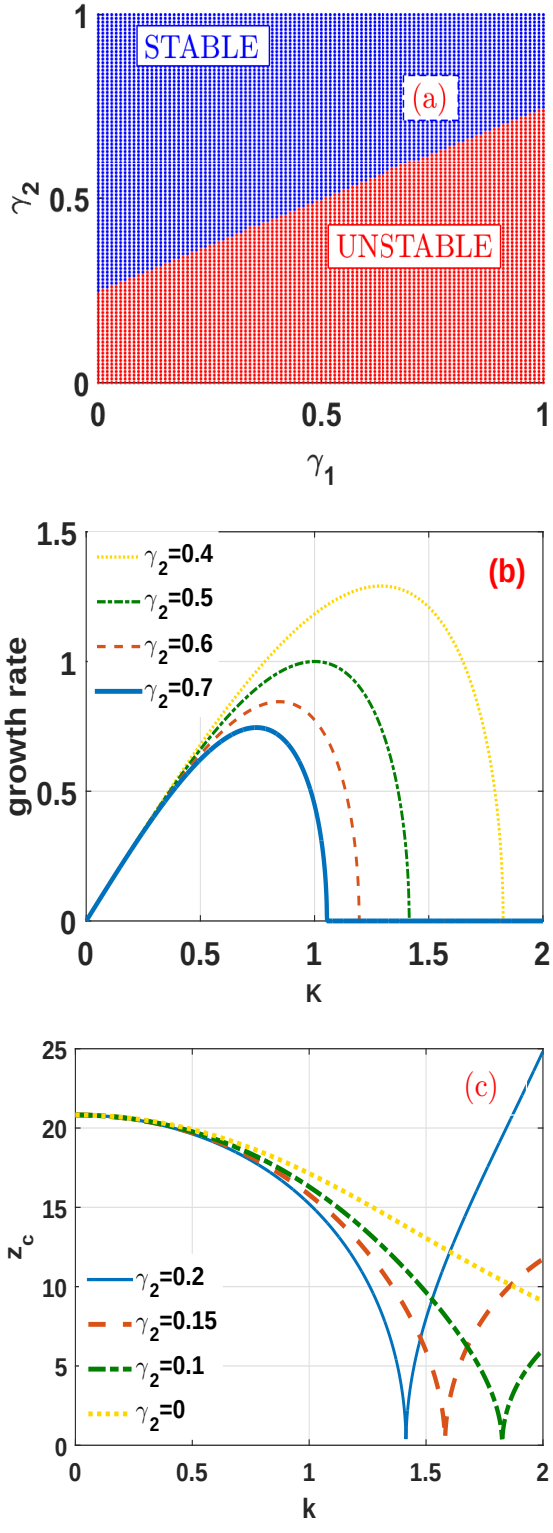

Figure 22: Analytical results on MI in the **RA** mode: (a) Stability/instability diagram illustrating two symmetrical areas. with the blue one being the region of stability and the red one, the region of instability, with $S_1 = 1, S_2 = -1, \eta_0 = 1, k = 1$. Panel (b) shows the profile of growth rate of instability for different values of the nonlocal quintic nonlinearity, and panel (c) depicts critical distance scale $Z_c(k)$ with increasing values of nonlocal quintic nonlinearity. The used physical parameters are: (b) $\gamma_1 = 1$ and (c) $\gamma_1 = 1, \alpha = 0.0005$, while the other parameters remain unchanged.

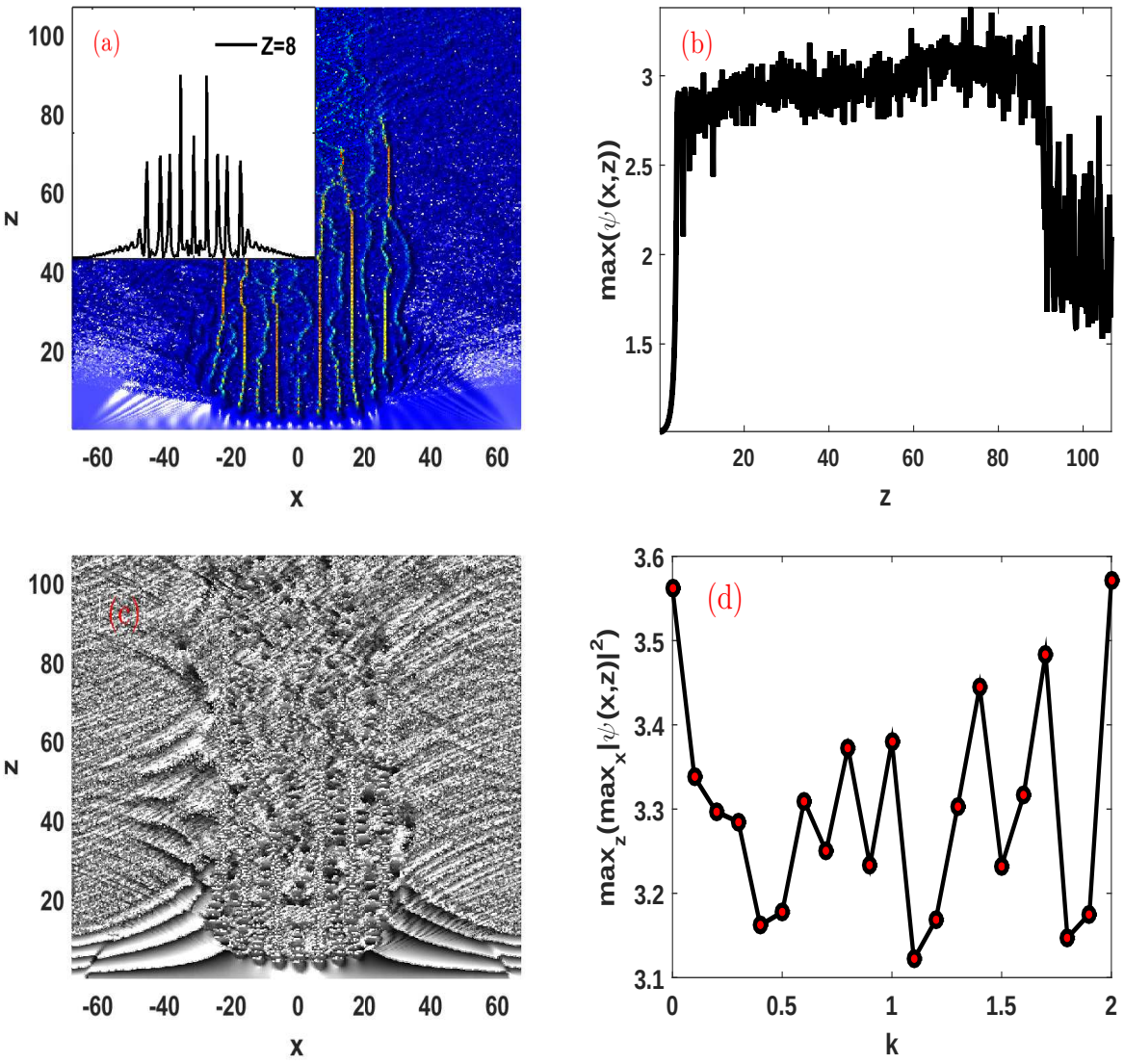

Figure 23: MI manifestation in the **RA** mode: (a) Spatiotemporal evolution of the modulated plane wave. (b) Evolution of the peak of intensity versus the propagation distance z. (c) Dynamics of phase and (d) Maximal peak versus the wave number. The characteristic parameters of the medium are: $S_1 = 1, S_2 = -1, \phi_0 = 1, k = 1,\ \gamma_1 = 1,\ \gamma_2 = 0.4, \alpha = 0.0005, \varepsilon = 0.01$.

3.3.3.3 Double-Attractive case (AA)

We follow the scheme in section (3.2) to investigate the system considering a medium where the cubic and quintic nonlinearities have the same sign ($S_1 = S_2 = -1$). Analytical results, obtained from Eqs. (3.16)-(3.17), are plotted in Fig. 24, where panel (a) shows the stability diagram of the plane wave. We note a large domain of nonlocality parameter, where MI occurs. The gain spectra of the MI for different values of the quintic nonlocality is illustrated in Fig. 24(b), where we also observe values of the quintic nonlocal parameter. This reduction is characterized by the shrinking of the bandwidth and decreasing of the maximum growth rate. In Fig. 24(c), we observe, with increasing values of nonlocality γ_2, the decreasing of critical distance with increasing of wave number. Fig. 25 illustrates the numerical evolution of MI of the plane wave with double focusing nonlinearities.

Fig. 25(a) considers the propagation with $\gamma_1 = 1$ and $\gamma_2 = 0.4$, where the inset presents the transverse intensity of plane wave at position $z = 8$. This position shows 13 sub-pulses chain with the maximal sub-pulse intensity occurring at $x = 0$. In Fig. 25(b), we observe the evolution of the maximum of intensity. The dynamics of phase wave is illustrated in Fig. 25(c). Fig. 25(d) shows the curve of the maximal amplitude (over space and time) where the discrete points indicate the maximum amplitude of the plane wave. It appears that with the wave number $k = 1.5$, MI is maximal. However, around $k = 1$, MI has its minimal amplitude. In general, MI appears for weakly nonlocal nonlinearities, where cubic and quintic terms can be of the same sign or not.

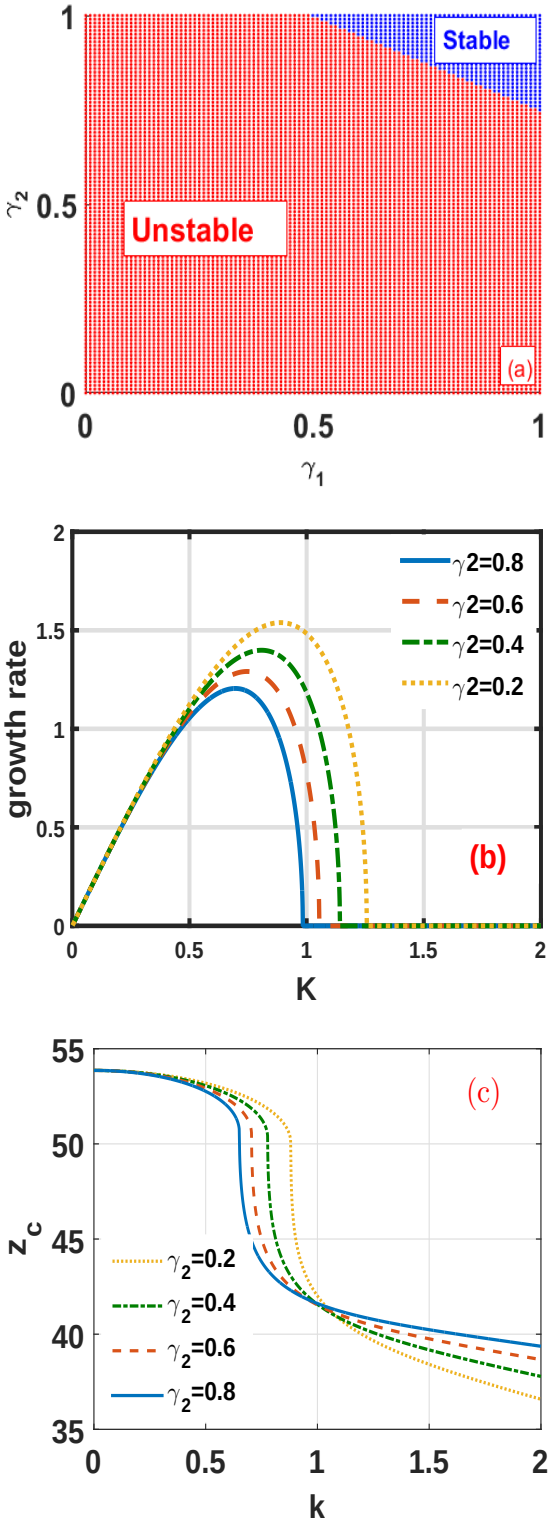

Figure 24: MI in the **AA** regime, where panel (a) shows the stability/instability diagram of plane wave, The blue region being for stability and red region being for instability. Panel(b) shows the profile of the growth rate of instability for different values of the three-body nonlocal interaction. Panel (c) depicts the critical distance scale $Z_c(k)$, when the three-body nonlocal interaction becomes stronger. The used physical parameters are: (a) $S_1 = -1$, $S_2 = -1$, $\eta_0 = 1$, $k = 1$. (b) $\gamma_1 = 1$, (c) $\gamma_1 = 1$, and $\alpha = 0.0005$.

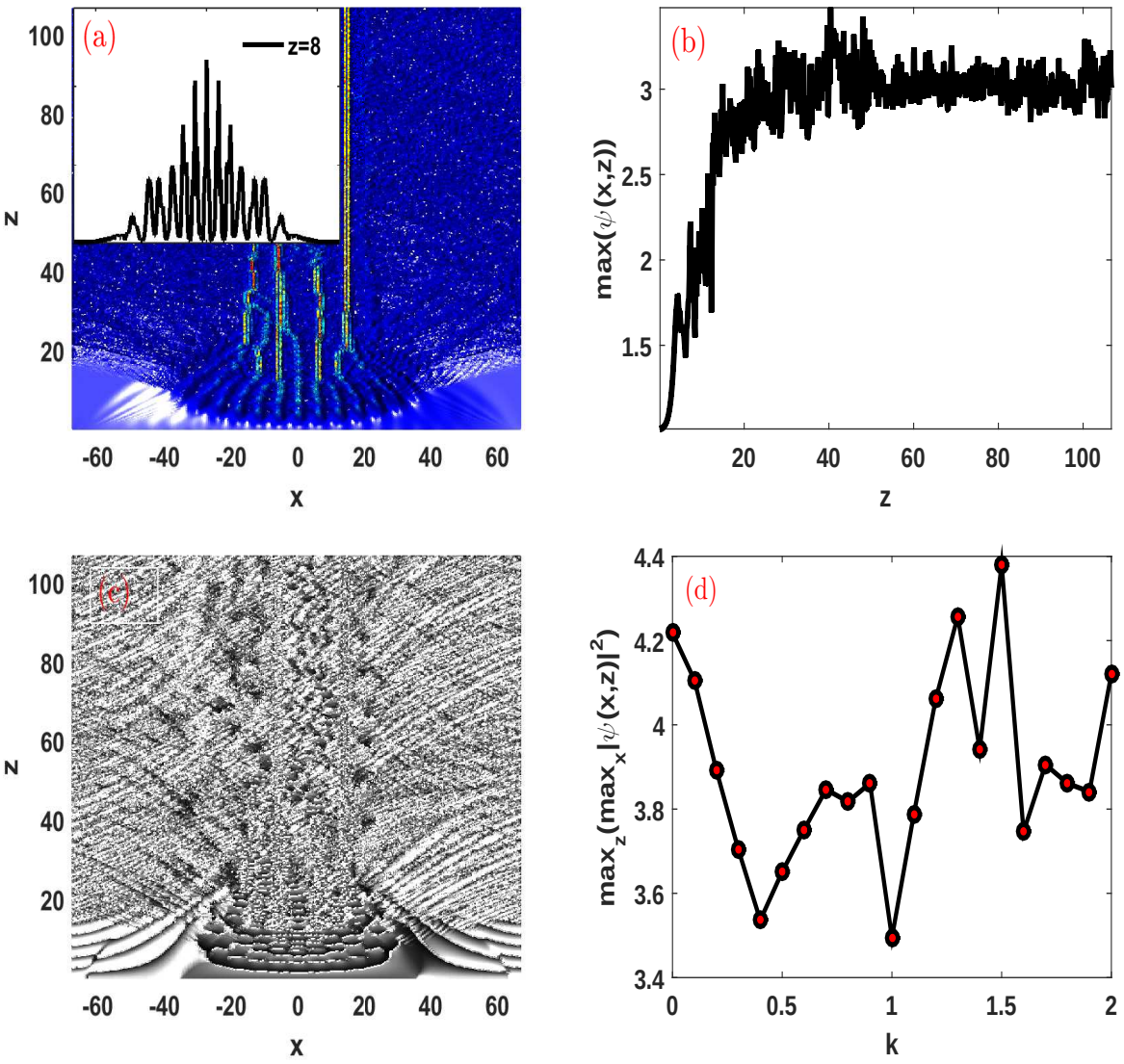

Figure 25: MI manifestation in the AA mode, where panel (a) pictures the spatiotemporal evolution of the modulated plane wave. Panel (b) shows the evolution of the peak of intensity versus the propagation distance. Panel (c) shows the dynamics of phase panel (d) shows the maximal peak versus the wave number, with the parameters: $S_1 = -1, S_2 = -1, \phi_0 = 1, k = 1$, $\gamma_1 = 0.4$, $\gamma_2 = 1$, $\alpha = 0.0005$, and $\varepsilon = 0.01$.

3.3.3.4 Effect of three-body interaction media

It has been well established that Rogue waves are the nonlinear manifestation of MI. This is due to the suitable balance between nonlinear and dispersive effects. In this particular study, the model involves competing nonlinearity, which implies that their combined effects are of importance in the emergence of nonlinear waves. In this regard, considering only the quintic nonlocal nonlinearity, we obtain the features of Fig. 26 which clearly show the appearance of trains of Akhmediev breathers (ABs), characterized by periodic peaks of the wave intensity during the propagation, as the result of the three-body interaction.

ABs describe the dynamics of MI for the NLSE in time and space and have been observed in a broad range physics areas actually related to plasma systems [173], biological molecules [174, 175], nonlinear optics [176, 177] and BECs [178], just to cite a few. For $\gamma_2 = 0.05$ and the parameter values $k = 0.75$, $S_2 = -0.5$, and $\varepsilon = 10^{-4}$, the ABs that initially appears thereafter adopts some erratic features as time increases. This is further demonstrated by Fig. 26(b) which shows the phase-plane between the imaginary part of the wave as a function of its real part. With increasing γ_2 to 0.1, the time and spatial expansion of the breathing patterns get affected as shown in Figs. 26(c) and (d). This situation appears particularly in some systems modeling the three-body interaction in BEC or extension of Tonk-Giradeau gaz with nonlocality [179]. In Fig. 27, the same calculations have been repeated, but in presence of both the cubic and quintic nonlinearities. Specifically, γ_2 taking the same values as previously, we have fixed $\gamma_1 = 1$. In Fig. 27(a) and (b), MI still manifests itself through the emergence of AB, which also get erratic when time increasing, with $\gamma_2 = 0.05$. The case $\gamma_2 = 0.1$ also shows ABs as displayed in Fig. 27(c), but the cyclic-like behavior of the phase plane of Fig. 27(d) confirms the robustness of ABs in the study of MI.

This however depends on the medium properties which can bring about new properties to the NLS equations as it is the case in this work. It has also been demonstrated that the emergence of ABs in NLS systems is closely related to the Fermi-Pasta-Ulam (FPU) recurrence phenomenon, mainly when some additional effects such as third-order dispersion or varying dispersion, or even the impact of initial excitation of MI are included [180, 181]. In the meantime, we should stress that the study of such phenomenon is not the concern of the present work, but we suspect it to take place when suitable values of all the parameters involved in the MI phenomenon are chosen. This study will comprehensively be addressed in a forthcoming work.

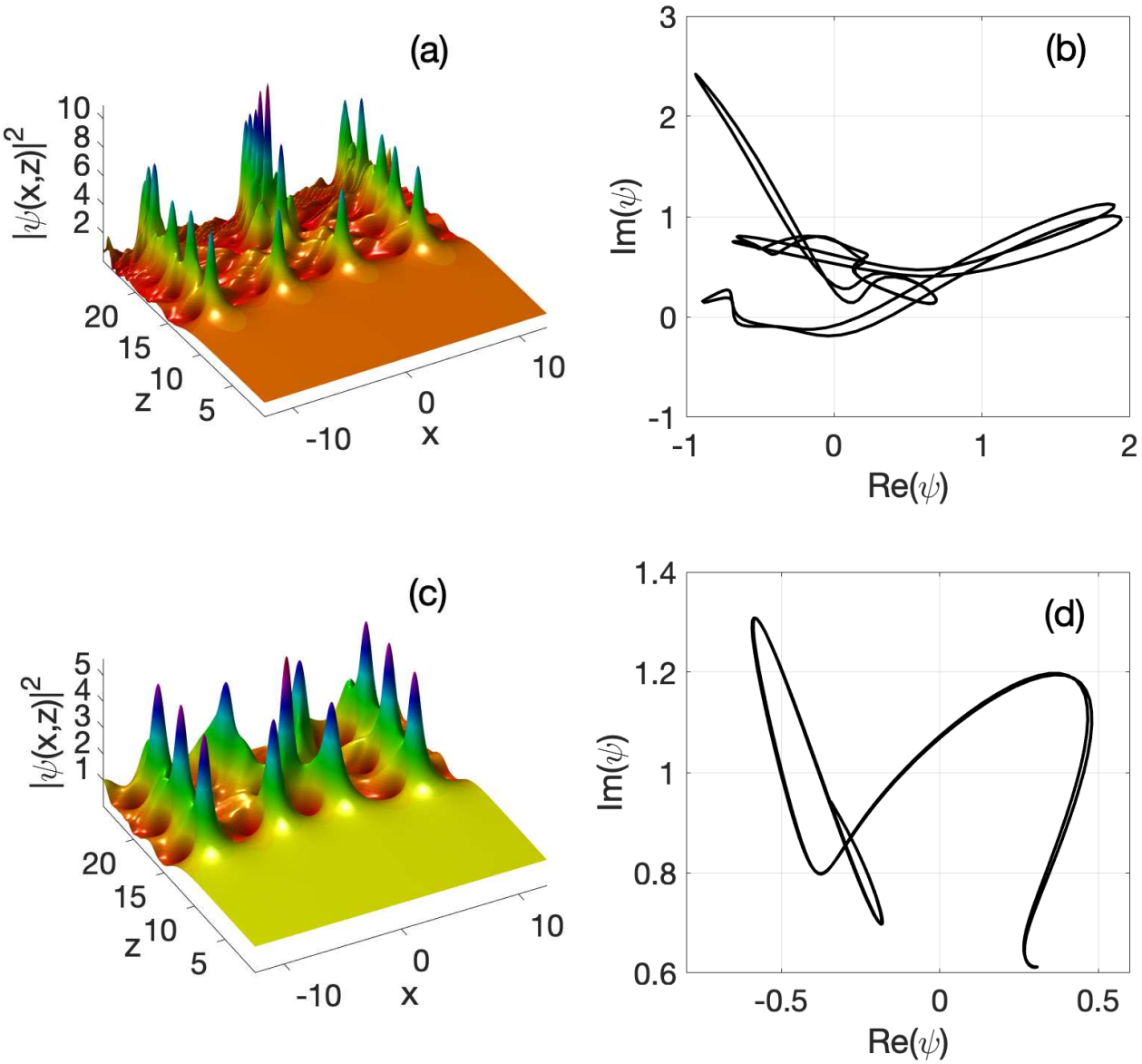

Figure 26: MI manifestation when the two-body nonlocal interaction is switch off, with $S_1 = 0$, $\phi_0 = 1$, $k = 1.5$, $\varepsilon = 0.0001$, $\alpha = 0$. The left panels (a) and (c) show the focusing case, $S_2 = -0.5$, with $\gamma_2 = 0.05$ and $\gamma_2 = 0.1$, respectively, and the right panels (b) and (d) show trajectory cycles of the phase.

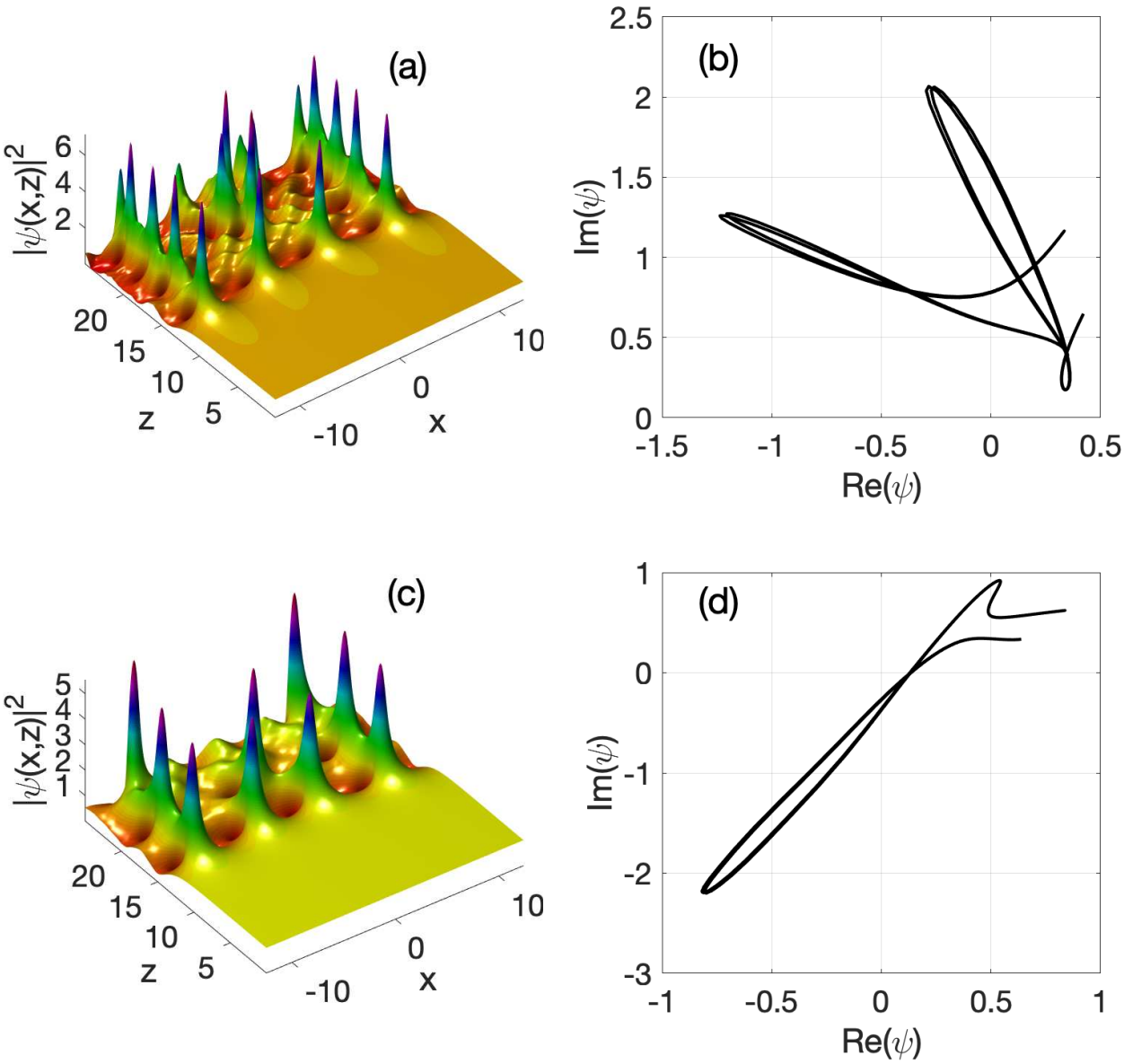

Figure 27: MI manifestation when the two-body nonlocal interaction is switch on, with $S_1 = 0.1$, $\phi_0 = 1$, $k = 1.5$, $\varepsilon = 0.0001$, $\alpha = 0$, $\gamma_1 = 1$. The left panels (a) and (c) show the focusing case, $S_2 = -0.5$, with $\gamma_2 = 0.05$ and $\gamma_2 = 0.1$, respectively, and the right panels (b) and (d) show trajectory cycles of the phase.

3.4 Generation of solitons in doped fiber with higher-order correction terms

In telecommunication systems, the principal role of a dopant is to boost the transmission of optical waves through the optical fiber. Often called the rare-earth or Lanthanide, the dopants form a group of 14 similar elements with atomic numbers ranging from 58 to 71 [145]. To understand the great contributions and specifications of any dopant, several publications were issued in the last three decades. For example, Ytterbium-doped fiber [182, 183, 184], Thulium doped fiber [185], and Erbium-doped fiber [186, 187, 188, 189, 190]. Their ionized forms confered to them particular proprieties when they are doped in silica or glass fiber. This singularity is exhibited by the susceptibilities where orders and combinations play an important role in its specification. Furthermore, the competing between susceptibilities was observed, when silica was doped in the case of semiconductor and for optical fiber [191]. Beneath the action of the dopant, the order of susceptibility may increase up to **7**. Then, the material may exhibit χ^3 χ^5 and χ^7 (cubic, quintic and septic) susceptibilities [192, 193]. It is important to point out that those materials exhibit a saturation of the third-order nonlinear susceptibility χ^3 which is equivalent to the presence of fifth and seventh-order nonlinear susceptibilities χ^5 and χ^7. Experimental results have been obtained with the material sample A_{s2s3} enabling the measure of the septic order susceptibility. Recent researches experimented with this new chalcogenide material, and it was used in the propagation of ultrashort femtosecond optical pulse [192, 193]. The dopant introduces linear and nonlinear effects such as dispersion with higher-order, which plays a crucial role in the propagation of optical pulses [34, 146, 147, 148, 194, 195, 196, 197, 198, 199].

Optical solitons through a doped or undoped fiber leads to several applications like optical atomic clocks, photonic radar, coherent communications, ultrafast distance measurements, optical frequency synthesizer [22].

A great interest is noted for higher order nonlinear systems [34, 146, 147, 148, 126, 200]. These systems can be used to exhibit ultra-short optical solitons at a very high bit rate and for performance improvement along with trans-oceanic and trans-continental distances. The aim of this paper is to study the generation of optical soliton in doped fiber where many nonlinear phenomena such as self-steeping effect and their correct terms, self-shifting effect, and their correction terms are taken into account. In this study, we shall investigate the MI gain of the CGL equation which contains higher -order dispersion, higher order non-Kerr nonlinearities, as well as higher-order self-steepening and self-shifting terms.

3.4.1 Theoretical model

In this subsection, we consider the higher-order CGL equation with non-Kerr nonlinearities terms, written as [201]

$$i\psi_{\xi}+\sum_{j=2}^{6}d_{jrs}\psi_{j\tau}+\gamma_{rs}\psi+\sum_{k=1}^{3}\left[\left(q_{krs}|\psi|^{2k}+m_{kr}|\psi|_{\tau}^{2k}\right)\psi+in_{ks}\left(|\psi|^{2k}\psi\right)_{\tau}\right]=0, \tag{3.24}$$

where $\psi(\xi,\tau)$ is a paraxial beam. The coordinate ξ is the propagation distance and τ is the retarded time in the frame moving with the pulse. The expressions of the parameters in (3.24) are given in Appendix A.

3.5 Linear stability analysis

In this section, we investigate the MI, based on (3.24). The general idea of linear stability analysis is to perturb the steady-state solution and then analyze whether this small perturbation decays or grows with the propagation. The continuous wave (CW) solution to (3.24) is assumed to be of the form

$$U(\xi)=\sqrt{P_0}\exp\left(i\chi(\xi)-(\gamma_s-i\gamma_r)\,\xi\right), \tag{3.25}$$

where P_0 is the input power of CW, $\chi(\xi)$ is the nonlinear phase shift given by:

$$\chi(\xi)=iq_{1r}\left(\int_0^{\xi}P_0\exp\left(-2\gamma_s\xi\right)d\xi\right)+iq_{2r}\left(\int_0^{\xi}P_0^2\exp\left(-4\gamma_s\xi\right)d\xi\right)+iq_{3r}\left(\int_0^{\xi}P_0^3\exp\left(-6\gamma_s\xi\right)d\xi\right). \tag{3.26}$$

To study the MI phenomena, we add a small perturbation to the CW solution and explore the growth of the perturbation as

$$U(\xi,\tau)=\left(\sqrt{P_0}+u(\xi,\tau)+iv(\xi,\tau)\right)\exp\left(i\chi(\xi)-(\gamma_s-i\gamma_r)\,\xi\right), \tag{3.27}$$

where $u(\xi,\tau)$ and $v(\xi,\tau)$ are the real and imaginary parts of small perturbation, respectively. Substituting (3.27) into (3.24) and after some mathematical manipulations, we obtain the following set of linearized equations for disturbance behaviours:

$$\begin{aligned}&u_{\xi}+\sum_{n=2}^{6}\left(d_{ns}u_{n\tau}+d_{nr}v_{n\tau}\right)+P_0\left(3\,n_{1s}+5\,n_{2s}P_0A_{\xi}^2+7\,n_{3s}{P_0}^2A_{\xi}^4\right)A_{\xi}^2u_{\tau}\\&+2{P_0}^2\left(q_{2s}+2\,q_{3s}P_0A_{\xi}^2\right)A_{\xi}^4u=0,\end{aligned} \tag{3.28}$$

$$\begin{aligned}&v_{\xi}+\sum_{n=2}^{6}\left(d_{ns}v_{n\tau}-d_{nr}u_{n\tau}\right)+P_0\left[\sum_{n=1}^{3}\left(-2nP_0^{(n-1)}\,m_{rn}u_{\tau}+n_{ns}v_{\tau}\right)A_{\xi}^{2(n-1)}\right]A_{\xi}^2\\&-2P_0\left(q_{1r}+4\,q_{2r}P_0A_{\xi}^2+6\,q_{3r}{P_0}^2A_{\xi}^4\right)A_{\xi}^2u=0.\end{aligned} \tag{3.29}$$

We acknowledge the presence of n_{ns} in those equations and $A_\xi = \exp(\gamma_r \xi)$. To solve the set of linear differential equations above, we assume the following ansatz states [202]:

$$u(\xi,\tau) = u_0 \exp\left[i \int K(\xi)\, d\xi - i\Omega\tau\right], \tag{3.30}$$

$$v(\xi,\tau) = v_0 \exp\left[i \int K(\xi)\, d\xi - i\Omega\tau\right], \tag{3.31}$$

where K and Ω are the waves vector and the frequency of the perturbation amplitude, respectively. Here, u_0 and v_0 are the perturbation amplitudes of anti-Stokes or backward (if its argument is negative) and Stokes sidebands or forward (if its argument is positive), respectively. Introducing (3.30) and (3.31) into (3.28) and (3.29), we obtain a set of two linearly coupled equations satisfied by u_0 and v_0 for non-trivial solutions. The nontrivial solution is such that

$$(K(\xi,\Omega) + g_{rs})^2 = \Gamma + i\Lambda, \tag{3.32}$$

where the real part of g_{rs} is given as :

$$g_r = P_0 A_\xi^2 \left(2n_{1s} + 3A_\xi^2 n_{2s} P_0 + 4A_\xi^4 n_{3s} {P_0}^2\right)\Omega + d_{5s}\Omega^5 - d_{3s}\Omega^3, \tag{3.33}$$

and the imaginary part is defined as :

$$g_s = -d_{6s}\Omega^6 + d_{4s}\Omega^4 - d_{2s}\Omega^2 + {P_0}^2 A_\xi^4 \left(2\, q_{3s} P_0 A_\xi^2 + q_{2s}\right). \tag{3.34}$$

Γ and Λ are expressed as the sum of the even and odd order of Ω, respectively. $\Gamma = \sum_{n=0}^{6} A_{2n}\Omega^{2n}$, and $\Lambda = \sum_{n=1}^{6} A_{2n-1}\Omega^{2n-1}$, A_n coefficients are defined in Appendix B. The roots of (3.32) are related to the sign of Λ. We will obtain two distinguishable cases.

(i) $\Lambda < 0$, the expressions of these roots are written as :

$$K_1(\xi,\Omega) = g_r + h_1 + i(g_s - h_2), \tag{3.35}$$

$$K_2(\xi,\Omega) = g_r - h_1 + i(g_s + h_2), \tag{3.36}$$

where

$$h_1 = \sqrt{\frac{1}{2}\left(\Gamma + \sqrt{\Gamma^2 + \Lambda^2}\right)},$$

$$h_2 = \sqrt{\frac{1}{2}\left(-\Gamma + \sqrt{\Gamma^2 + \Lambda^2}\right)}.$$

(ii) $\Lambda > 0$, we have

$$K_1^*(\xi,\Omega) = g_r - h_1 + i(g_s - h_2), \tag{3.37}$$

$$K_2^*(\xi,\Omega) = g_r + h_1 + i(g_s + h_2), \tag{3.38}$$

leading to solutions with the same asymptotic behavior as those obtained from K_1, and K_2. The complex form of K_1 and K_2 make it difficult to predict their signs. Nevertheless, their imaginary parts contribute on the system. Introducing (3.37) into two ansatzes, (3.30) and (3.31) provides a good and clear understanding of the behavior of these wave solitons. The quantity h_2 is always positive that is $g_s - h_2 < g_s + h_2$ holds, this behaviour depends on the sign of the quantity $g_s - h_2$ which corresponds to the imaginary part of K_1. The asymptotic behaviour of (3.30) and (3.31) is related to the constant $g_s - h_2$. If $g_s < 0$, then $h_2 - g_s$ is always positive and the solution of (3.30) and (3.31) increases exponentially when ξ goes towards to infinity. The system remains unstable under modulation. In this case, the boundaries of the domain of the MI are then given by $-\Omega_0(\xi) \ll \Omega(\xi) \ll \Omega_0(\xi)$, where

$$\Omega_0^2(\xi) = \sqrt[3]{C_0 + \frac{C_1}{18}} + \sqrt[3]{C_0 - \frac{C_1}{18}} + \frac{d_{6s}}{3d_{4s}}, \tag{3.39}$$

If $g_s > 0$, the asymptotic behaviour of wave solution will depend on the sign of $h_2 - g_s$.

When $\omega = \omega_0$, it is easy to distinguish two cases. For $h_2 - g_s > 0$, i.e, $g_s - h_2 < 0$, i.e., $I_m(K_1) < 0$, where $I_m(K_1)$ represents the imaginary part of K_1, the solutions (3.30) and (3.31) diverge without limitation as ξ increases and the corresponding solution is said to be modulationally unstable. The criterion for the modulutional instability of stokes waves is such that

$$0 > -\frac{(2g_s^2 - h_{11})}{2P\Omega^2} > -Y + d_{2r}q_{1r} - d_{2s}q_{1s}, \tag{3.40}$$

where h_{11} is defined as :

$$h_{11} = -18\,P_0^6 {q_{3s}}^2 - 24\,P_0^5 q_{2s}q_{3s} + \left(-8\,{q_{2s}}^2 - 12\,q_{3s}q_s\right)P_0^4 - 8\,P_0^3 q_{2s}q_{1s} - 2\,P_0^2 {q_{1s}}^2,$$

where $Y = Y_{11} + Y_0 + 2\left(d_{4s}q_{2s} - d_{4r}q_{2r}\right)P_0\Omega^2 + 3\left(d_{6r}q_{3r} - d_{6s}q_{3s}\right)P_0^2\Omega^4$, with

$$Y_0 = {d_{6\,r}}^2\Omega^{12} + {d_{4\,r}}^2\Omega^8 + {d_{5s}}^2\Omega^{10} + {d_{3s}}^2\Omega^6 + {d_{2\,r}}^2\Omega^4 + \left(25\,{n_{s3}}^2 P_0^6 + 13\,{n_{s2}}^2 P_0^4\right)\Omega^2,$$

and Y_{11} is given in Appendix B. From Lange-Newell's criterion, our system is such that

$$-Y_{11} + d_{2r}q_{1r} - d_{2s}q_{1s} + 2\left(d_{4s}q_{2s} - d_{4r}q_{2r}\right)P_0\Omega^2 + 3\left(d_{6r}q_{3r} - d_{6s}q_{3s}\right)P_0^2\Omega^4 < 0. \tag{3.41}$$

It is important to recall that Lange-Newell's criterion was derived for the first time for the Hamiltonian system in Ref [203], and for discrete and continuous dissipative systems [204, 205, 206]. The numerical results from the previous analytical treatments are presented below.

3.5.1 Numerical simulations

Theoretical investigation of MI through the model under consideration in (3.24), indicates the possibility of observing the regions of instability in the frequency spectra. The MI spectra are given by the negative imaginary part of the dispersion relation. In this study, we have two opportunities to obtain the MI gain. Firstly, when $\omega_0 = \omega_a$, the growth rate is defined as:

$$g(\Omega) = 2(g_s + h_2), \tag{3.42}$$

and when $\omega_0 \neq \omega_a$, the growth rate is given in the following integral form

$$g(\Omega) = -2\int_0^L (g_s + h_2)\, d\xi \tag{3.43}$$

[144, 202]. Below, it is referred to the integrated MI. This analysis is necessary however it is also limited to give the proprieties of MI phenomena. We use the split-step Fourier method to observe numerical evolution of the disturb wave as well as the dynamics of soliton. Therefore, we consider the initial condition as [202]

$$\psi(0,\tau) = \sqrt{P_0}\,(1 + a_m \sin(f_m \tau)) \exp(i\phi_{NL}), \tag{3.44}$$

with,

$$\phi_{NL} = \frac{P_0}{2\gamma_s}\left(q_{1r} + \frac{q_{2r}P_0}{2} + \frac{q_{3r}{P_0}^2}{3}\right),$$

where P_0 is the power, a_m and f_m are the modulated amplitude and frequency of a weak sinusoidal modulation imposed on CW beam respectively. We use the sensitivity analysis (SA) to observe a simultaneous physical effect, on the boundary conditions of the domain of the MI [151, 152, 153, 154, 155].

3.5.1.2 Cubic-quintic-septic complex Ginzburg-Landau *(CQSCGL)* equation

Here, all dispersion coefficients greater than two are considered to have a value of zero i.e; $d_{jrs} = m_{kr} = n_{ks} = 0$ for $j > 2$ and $k > 1$. We obtain the cubic-quintic-septic complex Ginzburg-Landau equation. This physical situation corresponds to the cubic quintic complex Ginzburg-Landau with septic nonlinearity as a correction term. It appears in physical processes of strong focusing nonlinearity. It is important to also observe the role played by q_{3r} and q_{3s} terms on MI. From the Lange-Newell criterion, the boundary of the domains of the MI is such that $\Omega^2 < \Omega_c^2$, where Ω_c^2 is the critical frequency of the disturbing wave defined as:

$$\Omega_c^2 = 2d_{2s}^{-2}(q_{1s}d_{2s} - q_{1r}d_{2r})P_0 + 4d_{2s}^{-2}(q_{2s}d_{2s} - q_{2r}d_{2r})P_0^2 + 6d_{2s}^{-2}(q_{3s}d_{2s} - q_{3r}d_{2r})P_0^3, \tag{3.45}$$

corresponding to $\omega_0 = \omega_a$. In this dissertation, we will, focus only in **the** normal regime i.e., $d_{2r} < 0$, associated to the following parameters with values: $q_{1r} = 5.10^{-1}$, $q_{1s} = -48.10^{-2}$, $q_{2r} = -34.10^{-2}$, $q_{2s} = -34.10^{-2}$, $d_{2r} = -0.5$, $d_{2s} = 0.1$, $\gamma_s = -3.10^{-3}$, $L = 1500$, $f_m = 95.10^{-2}$ and $a_m = 95.10^{-3}$. Some values of parameters have been taken arbitrary, but closer to experiment values available in published papers in the literature [28, 128, 146, 195, 202]. Thus Figure 25 shows the MI spectrum as a function of second-order correction of Kerr nonlinearity and gain or loss nonlinearity, respectively. Figures 25(a) and (b) show that the MI gain increases

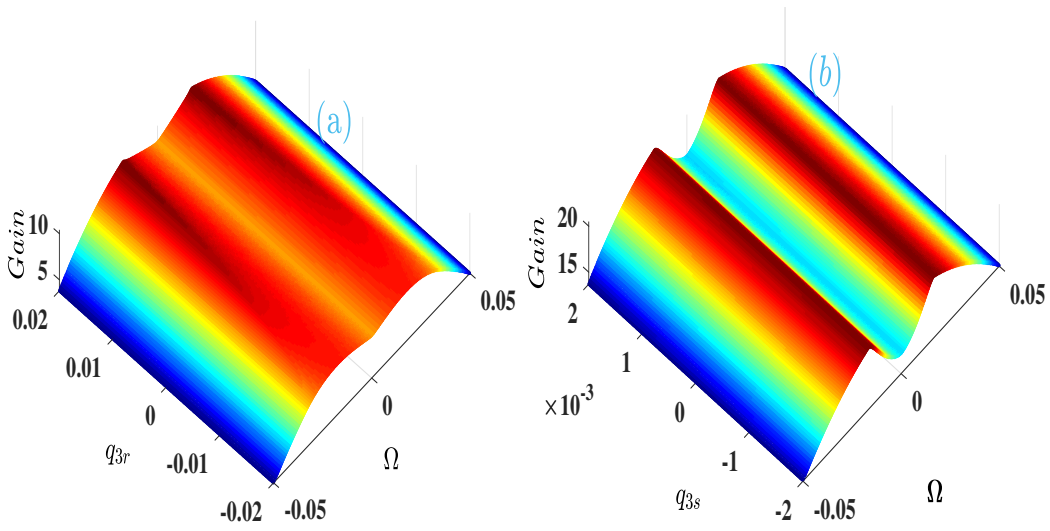

Figure 28: Instability gain spectra of CQSCGLE for : $P_0 = 1$, $\gamma_r = -9.10^{-3}$, (a) $q_{3s} = 1$, (b) $q_{3r} = 5.10^{-1}$

monotonously as septic non-Kerr nonlinearity increases. We observe uniform shapes of gain with an increase of septic gain/loss coefficient. In addition, two regions of instability of MI gain in the two diagrams above will appear. We also note that q_{3s} increases the modulation instability more than q_{3r}. This result is confirmed in Fig. 29, which illustrates the simultaneous physical effect in the boundary domain of MI. This result is obtained by sensitive analysis, where physical parameter values appear in (3.45). With this method, we have been able to obtain well-known results such as the growth of MI with an increase of the power input P_0, and the Kerr nonlinearity q_{1r}. At the same time, the first-order correction of gain nonlinearity q_{2s}, reduces the critical frequency which consequently reduces MI. We also observe a moderate influence of spectral filtering d_{2s}, dispersion d_{2r}, gain/ loss q_{1s} and quintic coefficient q_{2r}. To understand the physical effects of q_{3r} and q_{3s}, we introduce (3.44) into (3.24) and observe the numerical evolution of the perturb plane wave. Figure 27 illustrates the propagation of CW in the CQSCGL equation. Fig. 30(a) shows profile of CW in the plane (ξ, τ) , while in Fig. 30(b) we plotted the transverse distribution of the wave's intensity $\xi = 1$ (dashed line), $\xi = 225$ (dotted line) and $\xi = 1200$ (solid line). Initially, the plane wave has periodic transversal evolution

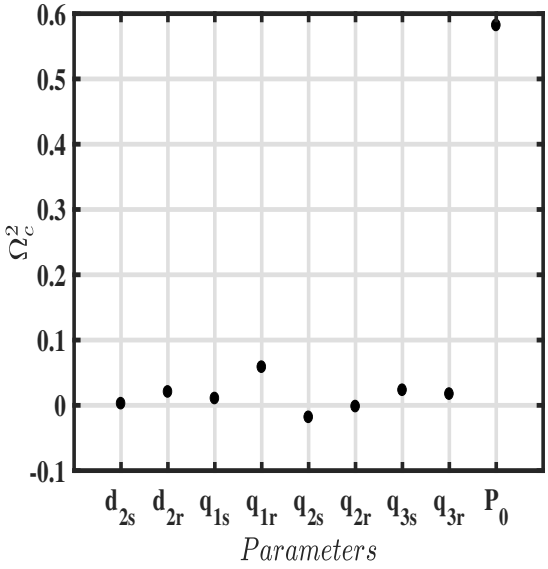

Figure 29: Influence of some physical effects on the frequency of the disturb wave using the sensitive analysis.

near the origin. Then, at $\xi = 225$, the intensity decreases, and sub-pulses occur between two pulses. So far, the intensity of CW increases and we observe a few generation of subpulses. The CW presents a chaotic behavior along with the distance of propagation. This is considered as a numerical property of MI in dispersive medium [144]. Fig. 30(c) shows evolution of CW when $q_{3r} < 0$ (defocusing case), and Fig. 30(d) presents evolution of Energy (solid line) and center-of-mass (dash line). These two quantities were already used in the bifurcation study of creeping solitons in dissipative systems [26]. Here, the position corresponding to the maxima of energy and dips of center-of-mass are the positions where the solitons are induced by the MI. The energy and center-of-mass are defined as:

$$Q = \int_{-\infty}^{\infty} |\psi(\xi,\tau)|^2 d\tau, \tag{3.46}$$

$$X_{CM} = \frac{\int_{-\infty}^{\infty} \tau |\psi(\xi,\tau)|^2 d\tau}{Q}.$$

The second order of correction of Kerr nonlinearity presents great advantages in dissipative system

3.5.1.2 Effects of higher-order dispersion coefficients

Now we will give our attention to the effects of high complex dispersion coefficients in MI. These physical situations appear in the optical fiber which presents the zero-dispersion wavelength.

3.5.1.3 Effect of the complex fourth order dispersion coefficient

We consider the optical fiber with complex third-order dispersion (TOD) and fourth-order dispersion (FOD) with the septic nonlinearity. The propagation model is equivalent to the

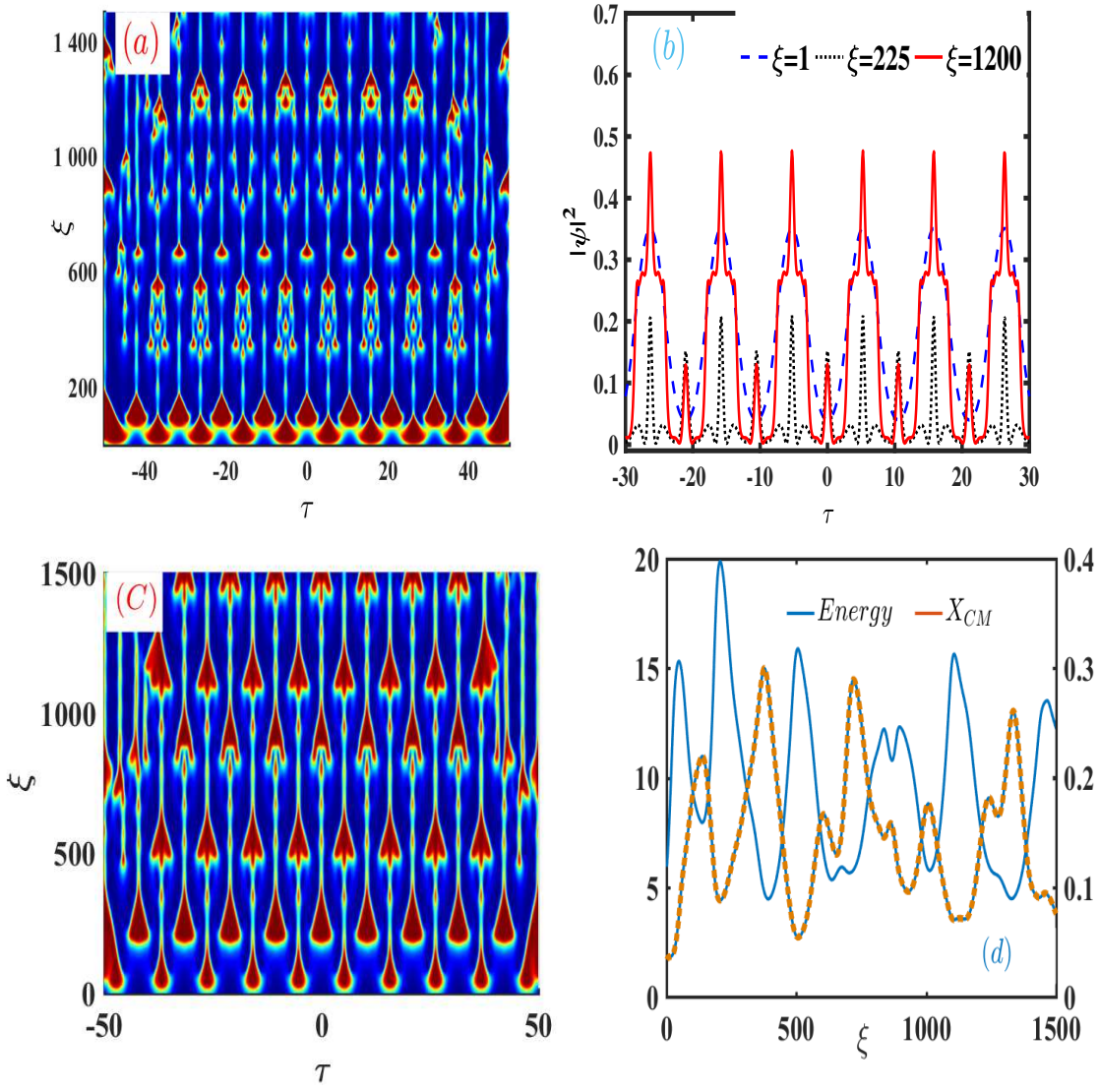

Figure 30: Second-order correction effect of Kerr nonlinearity on continuous wave propagation. Focusing case: (a) Propagation of Cw. (b) Distribution of intensity for $q_{3r} = 3.10^{-1}$. Defocusing case: (c) Propagation of Cw. (d) Comparison of energy and center-of-mass for $q_{3r} = -3.10^{-1}$.

modified complex Swift-Hohemberg equation (mCSHE), where $d_{3r} + id_{3s}$ will be considered as the lower-order correction of linear terms, γ_r the real linear loss, and the septic term conserves its previous value. Figure 28 illustrates the MI spectrum as a function of correction term d_{3r}.

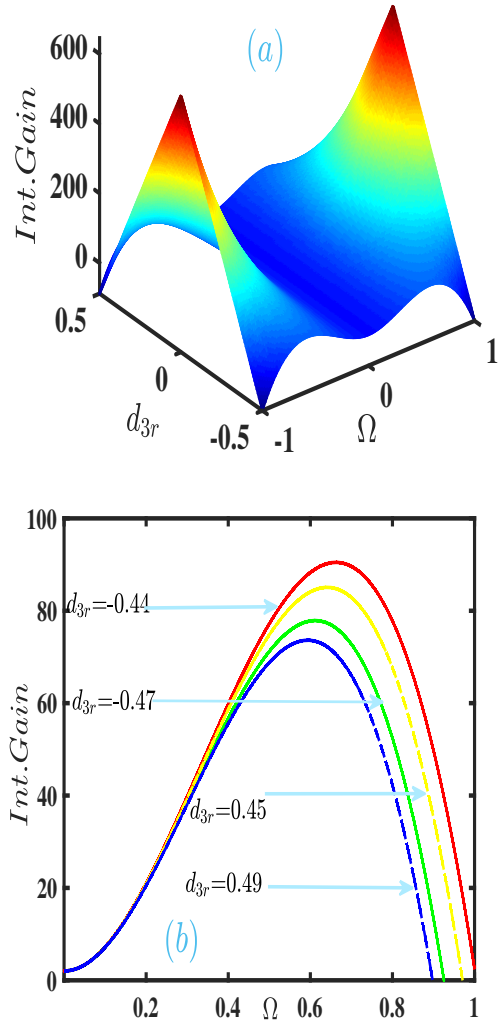

Figure 31: (a) 3D surface plot showing the integrated gain in the plane (Ω, d_{3r}) (b) Integrated gain in the plane (0, Ω) for the various values of d_{3r}, for $P_0 = 5.10^{-3}$, $d_{3s} = 4.10^{-2}$, $d_{4r} = 0$, $d_{4s} = -8.10^{-3}$. The other parameters are the same as in Fig1.

It appears that the integrated gain conserves their two regions of instability. As depicted in Fig. 31(a), we observe an increase of d_{3r} leading to an increase of the gain up to a maximum value, followed by a decrease. We note that this maximum value is obtained near the zero correction term. For a better understanding, Fig. 31(b) shows the variation of the integrated gain as a function of the frequency Ω, for different values of d_{3r}. The integrated gain increases

and decreases with increasing of the lower-order correction terms. Figure 29 shows the evolution of MI, beneath the correction effects. We observe the evolution of the pulse train along with the propagation distance as shown in Fig. 32(a). Fig. 32(b) also shows the energy for two different values of the correction term. The dashed curve is obtained for $d_{3r} = -15.10^{-3}$, for which the magnitude of energy decreases with the propagation distance. On the contrary, for solid curve, the magnitude of energy increases with ξ and the number of maxima is higher. It may be important to quantify the number of solitons induced by modulation instability for two different values of the physical effect. This is done using the bifurcation diagram.

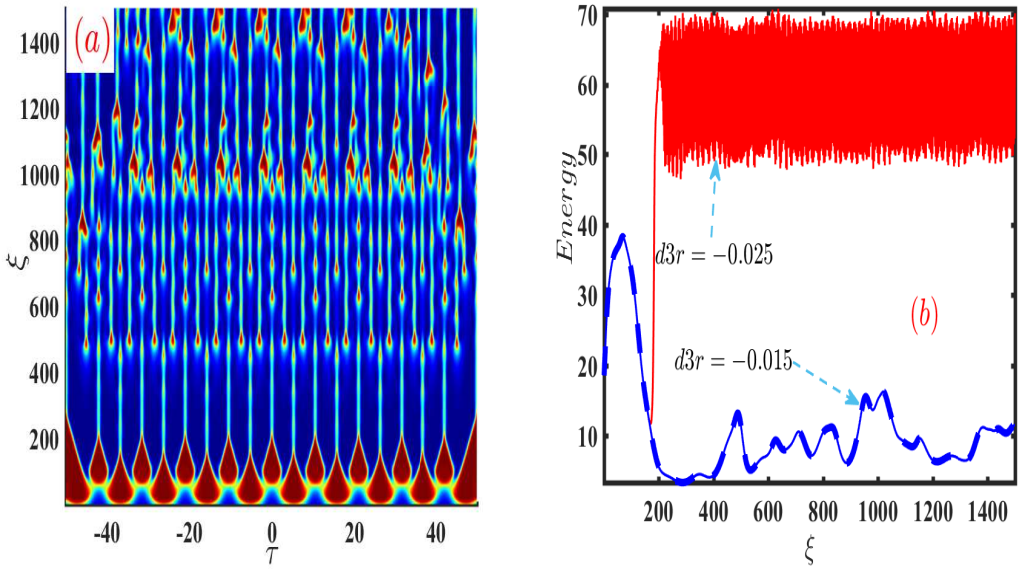

Figure 32: (a) Propagation of the perturbed wave. (b) Effect of dopant through the energy $d_{3r} = -25.10^{-3}$ (solide line), $d_{3r} = -15.10^{-3}$ (dashed line), the other physical parameters are: $P_0 = 1$, $q_{3r} = 3.10^{-1}$, $q_{3s} = 1$, $d_{3s} = 0.04$, $d_{4r} = 0$, $d_{4s} = -8.10^{-3}$, $\gamma_r = -99.10^{-4}$.

.

Figure 30 depicts the maxima (refering by Q_{max}) and minima (refering by Q_{min}) of energy as function of d_{3r}. The positions ofthe generation of solitons induced by the MI, the maxima obtained through the results of Q_{max}.

This diagram shows that for some values of the correction terms, the mCSHE produces many solitons with high energy. Depending on the value of d_{3r}, we observe that one, two, three, and four solitons having different energy can be generated simultaneously with the same propagation distance. That means that the lower-order correction term must not be neglected in optical fiber communications.

Figure 31 presents the integrated gain as a function of the frequency Ω and the fourth-order dispersion coefficient d_{4r}. The integrated gain is the same for positive and negative values of the frequency Ω for some selected values of the fourth-order dispersion (FOD) d_{4r} as can be

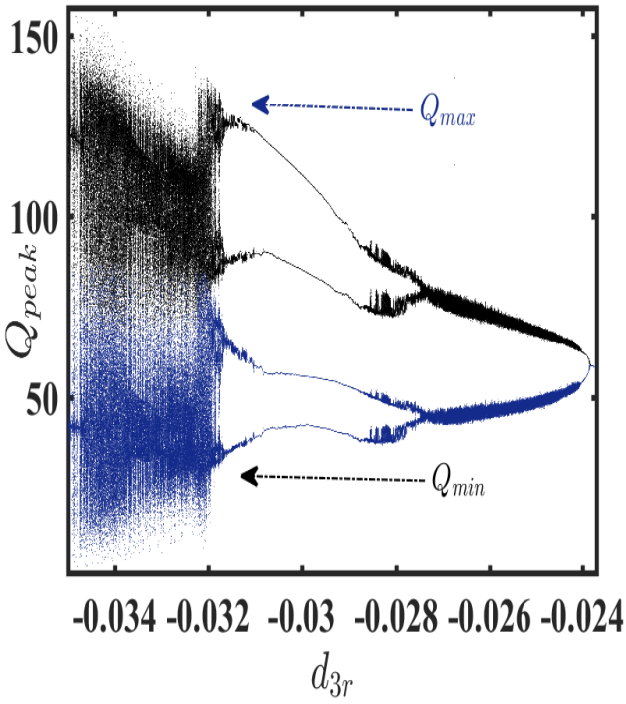

Figure 33: Bifurcation diagram as a function of the dopant effect. The physical parameters are the same as in Fig.5.

seen in Fig. 34(b). Figure 32 shows the evolution of the CW (inducing the MI (Fig. 35(a))) and the energy as a function of the higher-order spectral filtering d_{4s} (Fig. 35(b)). It appears that the MI is the precursor of the propagation of solitons in mCSHE.

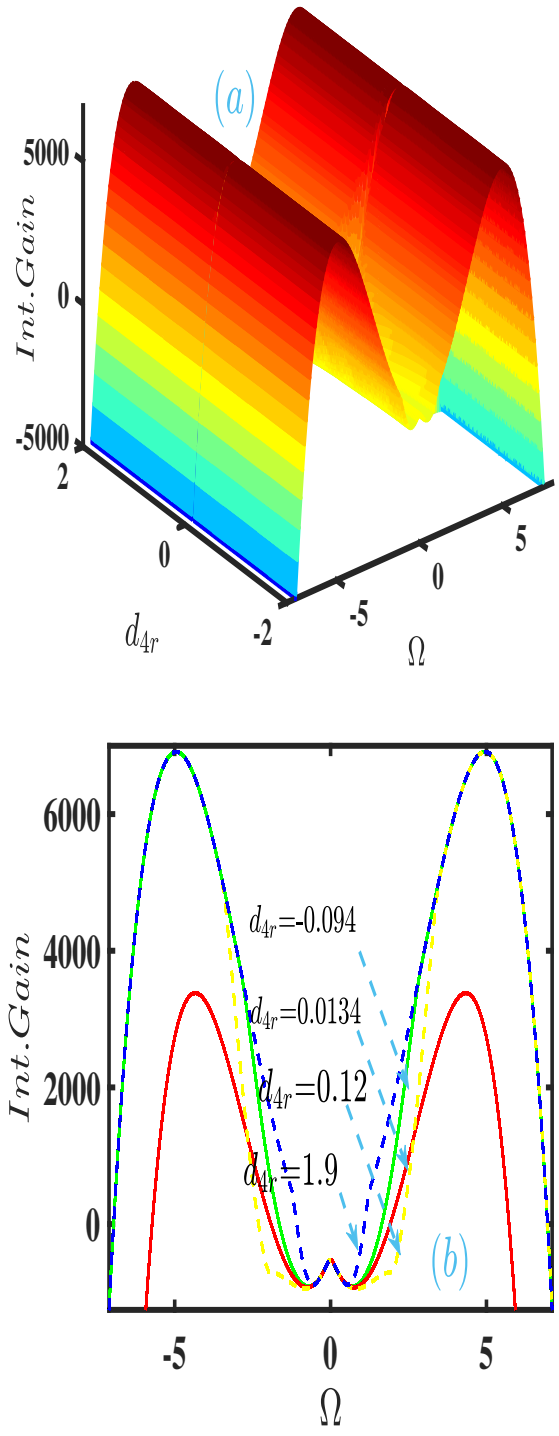

Figure 34: (a) 3D surface plot showing the integrated gain in the plane (Ω, d_{4r}); (b) Integrated gain as a function of the frequency Ω for various values of four-order dispersion coefficients for , $P_0 = 5.10^{-2}$, $q_{3r} = 5.10^{-1}$, $q_{3s} = 1$, $d_{3s} = -1.10^{-2}$, $d_{3r} = -1.10^{-2}$, $d_{4s} = 2.10^{-3}$, $\gamma_r = -9.10^{-3}$.

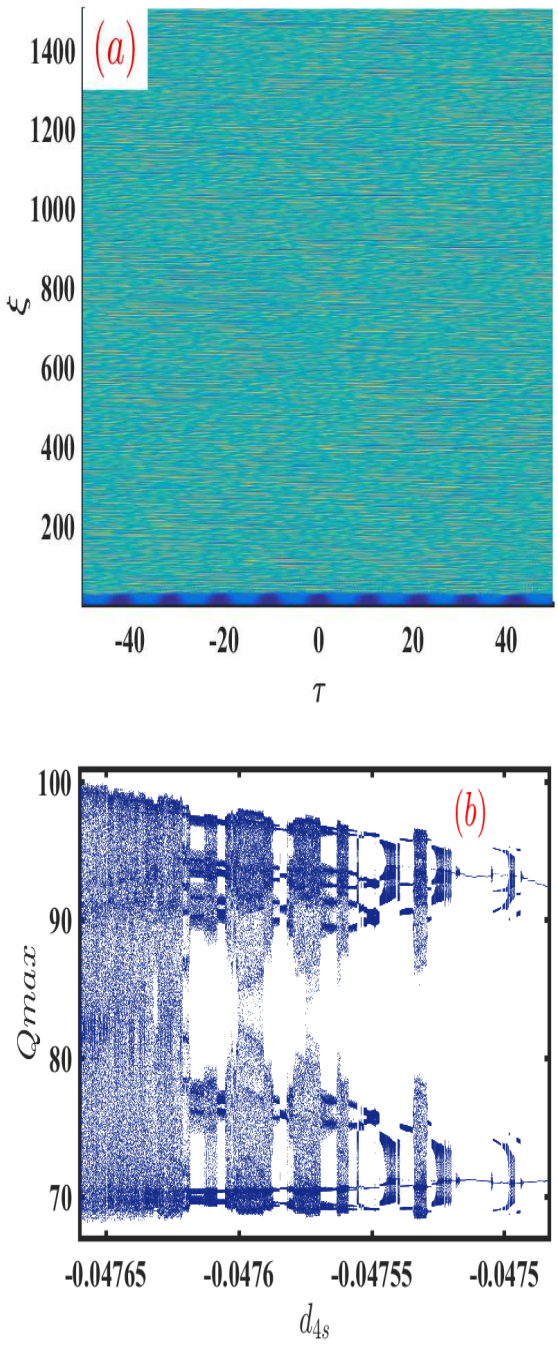

Figure 35: (a) Evolution of the modulational instability when (a) $d_{4s} = -6.10^{-2}$, and $P_0 = 1$, $q_{3r} = 3.10^{-1}$, $q_{3s} = 1$, $d_{3r} = d_{3s} = -1.10^{-2}$, $\gamma_r = -99.10^{-4}$. (b) Map soliton induced as a function of higher-order spectral filtering.

3.5.1.4 Effects of higher-order dispersion correction

Taking into account higher-order dispersion terms leading to CSH with higher-order dispersion. We note strong dependence of doped effect through d_{5r}, leading us to pay attention to the fifth-order dispersion. Like the third-order d_{3r}, the fifth-order d_{5r} produces the same behavior on the gain spectrum. Figure 33 shows the MI spectrum as a function of the high linear doped effect. We observe in Fig. 36(a) an increase and a decrease of the integrated gain while increasing values of the d_{5r}. Fig. 36(b) depicts the maximum gain as a function of the fifth-order dispersion. The pyramidal form of the maximum gain is obtained near the value of zero for d_{5r}. The generation of train of pulses along the propagation medium is observed in Fig. 37 (a) and bifurcation diagram as function of parameter d_{5r} is illustrated in Fig. 37 (b).

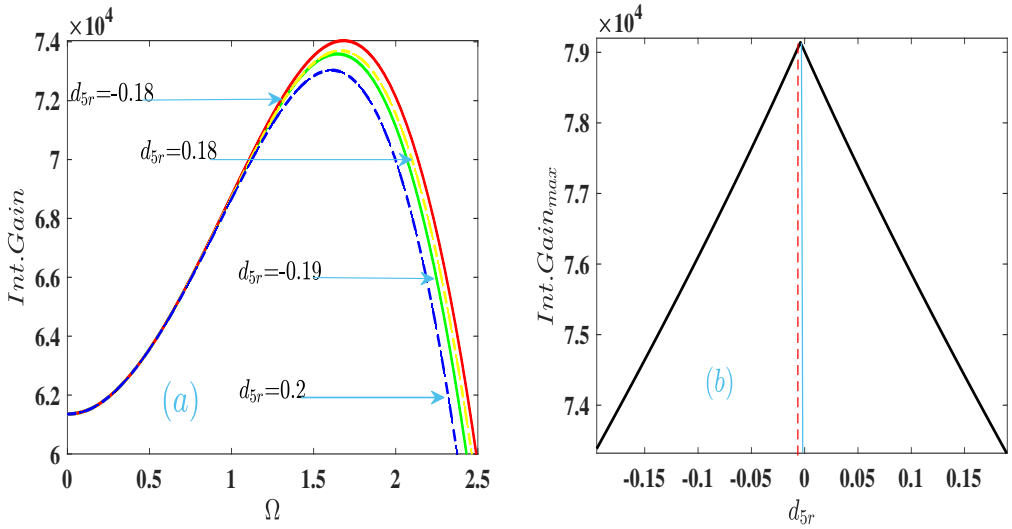

Figure 36: Effect of higher-order dopant on the instability spectrum. (a) Integrated gain as a function of Ω. (b) Maximum integrated gain as a function of d_{5r}, with $\Omega_{max} = 1.6$. The parameters used are : $P_0 = 5.10^{-1}$, $q_{3r} = 5.10^{-1}$, $d_{3r} = d_{3s} = -1.10^{-2}$, $d_{4r} = -5.10^{-2}$, $d_{4s} = -2.10^{-2}$, $d_{5s} = -1.10^{-3}$, $\gamma_r = -9.10^{-3}$.

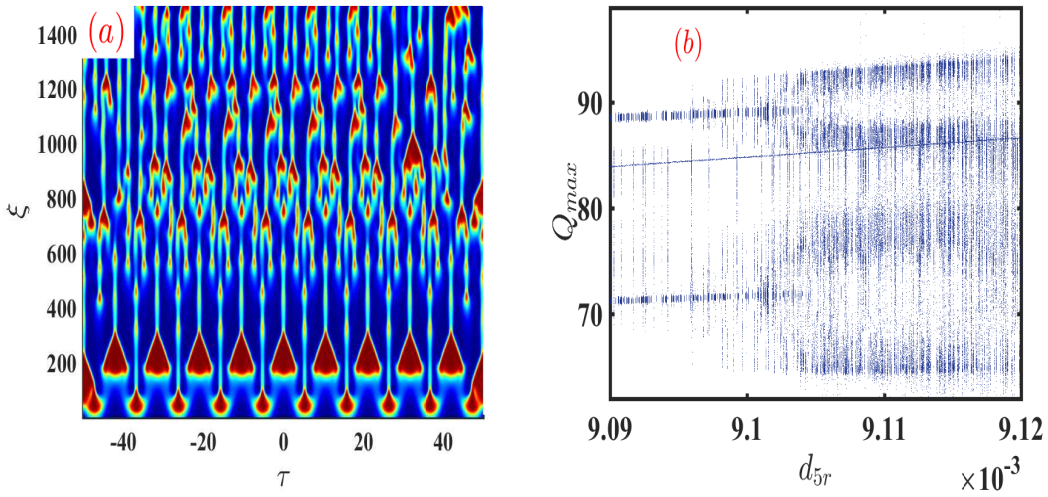

Figure 37: (a) Evolution of modulation instability for $d_{5r} = 7.10^{-3}$, and $P_0 = 1$, $q_{3r} = 8.10^{-1}$, $q_{3s} = 1.5$, $d_{3r} = d_{3s} = -1.10^{-1}$, $d_{4r} = -2.10^{-2}$, $d_{4s} = -2.10^{-2}$, $d_{5s} = -1.10^{-3}$, $\gamma_r = -99.10^{-4}$. (b) Map soliton induced as a function of higher-order dopant effect d_{5r}.

3.5.1.5 Sixth-order dispersion effect

We now consider the sixth-order complex dispersion term $(d_{6r} + id_{6s})$. The integrated gain maintains its shape by increasing the value of d_{6r}. The results are displayed in Fig. 35. The peak of integrated gain near to zero is shown in Fig. 38(b), while the bandwidth decreases when the d_{6r} value increases. The solid line illustrates the growth rate near zero.

Due to the large space of parameter values, Figure 36 presents an example of the stability investigation of the continuous wave in the plane (d_{6r}, q_{3r}) (Fig. 39 (a)). The white area indicates the stable domain and the blue area describes the unstable domain. When we consider a point in the stable domain, we have a stable evolution of the continuous wave $(z = 1170)$, witch oscillates periodically, as can be seen in Fig. 39(b)(solid line). When taking a point in the unstable domain, the evolution of continuous wave is presented by dash line in Fig. 39(b) witch is unstable. In Figure. 37, we plot the intensity distribution as a function of the retarded time τ, at the propagation distance $\xi = 1200$. We illustrate only the case with even dispersion (solid line in Fig. 38) and the full dispersion (dash line in Fig. 38). Higher values of the intensity distribution are obtained when considering the even dispersions. We note also the presence of sub-pulses. In this case, the amplitude of CW is high and the transversal distribution is symmetric.

In Fig. 38, we compare the map of solitons as a function of d_{6s} effect through energy (see Fig. 39(a)) and the dips of center-of-mass (see Fig. 40 (b)). These results are in good agreement with those of Fig.3(d).

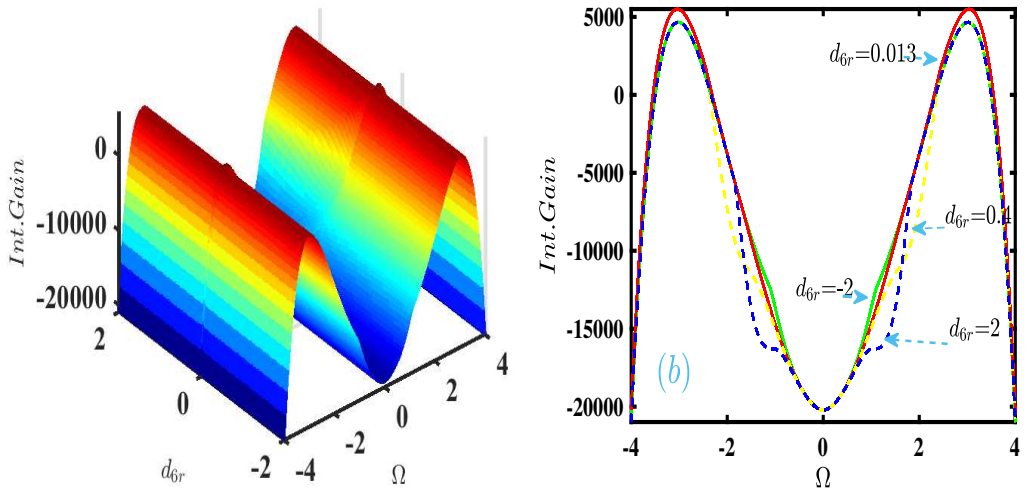

Figure 38: (a) 3D surface plot showing the integrated gain, in the plane (Ω, d_{6r}); (b) integrated gain as function of the frequency Ω, for the various of sixth-order of dispersion coefficient for, $P_0 = 2.10^{-1}$, $q_{3r} = 5.10^{-1}$, $q_{3s} = 5.10^{-1}$, $d_{2r} = -5.10^{-1}$, $d_{2s} = 5.10^{-1}$, $d_{3r} = d_{3s} = -1.10^{-2}$, $d_{4r} = -1.10^{-2}$, $d_{4s} = -18.10^{-3}$, $d_{5r} = -9.10^{-3}$, $d_{5s} = -1.10^{-3}$, $d_{6s} = 55.10^{-4}$, $\gamma_r = -9.10^{-4}$.

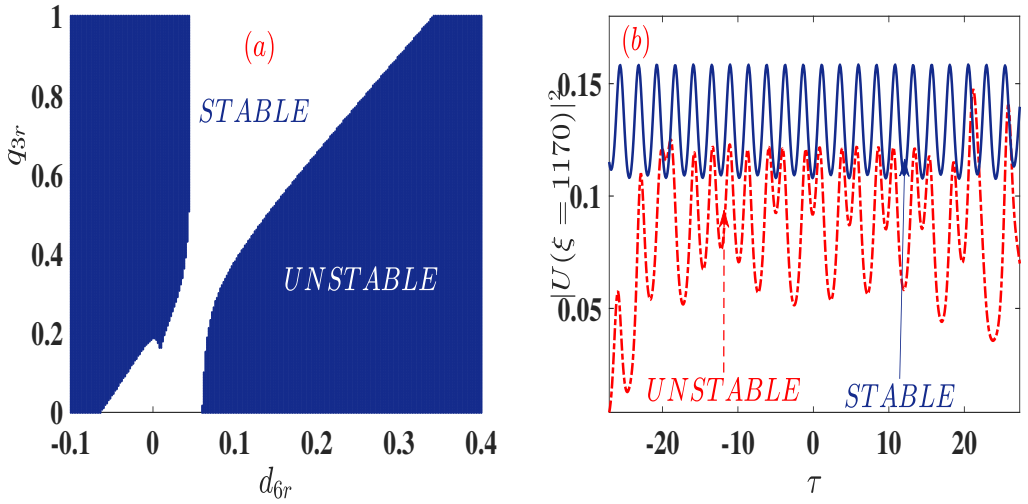

Figure 39: (a) The chart of stability. (b) Transversal distribution of the modulation instability at $\xi = 117.10^1$ for modulation stable (solid line) and modulation unstable (dash line). The physical parameters are: $P_0 = 2.10^{-1}$, $q_{3s} = 4.10^{-1}$, $d_{3s} = d_{3r} = -1.10^{-2}$, $d_{4r} = -2.10^{-2}$, $d_{4s} = -18.10^{-3}$, $d_{5r} = 9.10^{-3}$, $d_{5s} = -4.10^{-3}$, $d_{6s} = -9.10^{-4}$, $\gamma_r = -99.10^{-4}$, (b) solid line ($d_{6r} = 0$; $q_{3r} = 0$), dash line ($d_{6r} = 4.10^{-1}$; $q_{3r} = 1$).

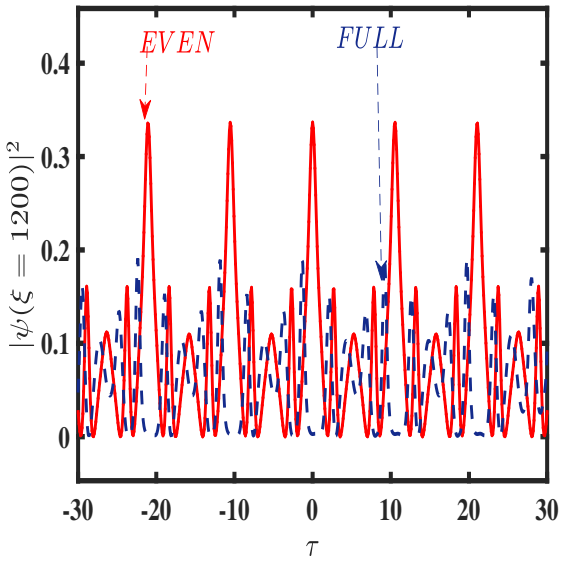

Figure 40: Transversal distribution of the modulation instability at $\xi = 12.10^2$ for even dispersion (solid line) and full dispersion (dash line). The physical parameters are: $P_0 = 1$, $q_{3s} = 1$, $q_{3r} = 4.10^{-3}$, $d_{3s} = d_{3r} = -1.10^{-2}$, $d_{4r} = -2.10^{-2}$, $d_{4s} = -2.10^{-2}$, $d_{5r} = 89.10^{-4}$, $d_{5s} = -1.10^{-3}$, $d_{6s} = -9.10^{-4}$, $d_{6r} = -1.10^{-4}$, $\gamma_r = -99.10^{-4}$.

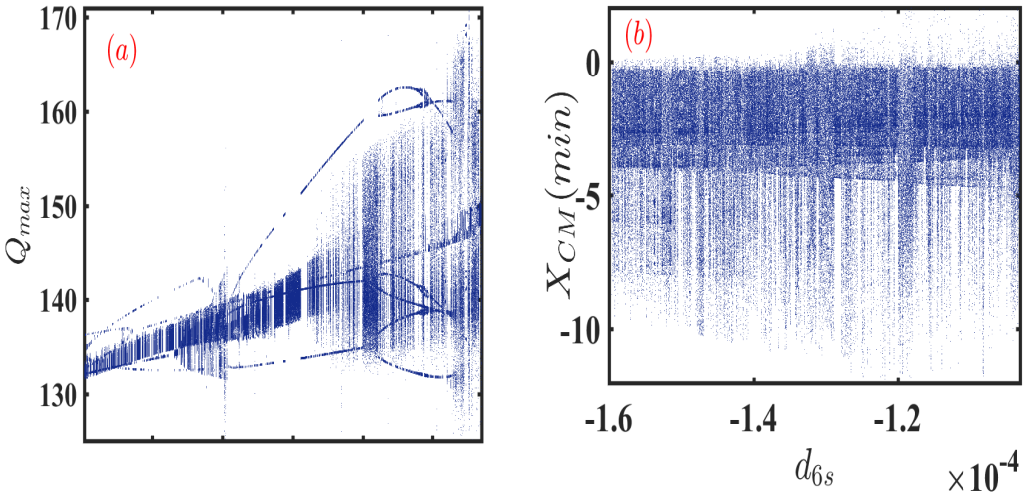

Figure 41: Comparison of map solitons as a function of higher-order d_{6i} term through: (a) energy and (b) center-of-mass.

3.5.1.5 Effect of intra-pulse Raman scattering and their correction terms

Here, we further analyzed the influence of self-frequency shift effects and their correction terms on the MI based in the CQSCGLE with higher-order dispersions. In general, the self-frequency shift effect is presented as the gradient of nonlinearity, which forms additional instability regimes on MI [220]. Figure 39 presents the integrated gain as a function of the input power P_0, taking into account the self-frequency shift effect associated with even dispersion effects (dark dashed line), the full dispersions effects (blue solid line). Neglecting the self-frequency shift effect, the result is displayed by the red dotted lines. The numerical evolution of the CW inducing the MI in this regime is illustrated in Fig.39. Figure 40 (a) depicts a case of full dispersion coefficient and Fig 16 (b) when the dispersion coefficients are even. For the second case, we observe a more concentration of train of pulses at $\xi = 6.10^2$.

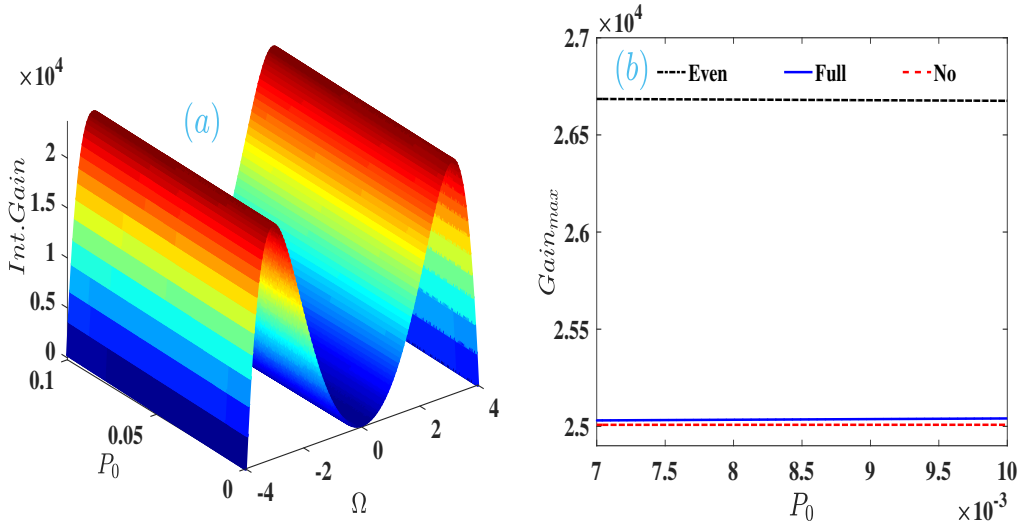

Figure 42: (a) 3D surface plot showing the integrated gain, in the plane (Ω, P_0). (b) Maximum gain as a function of P_0, with $\Omega_{max} = 3.1$, for different physical situations. The parameters are: $q_{3r} = 4.10^{-1}$, $q_{3s} = 1$, $d_{3r} = d_{3s} = -1.10^{-2}$, $d_{4r} = -1.10^{-2}$, $d_{4s} = -2.10^{-2}$, $d_{5r} = 6.10^{-3}$, $d_{5s} = -1.10^{-3}$, $d_{6s} = -6.10^{-2}$, $d_{6r} = 6.10^{-3}$, $\gamma_r = -1.10^{-3}$, $m_{1r} = 6.10^{-1}$, $m_{2r} = 8.10^{-2}$, $m_{3r} = 5.10^{-3}$.

From the presented figures, it comes that the self-frequency shift and their correction terms increase the gain of instability. This increase is higher when considering, the complex even dispersions.

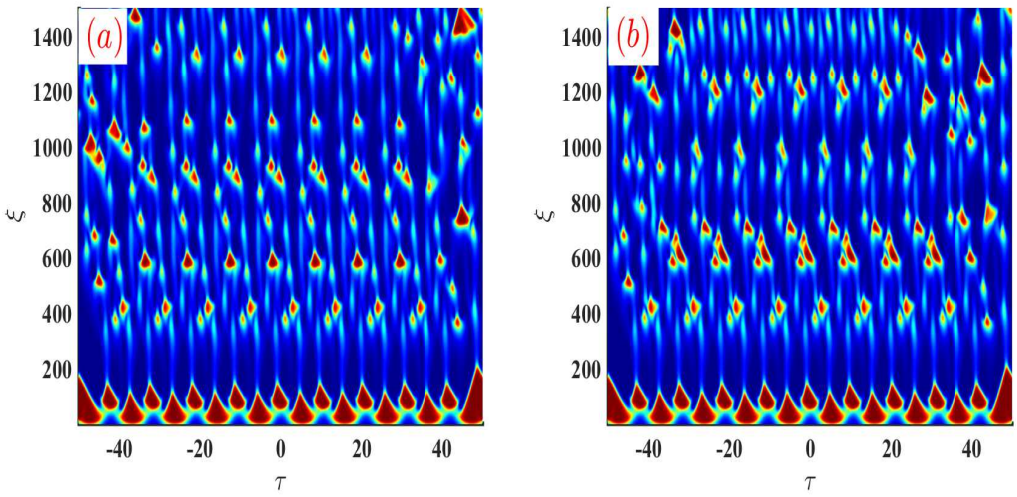

Figure 43: Evolution of modulational instability in the presence of self-frequency shift effect and their two correction terms. (a) Full dispersion, (b) Even dispersions. The others parameters are: $P_0 = 1$, $m_{1r} = 6.10^{-1}$, $m_{2r} = 8.10^{-2}$, $m_{3r} = 5.10^{-3}$.

3.5.1.6 Effect of higher-order term of self-steepening

Here, we study in detail the effect of self-steepening with correction terms on the MI using the CQSCGLE with higher-order complex dispersion coefficients. Neglecting the effects of the self-frequency and their correction, terms, Fig. 41 shows the maximum gain as a function of the input power P_0, where solid line represents the maximum gain with full complex dispersion coefficients, and dotted lines represent the case when even dispersion is considered.

Figure 42 illustrates the propagation of the CW in presence of a self-steepening in two dispersion cases. In Fig. 45(a), we investigated the case of full dispersion, where it appears that more train of optical pulses is generated since the beginning of the propagation. The map soliton obtained through the center-of-mass as a function of the self-steepening n_{1s} is depicted in Fig.43.

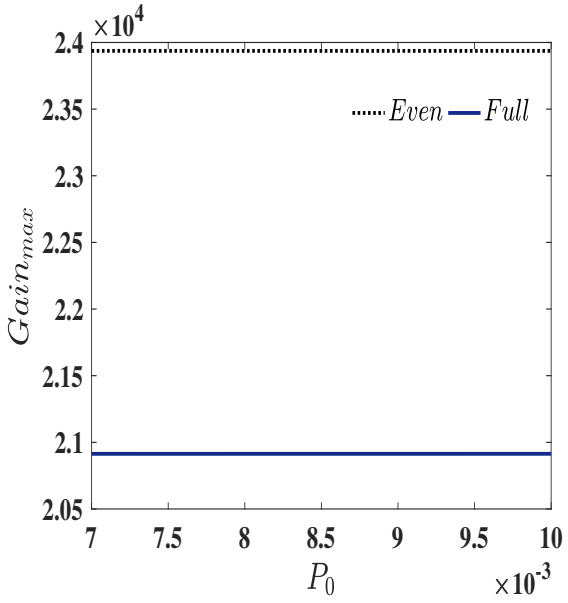

Figure 44: The maximum gain as function of power P_0 with $\Omega_{max} = 3.1$, for different physical situations. The physical parameters are: $n_{1s} = 4.10^{-1}$, $n_{2s} = 8.10^{-2}$, $n_{3s} = 8.10^{-3}$.

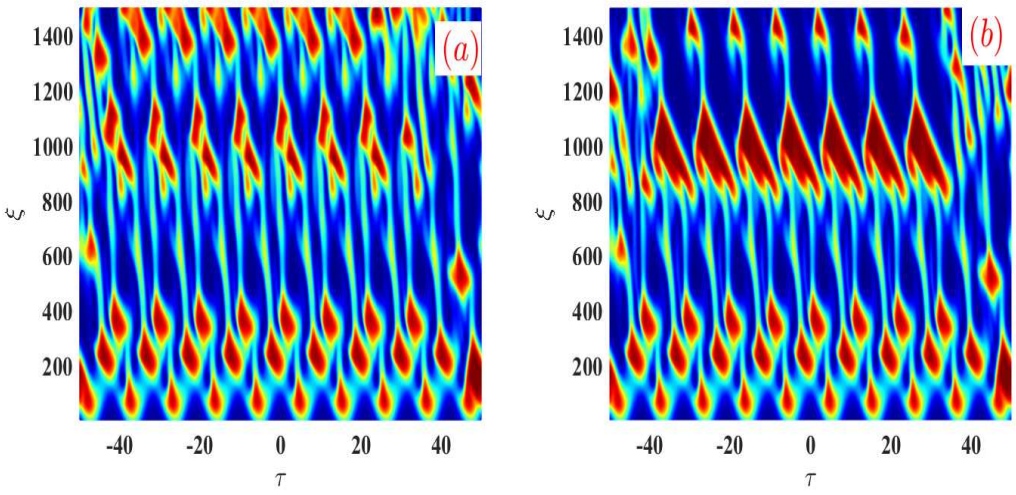

Figure 45: (a) Evolution of modulational instabilty in presence of self-steepening effect and their two correction terms. (a) Full dispersion. (b) Even dispersions. The other parameters are: $P_0 = 1$, $n_{1s} = 2.10^{-1}$, $n_{2s} = 1.10^{-2}$, $n_{3s} = 1.10^{-3}$.

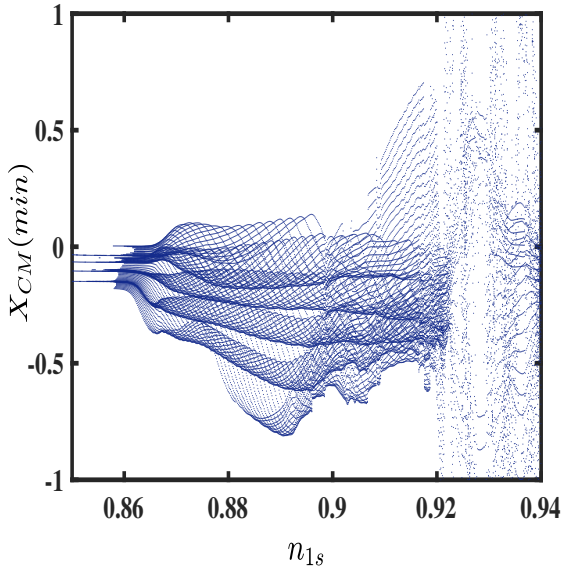

Figure 46: Map soliton through the dips of the center-of-mass as a function of the self-steepening n_{1s}.

3.5.1.7 Full model

We study the MI of CW solution within the full model (3.24). The critical frequency boundary of the MI has been determined analytically (see (3.44)) which does not depend on the real part dispersion and gradient of nonlinearity coefficients, respectively. Fig. 47 presents the statistical study showing the degree of influence of the different physical parameters that comes into consideration, on the boundaries of the frequency domain of the MI. Note that taking the horizontal line corresponding to the critical perturbation frequency at zero, the boundary domains of the MI decrease due to physical effect related to the presence of some points under this horizontal line, Whereas the points above the line increases the domain of frequency of MI.

We note also that the higher order of spectral filtering increases the boundaries of the MI more than anyother physical effect. The boundary domain of the MI is more sensitive to d_{4s}, d_{6s} and the propagation distance ξ, respectively. To investigate the MI, we show in Fig. 48(a) the dependence of the MI gain concerning P_0 and temporal detuning frequency Ω. In Fig. 48(b), we observe the influence of the input power in the MI spectrum. For small values of the input power, instability gain does not exist at $\Omega = 0$. An increase of the input power leads to an increase of the instability gain associated with two symmetrical side lobes which maintain their shapes. In with Fig. 48 (c) we observe the profile of the integrated gain as a function of Ω, and d_{4r}. In Fig. 48(d), we have three regions of instability (the first is located around the zero frequency Ω, and the two others are symmetric from the zero frequency) for a value of $d_{4r} = -3$. The region of instability associated with the gain can vary depending on the values of d_{4r} as we can observe in Fig. 48 (d) for $d_{4r} = -3.10^{-1}$ and $d_{4r} = 1.10^{-1}$.

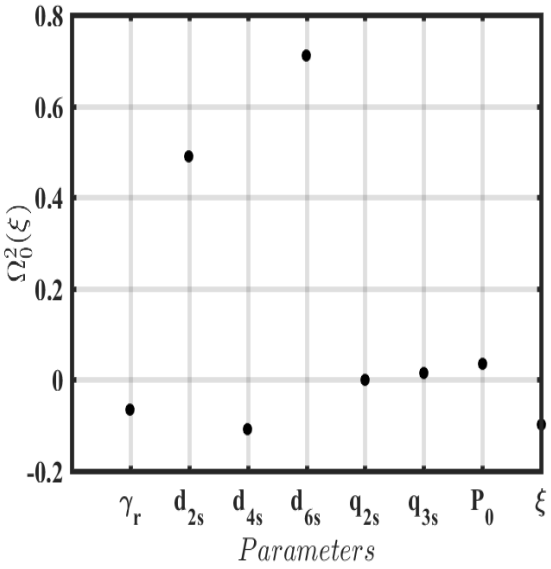

Figure 47: Influence of the physical parameters on the critical frequency using sensitive analyses.

Figure 47 shows the plot of the integrated gain as a function of the higher order dispersion coefficients d_{5r} and the frequency of the perturbation amplitude Ω. In Fig. 50 (a) and (b) an instability gain is developed induced by two higher order dispersion coefficients d_{5r} and d_{6r}, respectively.

Figure. 49(c) depicts the variation of the instability region. As we can see, the reversed phenomena from Fig. 49(d) are observed. Results from numerical simulations of the full model equation of the CW are shown in Fig.47. Figure 47 (b) gives the profile of CW for $P_0 = 1$. Also shown is the distribution of instability at $\xi = 1222$.

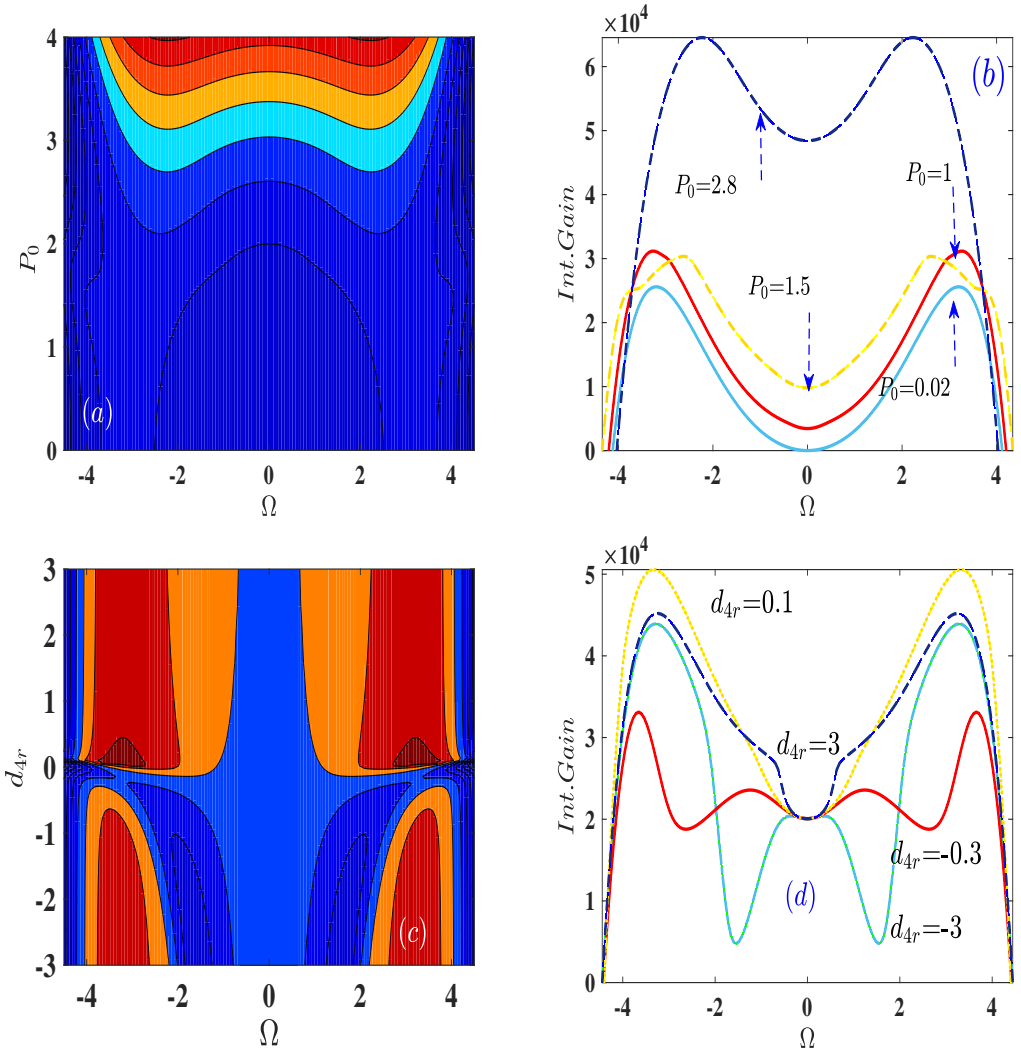

Figure 48: (a) 2D surface plot showing the integrated gain, in the plane (Ω, P_0). (b) 2D plot for various values of P_0. when $d_{4r} = -2.10^{-2}$. (c) 3D surface plot showing the integrated gain, in the plane (Ω, d_{4r}), $P_0 = 1$, (d) 2D a plot as a function of Ω for various values of d_{4r}. Parameters when are : $q_{3s} = 1$, $q_{3r} = 4.10^{-1}$, $d_{3r} = -34.10^{-3}$, $d_{3s} = -1.10^{-2}$, $d_{4s} = -48.10^{-3}$, $d_{5r} = 8.10^{-3}$, $d_{5s} = -1.10^{-3}$, $d_{6s} = -3.10^{-3}$, $d_{6r} = 6.10^{-3}$, $\gamma_r = -99.10^{-4}$, $n_{1s} = 2.10^{-1}$, $n_{2s} = 5.10^{-3}$, $n_{3s} = 2.10^{-3}$, $m_{1r} = 6.10^{-1}$, $m_{2r} = 8.10^{-2}$, $m_{3r} = 1.10^{-3}$.

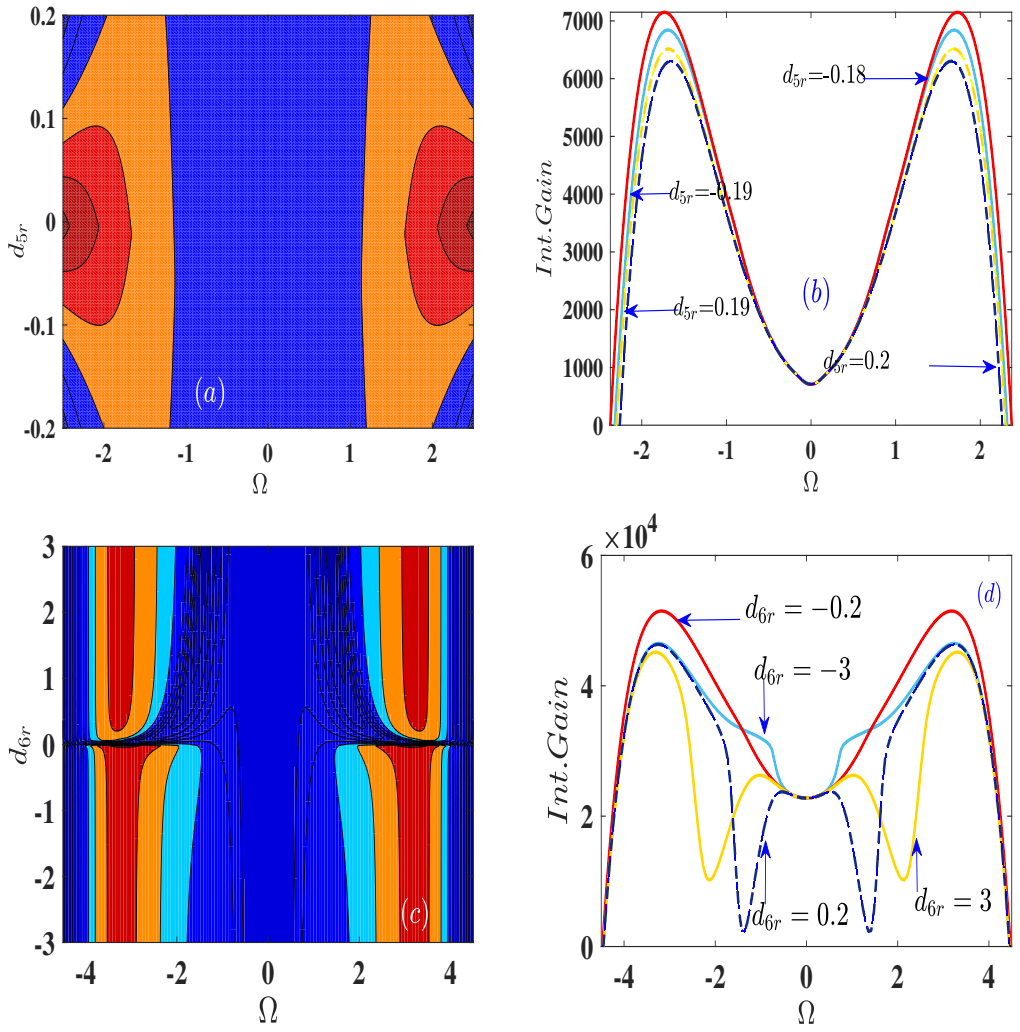

Figure 49: (a) 2D surface plot showing the integrated gain, in the plane (Ω, d_{5r}) when $d_{6r} = 6.10^{-3}$. (b) 2D plot for the various value of d_{5r}. (c) 2D surface plot showing the integrate**d** gain, in the plane (Ω, d_{6r}), when $d_{5r} = 8.10^{-3}$, and (d) 2D plot as function of Ω for various values d_{6r} Parameters are as follows : $P_0 = 5.10^{-1}$, $d_{4r} = -2.10^{-2}$, the other parameters are the same in Fig. 48

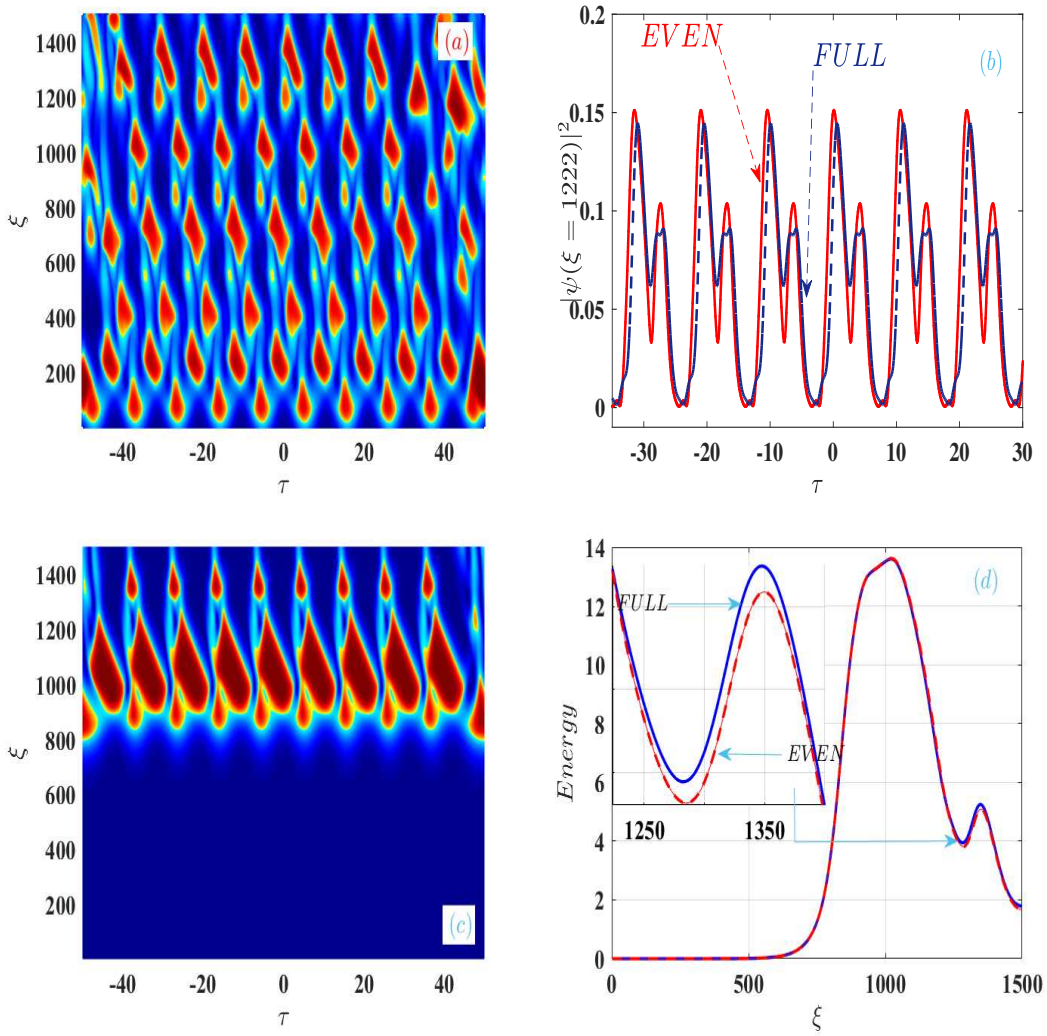

Figure 50: Numerical evolution of the modulational instability in the full model: (a) propagation of the CW when $P_0 = 1$. (b) Transverse distributions of the intensity at position $\xi = 1222$, considering full dispersion (solid line) and even dispersion (dash line). (c) Propagation when $P_0 = 1.5$. (d) Energy with full dispersion (solid line) and even dispersion (dash line). Parameters are the same in Fig. 48.

3.6 Conclusion

In this chapter, we have dealt with analytical and numerical studies of modulational instability for different models of nonlocal media. At first, we presented results of the models which we used to explain linear stability and SSFM of nonlocal media with magnetic effects. We note that the results from the modulational instability are not affected by a any change in the magnetic effects on the wave train. Our observation thus agrees with the results from Ref. [18], where MI was considered in the absence magnetic effects. We also examined modulation instability in weak nonlocal nonlinear media with competing Kerr and non-Kerr nonlinearities. We used Lenz transformation to transform the trapping equation into a management equation. We obtained a stability condition after the application Linear Stability. In this same order, we have obtained an analytical expression for the gain. The SSFM helped us to obtain the profile, maxima, and phase surface of the perturbed plane wave.

Later on, we investigated the generation of optical solitons in doped fiber with higher-order nonlinearities and high-order dispersion. In that contex, we used linear stability to obtain Lange-Newell's criterion for the model. The growth rate expression was also obtained, and we employed the sensitivity analysis method to observe the sensitivity of the physical parameters of the system. With the pseudo-spectral method, we observed the generation of optical solitons via their energy and center of mass. Finally, we dressed the soliton-map for different physical effects.

General Conclusion and Perspectives

In this thesis, we theoretically investigated the process of generation of soliton in nonlocal media. We considered two nonlinear dynamical systems, which are conservative systems governed by nonlocal nonlinear Schrödinger equations. Here, the nonlinearity competes between cubic Kerr and quintic non-Kerr at weakly regime of nonlocality. The dissipative system of our work is modeled by the cubic-quintic-septic with complex with higher-order Ginzburg-Landau equation modelling in doped, it has several properties such as high dispersion terms. To understand very well the process of generation of solitons, it was necessary to explain in detail the different notions that we have used in our investigations. Therefore, in chapter one, where we have defined the concept of soliton waves and described it in the context of nonlinear optics, with its different geometrical configurations. Next, we described the nature of linear and nonlinear effects. The origin and different types of nonlocal media were presented with the specification that rare earth chemistry elements originate from dissipation in optical fiber. We ended the chapter the notions on modulational instability phenomenon. In chapter two, we have at first derived the different models employed in this thesis. Next the conversion of nonlinear Schödinger equation to managed nonlinear Schödinger was done equation thanks to the Lenz transformation. We closed the chapter with the description of linear stability analysis, through the nonlocal nonlinear Schrodinger equation, and details of the numerical methods which help us to characterize the modulation instability. The main results of the thesis are summarized in the third chapter as follows. Firstly, we have investigated, analytically and numerically, MI in competing weakly nonlocal media. The contributions of cubic and quintic nonlocalities have been studied through the stability diagram collected from many regimes of nonlinearities. It has been found that MI can be suppressed by the weakly quintic term. In addition, analytical results have been verified numerically, through the maximum of peak of intensity in time and space. Competing effects from cubic and quintic nonlocalities have also been observed independently of the response function, leading to the generation in trains of pulses of the optical beam. The Attractive-Repulsive regime have been found to generate more trains of pulses than other regimes. The model under study has revealed other aspects of the nonlinear manifestation of MI such as the emergence of ABs, whose behavior over time and space has been found to be very sensitive to the three-body interaction. In fact, in the absence of cubic and quadratic potentials, the plane waves, similar to the Akhmediev Breathers, in presence of nonlocality, were obtained, with their

cycle of trajectory phase depending on the degree of nonlocality. Finally, the nonlocality can be identified as a dispersive term in presence of Akhmediev Breathers. Based on this cubic-quintic-septic complex Ginzburg-Landau equation with higher-order dispersion, gradient terms and using the linear stability analysis, the expression of the gain, boundaries domain of MI and the well known Lange-Newell criterion for the stability (instability) of Stokes waves have been obtained. Dopant effects have been analyzed analytically and numerically. Analytical results from the integrated gain reveal the presence of two side-bands of MI and pyramidal form of the maximum gain for the odd order dispersion coefficients. Numerically, the odd dispersion coefficients reduce the intensity of the continuous wave. Through the bifurcation diagram, we have generated several solitons with different energies at the same distance. The even dispersion coefficients produce several regions of instability through the integrated gain and increase the maximum gain, in the presence of gradient of nonlinearity and their correction terms. In addition, the center-of-mass is presented as a good physical characteristic to study MI. The particularity of this investigation is the use of the employed of SA method for the study of influences of physical parameters on the MI, in addition to the bifurcation diagram which shows many solitons generation. The future work of this thesis is oriented in many ideas

Perpective (Future orientation)

♦ Firstly we will concentrate on the propagation of solitons and their stability in doped optical fiber, and if it is possible to observe phenomena of multiple instabilities and intermittent bright soliton through this optical fiber. In the same order, it may be interesting to try to generate a fractal structure which can arise through the interaction of the Gaussian pulse in nonlocal competing Kerr and non-Kerr nonlinearities, distinguishing the cases of coherent and incoherent interactions.

♦ Secondly, we could investigate the vectorial aspect of the complex Ginzburg-Landau equation with the aim to generate the supercontinuum and study the cascading phenomena. We will investigate the modulational instability and bifurcation soliton.

♦ Thirdly, for the engineering application, it is necessary to obtain electronic equivalent or mechanic of the nonlocality with the idea to know the impact of nonlocality in the electronic and mechanic system. In addition, we have the ambition to study the nonlocality effect and dopant effects with machine learning with the aim to update the nonlocality and doped fiber.

Appendix

3.6.1 Appendix : Model

In equation (3.24), d_{jrs} are the complex dispersion coefficients (of the form $d_{jrs} = d_{jr} + id_{js}$, where d_{jr} is the real part and d_{js} the imaginary part). The coefficient expressions are given below

$$d_{2r} = -\left(\frac{\beta_2}{2} + \frac{g_p\left(-3\delta + \delta^3\right)T_2^2}{2n\left(1+\delta^2\right)^3}\right), \tag{3.47}$$

$$d_{2s} = -\frac{g_p\left(1 - 3\delta^2\right)T_2^2}{2n\left(1+\delta^2\right)^3}. \tag{3.48}$$

$$d_{3r} = -4\delta\frac{g_p\left(1-\delta^2\right)T_2^3}{2n\left(1+\delta^2\right)^4}, \tag{3.49}$$

$$d_{3s} = -\left(\frac{\beta_3}{6} + \frac{g_p\left(-1 - \delta^4 + 6\delta^2\right)T_2^3}{2n\left(1+\delta^2\right)^4}\right). \tag{3.50}$$

$$d_{4r} = \frac{\beta_4}{24} - \frac{g_p\left(-5\delta + 10\delta^3 - \delta^5\right)T_2^4}{2n\left(1+\delta^2\right)^5}, \tag{3.51}$$

$$d_{4s} = -\left(\frac{g_p\left(1 - 10\delta^2 + 5\delta^4\right)T_2^4}{2n\left(1+\delta^2\right)^5}\right). \tag{3.52}$$

$$d_{4s} = -\left(\frac{g_p\left(1 - 10\delta^2 + 5\delta^4\right)T_2^4}{2n\left(1+\delta^2\right)^5}\right). \tag{3.53}$$

$$d_{5s} = \frac{\beta_5}{120} + \frac{g_p\left(1 - 15\delta^2 + 15\delta^4 - \delta^6\right)T_2^5}{2n\left(1+\delta^2\right)^6}. \tag{3.54}$$

$$d_{6r} = -\frac{\beta_6}{720} - \frac{g_p\left(7\delta - 35\delta^3 + 21\delta^5 - \delta^7\right)T_2^6}{2n\left(1+\delta^2\right)^7}, \tag{3.55}$$

$$d_{6s} = -\frac{g_p\left(-1 + 21\delta^2 - 35\delta^4 + 7\delta^6\right)}{2n\left(1+\delta^2\right)^7}. \tag{3.56}$$

The constants q_{krs} represent the complex coefficients of nonlinearity, the real part are nonlinear coefficient and imaginary are nonlinear gain/loss.

For *k=1*, q_{1r} is the nonlinear Kerr coefficient, q_{1s} is the gain or loss term of nonlinearty and k the order of correction, with

$$q_{1r} = \frac{\partial\beta}{\partial\left|\psi\right|^2} + \left(\frac{n_2 k_0}{4}\right) A_{eff}^{-1}, \tag{3.57}$$

$$q_{1s} = \left(\frac{\alpha n_2}{4n}\right) A_{eff}^{-1}. \tag{3.58}$$

For *k=2*, it is the first correction of Kerr effect, commonly known as quintic nonlinearity coefficient,

$$q_{2r} = \frac{1}{2}\left(\frac{\partial\beta}{\partial\left|\psi\right|^4}\right) + \frac{k_0}{4}\left(\frac{n_2^2}{2n} + n_4\right) A_{eff1}^{-1}, \tag{3.59}$$

$$q_{2r} = \frac{1}{2}\left(\frac{\partial\beta}{\partial\left|\psi\right|^4}\right) + \frac{k_0}{4}\left(\frac{n_2^2}{2n} + n_4\right) A_{eff1}^{-1}, \tag{3.60}$$

For *k=3*, it is the second correction of**the** Kerr effect. It is commonly known as septic nonlinearity coefficient,

$$q_{3r} = \frac{1}{6}\left(\frac{\partial\beta}{\partial\left|\psi\right|^6}\right) + k_0\left(n_6 + \frac{n_2 n_4}{4n}\right) A_{eff2}^{-1}, \tag{3.61}$$

$$q_{3s} = \left(\frac{\alpha n_6}{4n}\right) A_{eff2}^{-1}. \tag{3.62}$$

Here A_{eff}^{-1}, A_{eff1}^{-1}, A_{eff2}^{-1}, keep the same definition as in Ref [146].

The coefficients m_{kr}, are the intra-pulse Raman scattering, m_{2r} and m_{3r} being the first and second order correction terms of m_{1r}, where

$$m_{1r} = \frac{\partial\beta}{\partial|\psi|_t^2}, \tag{3.63}$$

$$m_{2r} = \frac{1}{2}\frac{\partial\beta}{\partial|\psi|_t^4}, \tag{3.64}$$

$$m_{3r} = \frac{1}{6}\left(\frac{\partial\beta}{\partial|\psi|_t^6}\right). \tag{3.65}$$

The real parameters n_{ksi} denote self steepening coefficients coefficient, where

$$n_{1s} = \frac{\partial}{\partial_\omega}\left(\frac{\partial\beta}{\partial|\psi|^2}\right), \tag{3.66}$$

$$n_{2s} = \frac{1}{2}\left(\frac{\partial}{\partial_\omega}\left(\frac{\partial\beta}{\partial|\psi|^4}\right)\right), \tag{3.67}$$

$$n_{3s} = \frac{1}{6}\left(\frac{\partial}{\partial_\omega}\left(\frac{\partial\beta}{\partial|\psi|^6}\right)\right). \tag{3.68}$$

The complex coefficient of absorption, γ_{rs} is defined as

$$\gamma_{rs} = \gamma_r + i\gamma_s, \tag{3.69}$$

with

$$\gamma_r = \frac{g_p\delta}{2n\,(1+\delta^2)}, \tag{3.70}$$

$$\gamma_s = -\alpha + \frac{g_p}{2n\,(1+\delta^2)}. \tag{3.71}$$

3.6.2 Appendix: Modulational instability

Here we have the coefficients A_n of solution Eq.(3.32)

$$A_{12} = {d_{6\,r}}^2, \tag{3.72}$$

$$A_{11} = 2\,d_{5\,r}d_{6\,r}, \tag{3.73}$$

$$A_{10} = -\left(2\,d_{4\,r}d_{6\,r} + {d_{5\,r}}^2\right), \tag{3.74}$$

$$A_9 = -2\left(\,d_{4\,r}d_{5\,r} + \,d_{3\,r}d_{6\,r}\right), \tag{3.75}$$

$$A_8 = 2\left(\,d_{5\,r}d_{3\,r} + \,d_{2r}d_{6\,r}\right) + {d_{4\,r}}^2, \tag{3.76}$$

$$\begin{aligned} A_7 =& 2\left(\,d_{4\,r}d_{3\,r} + \,d_{5\,r}d_{2r}\right) + 2d_{6\,r}m_{r1}P_0A_\xi^2 \\ &+ 4d_{6\,r}m_{r2}{P_0}^2A_\xi^4 + 6d_{6\,r}m_{r3}{P_0}^3A_\xi^6, \end{aligned} \tag{3.77}$$

$$\begin{aligned} A_6 =& -2\,d_{2r}d_{4\,r} - {d_{3\,r}}^2 \\ &- 2P_0\left(\,d_{6\,r}d_{2r} + \,d_{5\,r}m_{r1}\right)A_\xi^2 \\ &- 4{P_0}^2\left(\,d_{5\,r}m_{r2} + \,d_{6\,r}q_{2r}\right)A_\xi^4 \\ &- 6{P_0}^3\left(\,d_{6\,r}q_{3r} + \,d_{5\,r}m_{r3}\right)A_\xi^6, \end{aligned} \tag{3.78}$$

$$\begin{aligned} A_5 =& -2\,d_{2r}d_{3\,r} - 2P_0\left(\,d_{4\,r}m_{r1} + \,d_{5\,r}q_{1r}\right)A_\xi^2 \\ &- 4{P_0}^2\left(\,d_{4\,r}m_{r2} + \,d_{5\,r}q_{2r}\right)A_\xi^2, \end{aligned} \tag{3.79}$$

$$
\begin{aligned}
A_4 =& {d_{2r}}^2 + 2P_0\,(\,d_{4\,r}q_{1r} + \,d_{3\,r}m_{r1})\,A_\xi^2 \\
&+ 4{P_0}^2\,(\,d_{4\,r}q_{1r} + \,d_{3\,r}m_{r2})\,A_\xi^4 \\
&+ 6{P_0}^3\,(\,d_{4\,r}q_{3r} + \,d_{3\,r}m_{r3})\,A_\xi^6,
\end{aligned}
\tag{3.80}
$$

$$
\begin{aligned}
A_3 =& 2\,P_0\,(d_{3\,r}q_{1r} + d_{2r}m_{r1})\,A_\xi^2 \\
&+ 4{P_0}^2\,(\,d_{3\,r}d_{4r} + \,p_r m_{r2})\,A_\xi^4 \\
&+ 6\,{P_0}^3\,(\,d_{2r}m_{r3} + \,d_{3\,r}q_{3r})\,A_\xi^6,
\end{aligned}
\tag{3.81}
$$

$$
\begin{aligned}
A_2 =& 9\,{P_0}^6{n_{3s}}^2A_\xi^{12} + 12\,{P_0}^5n_{3s}n_{2s}A_\xi^{10} \\
&+ 2{P_0}^4\left(2\,{n_{2s}}^2 + 3\,n_{1s}n_{3s}\right)A_\xi^8 \\
&+ 2{P_0}^3\,(2\,n_{i1}n_{i2} - 3\,q_{3r}q_{3r})\,A_\xi^6 \\
&+ {P_0}^2\left({n_{1s}}^2 - 4\,d_{2r}q_{2r}\right)A_\xi^4 - 2A_\xi^2 d_{2r}q_{1r}P_0,
\end{aligned}
\tag{3.82}
$$

$$
\begin{aligned}
A_1 =& 2\,{P_0}^3q_{2s}n_{1s}A_\xi^6 \\
&+ 4\,{P_0}^4\,(\,n_{2s}q_{3s} + 2\,q_{3s}n_{1s})\,A_\xi^8 \\
&+ 2\,{P_0}^5\,(3\,q_{2s}n_{3s} + 4\,q_{3s}n_{2s})\,A_\xi^{10} \\
&+ 12\,{P_0}^6q_{3s}n_{3s}A_\xi^{12},
\end{aligned}
\tag{3.83}
$$

$$
A_0 = -{P_0}^4\left({q_{2s}}^2A_\xi^8 + 4\,q_{3s}P_0A_\xi^{10}q_{2s} + 4\,{q_{3s}}^2{P_0}^2A_\xi^{12}\right). \tag{3.84}
$$

Coefficient of the frequency detuning in the full model defined in Eq.(3.39)

$$
C_0 = \frac{{d_{4s}}^3}{27{d_{6s}}^3} - \frac{d_{2s}d_{4s}}{6{d_{6s}}^2} + \frac{{P_0}^2A_\xi^4\left(2q_{3s}P_0A_\xi^2 + q_{3s}\right)}{2d_{6s}}, \tag{3.85}
$$

$$
C_1 = \left(81\,(\Xi)^2 + 12\left(\frac{d_{2s}}{d_{6s}} - \frac{{d_{4s}}^2}{3{d_{6s}}^2}\right)^3\right)^{1/2}, \tag{3.86}
$$

where

$$
\Xi = -\frac{2{d_{4s}}^3}{27{d_{6s}}^3} + \frac{d_{2s}d_{4s}}{3{d_{6s}}^2} - \frac{{P_0}^2A_\xi^4\left(2\,q_{3s}P_0A_\xi^2 + q_{2s}\right)}{d_{6s}}. \tag{3.87}
$$

Correction term of the Lange-Newlle's criterion defined in Eq.(3.41)

$$
\begin{aligned}
Y_{11} = & -\frac{{d_{6s}}^2 \Omega^{10}}{2P_0} + \frac{\left(2\, d_{6s} d_{4s} - 2\, d_{4\,r} d_{6\,r}\right) \Omega^8}{2P_0} \\
& + \frac{\left(-2\, d_{2s} d_{6s} + 2\, d_{2\,r} d_{6\,r} - 2\, d_{3s} d_{5s} - {d_{4s}}^2\right) \Omega^6}{2P_0} \\
& + \frac{\left(2\, P_0 q_{1s} d_{6s} + 4\, P_0^2 q_{2s} d_{6s} - 4\, d_{6\,r} P_0^2 q_{2r}\right) \Omega^4}{2P_0} \\
& + \frac{\left(6\, n_{i2} P_0^2 d_{5s} + 4\, n_{1s} P_0 d_{5s} + 8\, d_{5s} n_{3s} P_0^3\right) \Omega^4}{2P_0} \\
& + \frac{\left(-2\, d_{6\,r} P_0 q_{1r} - 2\, d_{4\,r} d_{2\,r} + 2\, d_{2s} d_{4s}\right) \Omega^4}{2P_0} \\
& + \frac{\left(-8\, d_{3s} n_{3s} P_0^3 + 2\, d_{4\,r} P_0 q_{1r} - 4\, d_{3s} n_{1s}\right) \Omega^2}{2P_0} \\
& + \frac{\left(6\, d_{4\,r} P_0^3 q_{3r} - 6\, P_0^3 q_{3s} d_{4s}\right) \Omega^2}{2P_0} \\
& + \frac{\left(-2\, P_0 q_s d_{4s} - 6\, d_{3s} n_{2s} P_0^2\right) \Omega^2}{2P_0} \\
& + \frac{\left(6\, d_{4\,r} P_0^3 q_{3r} - 6\, P_0^3 q_{3s} d_{4s} - {d_{2s}}^2\right) \Omega^2}{2P_0} \\
& + 2\, P_0 q_{2s} d_{2s} + \frac{5}{2}\, {n_{1s}}^2 P_0 + 18\, n_{2s} P_0^4 n_{3s} \\
& + 3\, P_0^2 q_{3s} d_{2s} + 11\, n_{1s} P_0^3 n_{3s} \\
& + 8\, n_{2s} P_0^2 n_{1s} - 3\, d_{2\,r} P_0^2 q_{3r} - 2\, d_{2\,r} P_0 q_{2r}
\end{aligned}
\tag{3.88}
$$

Bibliography

[1] G. P. Agrawal, *Nonlinear Fiber Optics, (San Diego, CA, Academic, 2001).*

[2] J. L. Baird, British Patent 285,738 (1928).

[3] C. W. Hansell, U. S. Patent 1,751,584 (1930).

[4] H. Lamm, Z, Flexible Optical Instrument ***Instrumentenk 50****, 579-81 (1930).*

[5] A. C. S. van Heel, A new method of transporting optical images without aberrations, ***Nature 173.4392****, 39 (1954).*

[6] H. H. Hopkins and N. S. Kapany, A flexible fibrescope, using static scanning, ***Nature 164****, 39 (1955); Transparent Fibres for the Transmission of Optical Images* ***Opt. Acta 1****, 164 (1955).*

[7] B. ÒBrian, U. S. Patent 2,825,260 (1958).

[8] B. I. Hirschowitz, U. S. Patent 3,010,357 (1961).

[9] R. H. Stolen, E. P. Ippen, and A. R. Tynes, Raman oscillation in glass optical waveguide, ***Appl. Phys. Lett****,* ***20.2****, 62-64(1972).*

[10] E. P. Ippen and R. H. Stolen, Stimulated Brillouin scattering in optical fibers ***Appl. Phys. Lett****,****21.11****, 539-541 (1972)*

[11] R. G. Smith, Optical power handling capacity of low loss optical fibers as determined by stimulated Raman and Brillouin scattering, ***Appl. Opt****,* ***11****, 2489-2494 (1972)*

[12] R. H. Stolen and A. Ashkin, Optical Kerr effect in glass waveguide, ***Appl. Phys. Lett****,* ***226****, 294-296 (1973)*

[13] R. H. Stolen, J. E. Bjorkholm, and A. Ashkin, Phase matched three wave mixing in silica fiber optical wave guides, ***Appl. Phys. Lett****,* ***24****, 308 (1974)*

[14] K. O. Hill, D. C. Johnson, B. S. Kawaski, and R. I. Mac Donald, Cw three wave mixing in single mode optical fibers, ***J. Appl. Phys****,* ***49****, 5098 (1974)*

[15] R. H. Stolen, Phase-matched-stimulated four-photon mixing in silica-fiber waveguides, **IEEE J. Quantum Electron**, **11**, 100-103 (1975)

[16] R. H. Stolen and C. Lin, Self-phase-modulation in silica optical fibers **Phys. Rev. A**, **17**, 1448 (1978).

[17] A. Snyder and J. Mitchell, Accessible solitons **Science**, **276**, 1538-1541 (1997).

[18] W. Krolikowski, O. Bang, J. J. Rasmussen and J. Wyller, Modulational instability in nonlocal nonlinear Kerr media, **Phys. Rev. E**, **276**, 016612 (2001).

[19] M. Peyrard, T. Dauxois, Physique des solitons, (EDP Sciences, CNRS Édition, 2004).

[20] Dissipative solitons, edited by N. Akhmediev, A. Ankiewicz, (Springer, Berlin, 2005).

[21] Dissipative solitons: From optics to Biology and Medicine Series, edited by N. Akhmediev and A. Ankiewicz, Lecture Notes in Physics Vol.751 (Springer, Berlin/Heidelberg, 2008).

[22] J. T. Kippenberg, A. L. Gaeta, M. Lipson, M. L. Gorodetsky, Dissipative Kerr solitons in optical microresonators, **Science. eaan 361**, 8083 (2018).

[23] A. Hasegawa and E. Tappert, Transmission of stationary nonlinear optical pulses in dispersive dielectric fibers. I. Anomalous dispersion, **Appl. Phys. Lett. 23**, 142 (1973).

[24] U. F. Mollenauer, R. H. Stolen, and J. P. Gordon, Experimental observation of picosecond pulse narrowing and solitons in optical fibers, **Phys. Rev. Lett. 45**, 1095 (1980).

[25] Y. S. Kivshar and G. P. Agrawal, Optical solitons: from fibers to photonic crystals, (San Diego, Academic Press, 2003).

[26] W. Chang, A. Ankiewicz, N. Akhmediev, Creeping solitons in dissipative systems and their bifurcations, **Phys. Rev. E 76**, 016607 (2007).

[27] J. M. Soto-Crespo, M. Grapinet, P. Grelu, N. Akhmediev, Bifurcations and multiple-period soliton pulsations in a passively mode-locked fiber, **Phys. Rev. E 70**, 066612 (2004).

[28] P. Grelu, N. Akhmediev, Dissipative solitons for mode-locked lasers, **nature photonics. 4**, 06 (2012).

[29] N. Akhmediev, J. M. Soto-Crespo, G. Town, Pulsating solitons, chaotic solitons, period doubling, and pulse coexistence in mode-locked lasers: Complex Ginzburg-Landau equation approach, **Phys. Rev. E 62**, 056602 (2001).

[30] J. M. Soto-Crespo, N. Akhmediev, A. Ankiewicz, Pulsating, Creeping, and Erupting solitons in dissipative systems, **Phys. Rev. E 85**, 14 (2000).

[31] W. Chang, J. M. Soto-Crespo, P. Vouzas, N. Akhmediev, Extreme soliton pulsations in dissipative systems, **Phys. Rev. E 92**, 022926 (2015).

[32] N. Akhmediev, J. M. Soto-Crespo, P. Vouzas, N. Devine, W. Chang, Dissipative solitons with extreme spikes in the normal and anomalous dispersion regimes, **Phil. Trans. R. Soc. A 0023**, 376(2018).

[33] M. Shen, B. Li, L. Ge, W. Chen, and D. Wu, Optics Communications **338**, 27 (2015).

[34] M. Djoko, C. B. Tabi, T. C. Kofané, Robust propagation of optical vortex beams, necklace-ring solitons, soliton clusters and uniform-ring beams generated in the frame of the higher-order (3+1)-dimensional cubic-quintic-septic complex Ginzburg-Landau equation. **Phys. Scr. 94**, 075501 (2019).

[35] D. R. Solli, C. Ropers, P. Koonath, and B. Jalali, Optical rogue waves **Nature 450**, 1054-1057 (2007).

[36] D. Buccoliero, H. Steffensen, H. Ebendorff-Heidepriem, T. M. Monro, and O. Bang, Mid-infrared optical rogue waves in soft glass photonic crystal fiber, **Opt. Exp 19**, 17973-17978 (2011).

[37] J. M. Soto-Crespo, Ph. Grelu, and N. Akhmediev, Bifurcations and multiple-period soliton pulsations in a passively mode-locked fiber laser, **Phys. Rev. E 84**, 016604 (2011).

[38] C. Lecaplain, Ph. Grelu, J. M. Soto-Crespo, and N. Akhmediev, Dissipative rogue waves generated by chaotic pulse bunching in a mode-locked laser, **Phys. Rev. E 108**, 233901 (2012).

[39] A. Zaviyalov, O. Egorov, R. Iliew, and F. Lederer, Rogue waves in mode-locked fiber lasers,**Phys. Rev. A 85**, 013828 (2012).

[40] M. G. Kovalsky, A. A. Hnilo, and J. R. Tredicce, Extreme events in the Ti: sapphire laser, **Opt. Lett. 36**, 4449 (2011).

[41] Lecaplain, Ph. Grelu, J. M. Soto-Crespo, and N. Akhmediev,, Dissipative rogue wave generation in multiple-pulsing mode-locked fiber laser,**Opt. Lett. 15**, 064005 (2013).

[42] S. A. Kolpakov, H. Kbashi, and S. V. Sergeyev, Dynamics of vector rogue waves in a fiber laser with a ring cavity, **Optica 15**, 870-875 (2016).

[43] M. Tlidi, K. Panajotov, M. l. Ferre, and M. G. Clerc, Drifting cavity solitons and dissipative rogue waves induced by time-delayed feedback in Kerr optical frequency comb and in all fiber cavities,**Chaos: An Interdisciplinary Journal of Nonlinear Science 27**, 114312 (2017).

[44] S. Residori, Bortolozzo, A. Montina, F. Lenzini, and F. T. Arecchi, Rogue waves in spatially extended optical systems, **Fluctuat. Noise Lett 11**, 1240014 (2012).

[45] A. Montina, U. Bortolozzo, S. Residori, and F. T. Arecchi, Non-Gaussian statistics and extreme waves in a nonlinear optical cavity,**Phys. Rev. Lett. 103**, 173901 (2009).

[46] P.-H. Hanzard, M. Talbi, D. Mallek, A. Kellou, H. Leblond, F. Sanchez, T. Godin, and A. Hideur, Brillouin scattering-induced rogue waves in self-pulsing fiber lasers, **Sci. Rep. 45868**, 173901 (2017)

[47] A. F. J. Runge, C. Aguergaray, N. G. R. Broderick, and M. Erkintalo, Raman rogue waves in a partially mode-locked fiber laser,**Opt. Lett 39**, 319-322 (2014).

[48] J. M. Dudley, F.Dias, M. Erkintalo, and G. Genty, Instabilities, breathers and rogue waves in optics,**Nat. Photonics8**, 755 (2014).

[49] N. Akhmediev et al., Roadmap on optical rogue waves and extreme events,**J. Opt.18**, 063001 (2016).

[50] M. Onorato, S. Residori, U. Bortolozzo, A. Montina, and F. Arecchi, Rogue waves and their generating mechanisms in different physical contexts,**Phys. Rep.528**, 47 (2013).

[51] W. Chang, J. M. Soto-Crespo, P. Vouzas, and N. Akhmediev, Extreme soliton pulsations in dissipative systems,**Phys. Rev. E92**, 022926 (2015).

[52] W. Chang, J. M. Soto-Crespo, P. Vouzas, and N. Akhmediev, Extreme amplitude spikes in a laser model descrebed by the complex Ginzburg-Landau equation, **Opt. Lett92**, 2949 (2015).

[53] E. Infeld, G. Rowlands, Nonlinear Waves Solitons Chaos, (Cambridge University Press, 1990)

[54] A. Scott, Nonlinear Science, (Oxford University Press, 2003).

[55] G. Assonto and M. Peccianti, IEEE. J. Quant. Electr. **39**, 13 (2003).

[56] G. Conti, M. Peccianti, and G. Assanto, Route to nonlocality and observation of accessible solitons,**Phy. Rev. Lett 91**, 073901 (2003).

[57] Snyder A. and Mitchell J. 1997 Science 276 1538.

[58] Rasmussen J. J. and Rydal K, Two-dimensional convection and interchange motions in fluids and magnetized plasmas,**Physical Scripta 33**, 481-497(1986).

[59] C. Sulem and P. L. Sulem, The Nonlinear Schrödinger Equation, Self-Focusing and Wave Collapse, Springer Verlag1999.

[60] Davydov a T. A. and Fishchuk A. I, Modulational and other types of parametric instabilities near plasma (upper-hybrid **Ukr. J. Phys. 40**, 487(1995).

[61] W. Krolikowski and O. Bang, Solitons in nonlocal nonlinear media: Exact solutions,**Phys. Rev. E63**, 016610(2000).

[62] Snyder A. and Mitchell J, Soliton dynamics in a nonlocal medium, **J. Opt. Soc. Am. B16**, 236(1999).

[63] Swartzlander G. A. Jr. and Law C. T, Optical vortex solitons observed in Kerr nonlinear media **Phys. Rev. Lett69**, 2503(1992).

[64] Dreischuh A. et al, Generation of multiple-charged optical vortex solitons in a saturable nonlinear medium,**Phys. Rev. E60**, 6111(1999).

[65] F. D. Dalfovo, S. Giorgini, L. P . Pitaevskii, S. Stringari, Theory of Bose Einstein condensation in trapped gases, **Rev. Mod. Phys71**, 463-512(1999).

[66] O. Bang, W. Krolikowski, J. Wyller, and J. J. Rasmussen, Collapse arrest and soliton stabilization in nonlocal nonlinear media, **Phys. Rev. E66**, 466191-466195(2002).

[67] D. Suter, T. Blasberg, Stabilization of trasverse solitary waves by a nonlocal response of the nonlinear medium,**Phys. Rev. A48**, 4583-4587(1993).

[68] WWW. alamy. Com.

[69] D. I. Kovsh, D. J. Hagan, and E. W. V. Stryland, Numerical modeling of thermal refraction in liquids in the transient regime, **Opt. Exp4**, 315-327(1999)

[70] S. Gatz and J. Hermann, Anisotropy , nonlocality , and space-charge

eld displacement in (2+1)-dimensional self-trapping in biased photorefractive crystals, **Opt. Lett23**, 1176-1178(1998).

[71] A. A. Zozulya, D. Z. Anderson, A. V. Mamaev, amd M. Saffman, Solitary attractors and low-order filamentation in anisotropic self-focusing media, **Phys. Rev. A57**, 522-534(1998).

[72] D. Suter and T. Blasberg, Stabilization of transverse solitary waves by a nonlocal response of the nonlinear medidium,**Phys. Rev. A48**, 4583-4587(1993).

[73] Y u. B. Gaididei, S. F. Mingaleev, P . L. Christiansen, Effect of nonlocal dispersion on self-interacting excitations, **Phys. Lett. A222**, 152-156(1996).

[74] D. I. Kovsh, D. J. Hagan, and E. W. V. Stryland, Numerical modeling of thermal refraction in liquids in the transient regime, **Opt. Exp4**, 315-327(1999).

[75] P . Brochard, V. Grolier-Mazza, and R. Cabanel, Temporal nonlinear refraction in dye solutions: a study of the transient regime, **J. Opt. Soc. Am.B14**, 405-414(1997).

[76] K. B. Dysthe, H. L. Pecseli, Non-liear langmuir wave modulation in collisionless plasmas, **Plasma Phys19**, 931-943(1997).

[77] H. L. Pecseli, J. J. Rasmussen, Nonlinear electron waves in strongly magnetized plasmas,**Plasma Phys22**, 421-438(1980).

[78] I.C. Khoo, Liquid crystals and nonlinear optical phenomena, (Wiley , New York, 1995).

[79] G. Assanto, M. Peccianti and C. Conti, Optical spatial solitons in nematic liquid crystals, **Opt. Phot. News14**, 45-488(2003).

[80] M. Peccianti, K. A. Brzdakiewicz, and G. Assanto, Nonlocal spatial soliton interactions in nematic liquid crystals, **Opt. Lett News27**, 1460-1462(2002).

[81] Xavier HUTSEBAUT, Étude expérimentale de l'optique non linéaire dans les cristaux liquides: Solitons spatiaux et instabilité de modulation, Thèse 2006-2007.

[82] S. Tzortzakis, L. Berge, A. Couairon, M. Franco, B. Prade, and A. Mysyrowicz, Breakup and fusion of self-guided femtosecond light pulses in air, **Phys. Rev. Lett86**,5470-5473(2001).

[83] A. Couairon and L. Berg é, Modeling the filamentation of ultra-short pulses in ionizing media,**Phys. Rev. Lett7**,193-209(2000).

[84] M. Mlejnek, E. M. Wright, J. V. Moloney, Dynamic spatial replenishment of femtosecond pulses propagating in air,**Opt. Lett23**,382-384(1998).

[85] T. B. Benjamin and J. E. Fei, The Disintegration of Wave Trains on Deep Water. Part. Theory, **Journal of Fluid Mechaics27**,417-430(1967).

[86] T. B. Benjamin, Instability of Wave train in Nonlinear Dispersive Systems, **Proceedings of the Royal Society of London, series A299**,59-75(1967).

[87] A. Hasegawa and W. F. Brinkman, Tunable Coherent IR and FIR Sources Utilizing Modulational Instabiltiy,**IEEE Journal of Quantum ElectronicsQE-I6**,694-697(1980).

[88] V. I. Bespalovand V. I. Talanov, Filamentary Structure of Light Beams in Nonlinear Liquids,**JETP. Lett3**,307-310(1960).

[89] N. F. Pilipetskil and A. R. Rustamov, Observation of Self-Focusing of Light in Liquids, **JETP. Lett2**,55-56(1965).

[90] P. L. Kelley, Self-Focusing of Optical Beams, **Phy. Rev. Lett15**,1005-1008(1965).

[91] R. Y. chiao, E. Garmire, and C. H. Townes, Self-Trapping of Optical Beams, **Phy. Rev. Lett15**,482-497(1964).

[92] C. K. W. Tam, Amplitude dispersion and nonlinear instability of whistlers, **Phys Fluids 12**,1028(1969).

[93] T. Taniuti and H. Washimi, Propagation of ion-acoustic solitary waves of small amplitude, **Phys. Rev. Lett 21**,209 (1968).

[94] A. Hasegawa, Plasma Instabilities and Nonlinear Effects, (Springer-Verlag Heidelberg, 1975).

[95] E. Kengne, S. T. chui and W. M. Liu, Modulational instability criteria for coupled nonlinear transmission lines with dispersive elements, **Phys. Rev. E 74**,036614(2006).

[96] C. L. Gninzanlong, F. T. Ndjomatchoua, and C. Tchawoua, Discrete breathers dynamic in a model for DNA chain with a finite stacking enthalpy,**Chaos28**,043105(2018).

[97] C. B. Tabi, A. Mohamadou and T.C Kofané, Modulational instability and pattern formation in DNA dynamics with viscosity, **J. Comput. Theor. Nansci5**,647(2008).

[98] C. B. Tabi, A. Mohamadou and T.C Kofané, Modulational instability in the anharmonic Peyrard-Bishop model of DNA, **Eur. Phys. J. B74**,151(2010).

[99] I. Maïna, C. B. Tabi, A. Mohamadou, H. P. F. Ekobena and T. C. Kofané,Discrete impulses in ephaptically coupled nerve fibers, **Chaos B25**,043118(2015).

[100] C. B. Tabi, I. Maïna, A. Mohamadou, H. P. F. Ekobena and T. C. Kofané, Long-range intercellular Ca^{2+} wave patterns **Physica A1**,435(2015).

[101] A. S. Etémé, C. B. Tabi and A. Mohamadou, Long-range patterns in Hindmarsh-Rose networks, **Commun. Nonl. Sci. Num. Simul1**, 435(2017).

[102] C. B. Tabi, A. S. Etémé, A. Mohamadou and T. C. Kofané, Unstable discrete modes in Hindmarsh-Rose neural networks under magnetic flow effect, **Chaos Solitons and Fractals123**, 116(2019).

[103] C. S. Panguetna, C. B. Tabi and T. C. Kofané, Electronegative nonlinear oscillating modes in plasmas, **Commun. Nonlinear Sci. Numer. Simul55**, 326(2018).

[104] C. S. Panguetna, C. B. Tabi and T. C. Kofané,Two-dimensional modulated ion-acoustic excitations in electronegative plasmas, **Phys. Plasmas24**, 092114(2017).

[105] C. B. Tabi, C. S. Panguetna and T. C. Kofané, Electronegative (3+1)-dimensional modulated excitations in plasmas, **Physica B 545**, 70(2018).

[106] G. Theacharis, Z. Rapti, P. G. Kevrekidis, D. J. Frantzeskaki, and V. V. Konotop, Modulational instability of Gross-Pitaevskii-type equations in dimensions, ***Phys. Rev. A67***, *063610(2003)*.

[107] J.-K. Xue, Modulational instability of the trapped Bose-Einstein condensates, ***Phys. Lett. A341***, *527(2005)*.

[108] W. Lei, Z. Jie- Fang, Chin. Phy. Lett ***246***, *1471 (2007)*.

[109] E. Wamba, A. Mouhamadou, and T. C. Kofanë, Modulational instability of a trapped Bose-Einstein condensate with two-and three-body interactions,***Phys. Rev. E77***, *0462167(2008)*.

[110] X. Ying Qi, and Ju- Kui Xui, Modulational instability of a modified Gross-Pitaevskii equation with higher-order nonlinearity, ***Phys. Rev. E86***, *017601(2012)*.

[111] F. Maucher, T. Pohl, S. Skupin, and W. Krolikowski, Self-organization of light in optical media with competing nonlinearities, ***Phys. Rev. Lett116***, *163902(2016)*.

[112] F. Maucher, T. Pohl, W. Krolikowski, and S. Skupin, Pattern formation in the nonlinear Schrödinger equation with competing nonlocal nonlinearities, ***Opt. Data Process. Storage3***, *13(2017)*.

[113] F. Baranio, M conforti, A. Degasperis, S. Lambardo, M. Onarato, and C. Wabnitz, Vector rogue waves and baseband modulation instability in the defocusing regime, ***Phys. Rev. Lett113***, *034101(2014)*.

[114] G. Zhang, Z. Yan, X-Y. Wen, Modulational instability and dynamics of multi-rogue wave solutions for the discrete Ablowitz-Ladik equation,***Proc. R. Soc. A473***, *20170243(2017)*.

[115] G. B. Whitham, A general approach to linear and non-linear dispersive waves using a Lagrangian, ***Journal of fluid mechanics22***, *273-283(1965)*.

[116] S. T. Sorensen, C. Larsen, U. Moller, P. M. Moselend, L. Carsten, Thomsen, and Ole Bang, Influence of pump power and modulation instability gain spectrum on seeded supercontinuum and rogue wave generation, ***J. Opt. Soc. Am. B 29***, *10 (2012)*.

[117] A. K. S. Ali, K. Nithyanandan, K. Porsezian And A. I. Maimistov, Modulation instability in a triangular three-core coupler with a negative-index material channel, ***J. Opt. 18***, *035102 (2016)*.

[118] D. Zanga, S. I. Fewo, C. B. Tabi, T. C. Kofané, Modulational instability in weak nonlocal nonlinear media with competing Kerr and non-Kerr nonlinearities, ***Commun Nonlinear Sci Numer Simulat. 80***, *104993 (2020)*.

[119] B. K. Esbensen, A. Wlotzka, M. Bache, O. Bang, W. Krolikowski, Modulational instability and solitons in nonlocal media with competing nonlinearities, **Phys. Rev. A 84**, 053854 (2011).

[120] R. Ganapathy, K. Senthilnathan and K. Porsezian, Modulational instability in a fibre and a fibre Bragg grating, J. Opt. B **6**, S436. (2004).

[121] K. Porsezian, K. Senthilnathan, Generation of Bragg solitons through modulation instability in a Bragg grating structure, Chaos. **15**, 037109 (2005).

[122] J. Ancemma, K. Senthilnathan, K. Porsezian, P. Tchofo Dinda, Gap solitons and modulation instability in a dynamic Bragg grating with nonlinearity management, J. Opt. A **11**, 015203 (2009).

[123] K. Porsezian, K. Senthilnathan, and S. Devipriya, Modulational Instability in fiber Bragg grating with Non-Kerr Nonlinearity, IEEE J. Quantum Electron. **6**, 41 (2005).

[124] K. Nithyanandan, R. V. J. Raja, and K. Porsezian, Modulational instability in a twin-core fiber with the effect of saturable nonlinear response and coupling coefficient dispersion, Phys. Rev. A **87**, 043805 (2013).

[125] R. Ganapathy, B. A. Malomed, K. Porsezian, Modulational instability and generation of pulse trains in asymmetric dual-core nonlinear optical fibers, Phys. Lett. A **354**, 366 (2006).

[126] R. Haldar, A. Roy, P. Mondal, V. Mishra, S. K. Varshney, Free-carrier-driven Kerr frequency comb in optical microcavities: Steady state, bistability, self-pulsation, and modulation instability, **Phys. Rev. A 99**, 033848 (2019).

[127] K. Nithyanandan, R. V. J. Raja, K. Porsezian, Theoretical investigation of modulational instability in semiconductor doped dispersion decreasing fiber and its cutting edge over the existing fiber systems, **J. Opt. Soc. Am. B 30**, 1 (2013).

[128] G. P. Agrawal, Modulation Instability in Erbium-doped fiber amplifiers, **IEEE Photonics. Technol. Lett. 4**, 06 (1992).

[129] M. J. Ablowitz, and P. A. Clarkson, Nonlinear Evolution Equations and Inverse Scattering, (Cambridge University Press, Cambridge 2000).

[130] M. J. Ablowitz , P. A. Clarkson . Solitons, Nonlinear Evolution Equations and Inverse Scattering, (Cambridge University Press, Cambridge, UK, 1991).

[131] G. Tanolu, Int. J. Nonlinear Sci. 1, 1479 (2006).

[132] S. Kakei, N. Sasa, and J. Satsuma, Bilinearization of a generalized derivative nonlinear Schrödinger equation, **J. Phys. Soc. Jpn. 64**, 1519 (1995).

[133] A. Ebaid, and E. H. Aly, Exact solutions for the transformed reduced Ostrovsky equation via the F-expansion method in terms of Weierstrass-elliptic and Jacobian-elliptic functions, **Wave Motion 49**, 296 (2012).

[134] A. Filiz, M. Ekici, and A. Sonmezoglu, Expansion Method and New Exact Solutions of the Schrödinger-KdV Equation, **The scientific World Journal 49**, 534063 (2014).

[135] S. Liu, Z. Fu, S. Liu, and Q. Zhao, Jacobi elliptic function expansion method and periodic wave solutions of nonlinear wave equations, **Phys. Lett. A 289**, 69 (2001).

[136] G.-T. Liu , and T.-Y. Fan, New applications of developed Jacobi elliptic function expansion methods, **Phys. Lett. A 345**, 161 (2005).

[137] D. Anderson, Variational approach to nonlinear pulse propagation in optical fibers, **Phys. Rev. A 27**, 0 (1983).

[138] E. Wamba, Matter waves of Bose-Einstein condensates with two- and three-body interactions, PhD thesis, University of Yaounde I, (2013).

[139] T. Miya, Y. Terunama, T. Hosaka and T. Miyashita, Ultimate low-loss single-mode fibres at 1-55 fim Electron, **Electron. Lett. 27**, 106 (1979).

[140] P. V. Mamyshev and S. V. Chernikov, Ultrashort-pulse propagation in optical fibers, **Opt. Lett. 15**, 1076 (1990).

[141] S. V. Chernikov and P. V. Mamyshev, Femtosecond soliton propagation in fibers with slowly decreasing dispersion, **J. Opt. Soc. Am. B 8**, 1633-1641 (1991).

[142] F. Dalfovo, S. Giorgini, L.P. Pitaevskii, and S. Stringari, Theory of Bose-Einstein condensation in trapped gases, **Rev. Mod. Phys 71**, 463 (1999); K. Goral, K. Rzazewski, and T. Pfau, Bose-Einstein condensation with magnetic dipole-dipole forces, **Phys. Rev. A 61**, 051601 (2000); V. M. Perez-Garcia, V. V. Konotop, and J.J. Garcia-Ripoll, Dynamics of quasicollapse in nonlinear Schrödinger systems with nonlocal interactions, **Phys. Rev. E 62**, 4300 (2000).

[143] D. Mihalache, D. Mazilu, F. Lederer, L-C Crasovan, Y. V. Kartashov,L. Toner and B. A. Malomed, Stable solitons of even and odd parities supported by competing nonlocal nonlinearities, **Phys. Rev. E 74**, 066614 (2006).

[144] G. P. Agrawal, Optical pulse propagation in doped fiber amplifiers, Phys. Rev. A **44**, 11 (1991).

[145] G. P. Agrawal, (eds), Applications of nonlinear fiber optics (Nonlinear fiber Optics, 2001).

[146] M. Djoko and T. C. Kofané, Dissipative optical bullets modeled by the cubic-quintic-septic complex Ginzburg-Landau equation with higher-order dispersions, **Commun Nonlinear Sci Numer Simulat. 48**, 179 (2017).

[147] M. Djoko, T. C. Kofané, The cubic-quintic-septic complex Ginzburg-Landau equation formulation of optical pulse propagation in 3D doped Kerr media with higher-order dispersions, **Opt. Commun. 416**, 190 (2018).

[148] M. Djoko, T. C. Kofané, Dissipative light bullets: from stationary light bullets to double, quadruple, six fold, eight fold and ten fold bullet complexes, **Commun Nonlinear Sci Numer Simulat. 68**, 169 (2019).

[149] A. Trombettoni and A. Smerzi, Discrete solitons and breathers with dilute Bose-Einstein condensates,**Phys. Rev. Lett 86**, 2353 (2001).

[150] F. K. Abdullaevet al, Nonlinear excitations in arrays of BoseEinstein condensates, **Phys. Rev. A 64**, 043606 (2001).

[151] S. Marino, I. B. Hogue, C. J. Ray, D. E. Kirschner, A methodology for performing global uncertainty and sensitivity analysis in systems biology, **J. Theor. Biol. 254**, 178 (2009).

[152] S. A. Pedro, H. E. Z. Tonnang, S. Abelman, Uncertainty and Sensitivity Analysis of a Rift Valley fever model, **Comput. Math. Appl 279**, 170 (2016).

[153] M. M. Foudjio, F. T. Ndjomatchoua, C. L. Gninzanlong, C. Tchawoua, Collective escape and supratransmission phenomena in a nonlinear oscillators chain **Chaos** , **30**, 123122 (2020).

[154] B. S. Djouda, F. T. Ndjomatchoua, F. M . Moukam Kakmeni, C. Tchawoua and H. E. Z. Tonnang, Understanding biological control with entomopathogenic fung-Insights from a stochastic pest-pathogen model **Chaos** , **31**, 023126(2021).

[155] S. F. Kamga, F. T. Ndjomatchoua, R. A. Guimapi, I. Klingen, C. Tchawoua, A. G. R. Hjelkrem, K. H. Thunes, F. M. Kakmeni, The efect of climate variability in the efcacy of the entomopathogenic fungus Metarhizium acridum against the desert locust Schistocerca gregaria **Sci. Rep**, **12**, 7535(2022).

[156] P. G. Kevrekidis, The discrete nonlinear schrödinger equation: Mathematical Analysis, Numerical Computations and physical perspectives, STMP 233 (Springer, berlin Heidelberg, 2009).

[157] V. G. S. Murti and C. Vijayan, Essentials of Nonlinear optics, (Wiley, 2014).

[158] A. Visiniscu, and D. Grecu, Proc. Inst. Math. NAS Ukr. **50**, 3 (2004).

[159] R. Carretero-Gonzalez, J. D. Talley, C. Chong and B. A. Malomed, Multistable solitons in the cubic-quintic discrete nonlinear Schrödinger equation, **Physica D 216**, 77 (2006).

[160] R. I. Ben, L. C. Ake and A. A. Minzoni and P. Panayotaros, Localized solutions for a nonlocal discrete NLS equation, **Phys. Lett. A 379**, 1705 (2015).

[161] T. Lahaye, C. Menotti, L. Santos, M. Lewenstein and T. Pfau, The physics of dipolar bosonic quantum gases, **Rep. Prog. Phys 72**,126401 (2009).

[162] J. Cueves B. A. Malomed, P. G. Kevrekidis and D. J. Frantzeskakis, Mobility of discrete solitons in quadratically nonlinear media **Phys. Rev. Lett. 97**,124101 (2007).

[163] A. Griesmaier, J. Stuhler, T. Koch, M. Fahori, T. pau and S. Giovanatti, Comparing contact and dipolar interactions in a Bose-Einstein condensate, **Phys. Rev. Lett. 97**,250402 (2006)

[164] M. Warenghem, J. F. Blach and J. F. Henninot, Thermo-nematicon: an unnatural coexistence of solitons in liquid crystals ?,**J. Opt. Soc. Am 25**,1882 (2008)

[165] B. K. Esbensen, M. Bache, O. Bang and W. Krolikowski, Modulational instability and solitons in nonlocal media with competing nonlinearities, **Phys. Rev. A 86**,033838 (2012)

[166] D. Trejo-Garcia, D. Gonzalez-Hermandez, D. López-Aguayo, and S. Lopez-Aguayo, Stable Hermite-Gaussian solitons in optical lattices, **J. Optics 20**,125501 (2018).

[167] M. Peccianti, C. Conti, G. Assanto, A. De Luca and C. Umeton,Routing of anisotropic spatial solitons and modulational instability in liquid crystals,**Nature 432**,733-737, (2004).

[168] H. Tagwo, G. G. L. Tiofack, O. Dafounansou, A. Mouhamadou and T. C. Kofané, Effect of competing cubic-quintic nonlinearities on the modulational instability in nonlocal Kerr-type media, **J. Mod. Opt. 63**,558-565, (2016).

[169] C. G. L. Tiofack, H. Tagwo, O. Dafounansou, A. Mouhamadou and T. C. Kofané, Modulational instability in nonlocal media with competing non-Kerr nonlinearities, **J. Mod. Opt. 357**,7, (2015).

[170] Z. Zhou, Y. Du, C. Hou, H. Tian and Y. Wang, Dark-type solitons in media with competing nonlocal non-Kerr nonlinearities, **J. Opt. Soc. Am. B 28**,1583, (2011).

[171] Q. Kong, M. Shen, Z. Chen, Q. Wang, R-K. Lee and W. Krolikowski, Dark solitons in nonlocal media with competing nonlinearities, **Phys. Rev. A 87(6)**,063832, (2013).

[172] E. I. Duque and S. Lopez-Aguayo, Phys. Rev. A, Generation of solitons in media with arbitrary degree of nonlocality using an optimization procedure, **Phys. Rev. A 99**,013831, (2019).

[173] C. S. Panguetna, C. B. Tabi and T. C. Kofané, Low relativistic effects on the modulational instability of rogue waves in electronegative plasmas, **J. Theor. Appl. Phys. 3**,237-249, (2019).

[174] C. B. Tabi, Fractional unstable patterns of energy in α- helix proteins with long-range interactions,**PChaos Solit. Fract. 116**,386, (2018).

[175] J. D. T. Tchinang, A. B. M. Togueu and C. Tchawoua, Biological multi-rogue waves in discrete nonlinear Schrödinger equation with saturable nonlinearities, **Phys. Lett. A 380**,3057, (2016).

[176] M. Erkintalo, G. Genty, B. Wetzel and J.M. Dudley, Akhmediev breather evolution in optical fiber for realistic initial conditions, **Phys. Lett. A 375**,2029, (2011).

[177] B. Frisquet, B. Kibler and G. Millot, Collision of Akhmediev breathers in nonlinear fiber optics, **Phys. Rev. X 3**,041032 , (2013).

[178] K. Manikandan, P. Muruganandam, M. Senthilvelan, and M. Lakshmanan, Manipulating matter rogue waves and breathers in Bose-Einstein condensates, **Phys. Rev. E 90**,062905, (2014).

[179] B. B. Baizakov, F. Kh. Abdullaev, B. A. Malomed, and M. Salermo, Solitons in the Tonks-Girardeau gas with dipolar interactions,J. Phys. B. At. Mol. Opt. Phys. **42**, 175302 (2009).

[180] O. Kimmoun, H. C. Hsu, H. Branger, M. S. Li, Y. Y. Chen, C. Kharif, M. Onorato, E. J. R. Kelleher, B. Kibler, N. Akhmediev and A. Chabchoub, Modulation instability and phase-shifted Fermi-Pasta-Ulam recurrence,Sci. Rep. **6**, 28516 (2016).

[181] N. Akhmediev and A. Ankiewicz, Modulation instability, Fermi-Pasta-Ulam recurrence, rogue waves, nonlinear phase shift, and exact solutions of the Ablowitz-Ladik equation, Phys. Rev. E **83**, 046603 (2011).

[182] X. Feng, Y. Liu, S. Fu, S. Yuan, X. Dong, Switchable dual-wavelength Ytterbium-doped fiber laser based on a few-mode fiber grating, IEEE Photonics. Technol. Lett. **16**, 3 (2004).

[183] Y. Jeong, J. K. Sahu, D. N. Payne, J. Nilsson, Ytterbium-doped large-core fiber laser with 1.36 kW continuous-wave output power, Opt.Express **12**, 25 (2004).

[184] L. M. Zhao, D. Y. Tang, H. Zhang, X. Wu, Q. Bao, K. P. Loh, Dissipative soliton operation of an Ytterbium-doped fiber laser mode locked with atomic multilayer Graphene, Opt. Lett. **35**, 21 (2010).

[185] M. Zhang, E. J. R. Kelleher, F. Torrisi, Z. Sun, T. Hasan, D. Popa, F. Wang, A. C. Ferrari, S. V. Popov, J. R. Taylor, Tm-doped fiber laser mode-locked by graphene-polymer composite, Opt.Express **20**, 22 (2012).

[186] Z. Luo, M. Zhou, J. Weng, G. Huang, H. Xu, C. Ye, Z. Cai, Graphene-based passively Q-switched dual-wavelength Erbium-doped fiber laser, Opt.Lett **35**, 21 (2010).

[187] Y. Chen, C. Zhao, S. Chen, J. Du, P. Tang, G. Jiang, H. Zhang, S. Wen, D. Tang, Large energy, wavelength widely tunable, topological insulator Q-switched Erbium-doped fiber laser, IEEE J. Sel. Top. Quantum Electron **20**, 5 (2014).

[188] H. Zhang, D. Y. Tang, L. M. Zhao, Q. L. Bao, K. P. Loh, Large energy mode locking of an Erbium-doped fiber laser with atomic layer Graphene, Opt.Epress **17**, 20 (2009).

[189] F. Sanchez, P. le Boudec, F. Pierre-Luc , G. stephan, Effects of ion pairs on the dynamics of erbium-doped fiber laser. Phys. Rev. A **48**, 3 (1993).

[190] L. Luo, T. J. Tee, P. L. Chu, Chaotic behavior in Erbium-doped fiber-ring lasers. J. Opt. Soc. Am. B **15**, 3 (1998).

[191] S. Gatz, J. Herrmann, Opt. Lett. **17**, 484 (1992).

[192] C. Yi-Fan, K. Beckwitt, F. W. Wise, B. G. Aitken, J. S. Sanghera, I. D. Aggarwal, Measurement of fifth-and seventh-order nonlinearities of glasses, **J. Opt. Soc. Am. B 23**, 02 (2006).

[193] A. Mohamadou, C. G. Latchio Tiofack, T. C. Kofané, Wave train generation of solitons in systems with higher-order nonlinearities, **Phys. Rev. E 82**, 016601 (2010).

[194] S. I. Fewo, C. M. Ngabireng and T. C. Kofané, Ultrashort Optical Solitons in the Cubic-Quintic Complex Ginzburg-Landau Equation with Higher-Order Terms, **Phys. Soc. Jpn. 77**, 07 (2008).

[195] S. I. Fewo, T. C. Kofané, A collective variable approach for optical solitons in the cubic-quintic Complex Ginzburg-Landau Equation with third-order dispersion, **Opt. Commun. 281**, 2893 (2007).

[196] K. Porsezian, K. Nithyanandan, R. V. J. Raja, P. K. Shukla, Modulational instability at the proximity of zero dispersion wavelength in the relaxing saturable nonlinear system, **J. Opt. Soc. Am. B 29**, 10 (2012).

[197] R. V. J. Raja, K. Porsezian, K. Nithyanandan, Modulational-instability-induced supercontinuum generation with saturable nonlinear response, **Phys. Rev. A 82**, 013825 (2010).

[198] P. Tchofo Dinda, C. M. Ngabireng, K. Porsezian, B. Kalithasan, Modulational instability in optical fibers with arbitrary higher-order dispersion and delayed Raman response, Opts. Commun. **266**, 142 (2006).

[199] K. Nithyanandan, R. V. J. Raja, K. Porsezian, B. Kalithasan, Modulational instability with higher-order dispersion and walk-off in Kerr media with cross-phase modulation, **Phys. Rev. A 86**, 023827 (2012).

[200] S. V. Gurevich, C. Schelte, J. Javaloyes, Impact of high-order effects on soliton explosions in the complex cubic-quintic Ginzburg-Landau equation, **Phys. Rev. A 99**, 061803(R) (2019).

[201] K. K. Ndebele, C. B. Tabi, T. C. Kofané, Modulational instability in nonlinear doped optical fiber induced by the cubic-quintic-septic complex Ginzburg-Landau equation with higher-order dispersions, **J. Opt SOC. Am. B 37**, 11 (2020).

[202] C. G. Latchio Tiofack, A. Mohamadou, T. C. Kofané and A. B. Moubissi, Generation of pulse trains in nonlinear optical fibers through the generalized complex Ginzburg-Landau equation, **Phys. Rev. E 80**, 066604 (2009).

[203] C. G. Lange, A. C. Newell, A stability criterion for envelope equation, **Siam J. Appl. Math. 27**, 3 (1974).

[204] F. II. Ndzana, A. Mohamadou, T. C. Kofané, Discrete Lange-Newell criterion for dissipative systems, **Phys. Rev. E 79**, 056611 (2009).

[205] F. B. Pelap, T. C. Kofané, Modulation Instability in some physical systems, . **Phys. scr. 64**, 410 (2001).

[206] A. Mohamadou, B. E. Ayissi, T. C. Kofané, Instability criteria and pattern formation in the complex Ginzburg-Landau equation with higher-order terms, **Phys. Rev. E 74**, 046604 (2006).

[207] E. Doktorov and M. A. Molcham, Discrete nonlinear Schrödinger equation with arbitrary nonlocality: Linear stability analysis and localized solution, **Phys. Lett. A.**, **373**, 1031 (2009).

[208] L. Zhong, Y. Li, Y. Chen, W. Hong, W. Hu and Q. Guo, Chaoticons described by nonlocal nonlinear Schrödinger equation,**Sci. Rep.**, **7**, 41438 (2017).

[209] L. Zhong, J. Yang, Z. Ren and Q. Guo, Hermite-Gaussian stationary solutions in strongly nonlocal nonlinear optical media, **Opt. Com**, **383**, 274 (2017).

[210] A. Hasegawa, An historical review of application of optical solitons for high speed communications, **Chaos: An Interdisciplinary Journal of Nonlinear Science**, **10**, 475-485 (2000).

[211] M. I. Carvalho, M. Facão, Dissipative solitons for generalizations of the cubic complex Ginzburg-Landau equation, **Phys. Rev. E 100**, 032222 (2019).

[212] M. I. Carvalho, M. Facão, Plain and oscillatory solitons of the cubic complex Ginzburg-Landau equation with nonlinear gradient terms, **Phys. Rev. E 96**, 042220 (2017).

[213] M. I. Carvalho, M. Facão, Existence and stability of solutions of the cubic complex Ginzburg-Landau equation with delayed Raman scattering, **Phys. Rev. E 92**, 022922 (2015).

[214] R. Murali, K. Porsezian, Modulational instability and moving gap soliton in Bose-Einstein condensation with Feshbach resonance management, Physica. D **239**, 1 (2010).

[215] T. S. Raju, P. K. Panigrahi, K. Porsezian, Modulational instability of two-component Bose-Einstein condensates in a quasi-one-dimensional geometry. **Phys. Rev. A 71**, 035601 (2005).

[216] T. Mithun, K. Porsezian, Modulational instability of $F = 2$ spinor condensates. **Phys. Rev. A 85**, 013616 (2012).

[217] N. Kumar, A. Pukhov, K. Lotov, Self-Modulation Instability of a Long Proton Bunch in Plasmas, **Phys. Rev. Lett. 104**, 255003 (2010).

[218] A. Hasegawa, Plasma instabilities and nonlinear effects (Springer-Verlag Heidelberg, 1975).

[219] T. Taniuti, H. Washimi, Self-trapping and instability of hydromagnetic waves along the magnetic field in a cold plasma, **Phys. Rev. Lett 21**, 209 (1968).

[220] A. K. S. Ali, K. Porsezian, and T. Uthayakumar, Influence of self-steepening and intrapulse Raman scattering on modulation instability in oppositely directed coupler, Phys. Rev. E **90**, 042910 (2014).

Related works of the thesis

★.**Dieudonné Zanga**, Serge. I. Fewo, Conrad. B. Tabi, Timoléon. C. Kofané, Modulational instability in weak nonlocal nonlinear media with competing Kerr and non-Kerr nonlinearities, **Commun Nonlinear Sci Numer Simulat. 80**, 104993 (2020).

★. **Dieudonné Zanga**, Serge. I. Fewo, Conrad. B. Tabi, Timoléon. C. Kofané, Generation of dissipative solitons in a doped optical fiber modeled by the higher-order dispersive cubic-quintic-septic complex Ginzburg-Landau equation, **Physical Review A 105**, 023502 (2022).